PRENATAL EXPOSURE TO A WESTERN-STYLE DIET: IMPACTS TO SENSORY CONNECTIVITY AND NEUROINFLAMMATION IN THE CONTEXT OF SENSORY PROCESSING DISORDER

By

Samantha Lauren Papadakis

A DISSERTATION

Presented to the Department of Behavioral Neuroscience

and the Oregon Health & Science University

School of Medicine

In partial fulfillment of the requirements for the degree of

Doctor of Philosophy

January 12th, 2023

School of Medicine

Oregon Health & Science University

CERTIFICATE OF APPROVAL

This is to certify that the PhD dissertation of

Samantha L. Papadakis

has been approved

Damien Fair, PA-C, PhD, Mentor/Advisor

Elinor Sullivan, PhD, Mentor/Advisor

Stephen David, PhD, Committee Chair

John Williams, PhD, Member

Oscar Miranda-Dominguez, PhD, MS, Member

TABLE OF CONTENTS

FIGURES CONTENTS

TABLE CONTENTS

ABBREVIATIONS

αMSH – alpha-melanocyte-stimulating hormone

AAC – auditory association cortex

ABCD – Adolescent Brain Cognitive Development

ABIDE – Autism Brain Imaging Data Exchange

ADHD – Attention-deficit/hyperactivity disorder

AgRP – agouti-related peptide

AI – primary auditory cortex

AIC – Akaike information criterion

AII – secondary auditory cortex

Amyg-Any – amygdala-any network

ANOVA – analysis of variance

ANTs – Advanced Normalization Tools

ARC – arcuate nucleus of the hypothalamus

ASD – Autism Spectrum Disorder

Aud-Aud – auditory-auditory

AVMA – American Veterinary Medical Association

BBB – blood-brain barrier

BICEPS – Brain Imaging Connectivity Extraction Program Solution

BMI – body mass index

BOLD – blood oxygen level dependent

Chisq – chi-squared test statistic

CIFTI – Connectivity Informatics Technology Initiative

CNS – central nervous system

CTR – control diet

DAIC – Data Analytics and Informatics Core

DAIRC – Data Analysis, Informatics & Resource Center

DAPI – 4′,6-diamidino-2-phenylindole

DCAN – Developmental Cognition and Neuroimaging Labs

Df – degrees of freedom

DSM-5 – Diagnostic and Statistical Manual of Mental Disorders

DTI – diffusion tensor imaging

EBZ – ear-bar zero

EGF – epidermal growth factor

ELISA – enzyme-linked immunosorbent assay

EPI – echoplanar imaging

FA – flip angle

FD – framewise displacement

FDA – Food and Drug Administration

Fiji – Fiji Is Just ImageJ

FMRIB - Functional Magnetic Resonance Imaging of the Brain

FOV – field of view

FRF – Functional Random Forest

FSL – FMRIB Software Library

GABA - γ-aminobutyric acid

GMA – Gamma-Minimum-Average

GPR56 – G protein-coupled receptor 56

GUI – graphical user interface

HCP – Human Connectome Project

HFD – high-fat diet

HSB – Hue, Saturation, and Brightness

Iba1 – ionized calcium-binding adaptor protein-1

ICC – inferior colliculus, central nucleus

ICC – intraclass-correlation coefficient

ICx – inferior colliculus, exterior nucleus

IEC – intestinal epithelial cell

IFNg – interferon gamma

IL-12 – interleukin 12

IL-17 – interleukin-17

IL-1b – interleukin 1 beta

IL-1RA – interleukin 1 receptor antagonist

IL-1β – interleukin-1 beta

IL-6 – interleukin-6

I-TAC – interferon-inducible T-cell alpha chemoattractant

KPBS – potassium phosphate buffered saline

LL – lateral lemniscus

logLik – log-likelihood

LP – lamina propria

LPS – lipopolysaccharide

LTu – lateral tuberal nucleus

MAE – mean absolute error

MCP-1 – monocyte chemoattractant protein-1

MDC – macrophage-derived chemokine

ME – median eminence

MGB – medial geniculate body

MIF – macrophage migration inhibitory factor

MIP-1b – macrophage inflammatory protein-1 beta

MRI – magnetic resonance imaging

NaPO4 – sodium phosphate

NCAP – non-classical auditory pathway

NDA – NIMH Data Archive

NHP – non-human primate

NIMH – National Institute of Mental Health

npar – number of parameters

NPY – neuropeptide Y

NS – non-significant

ONPRC – Oregon National Primate Research Center

OPT – optic tract

PF – paraformaldehyde

PLSR – partial least squares regression

POMC – pro-opiomelanocortin

Pr(>Chisq) – p-value

PS – phosphatidylserine

R – Pearson's correlation coefficient

RANTES – regulated upon activation, normal T cell expressed and secreted

ROI – region of interest

rs-fcMRI – resting-state functional connectivity magnetic resonance imaging

SARS-CoV-2 – Severe acute respiratory syndrome coronavirus 2

SBMD – Sensory-based Motor Disorder

SC – sensory craving

SDD – Sensory Discrimination Disorder

SEM – standard error of the mean

SFB – segmented filamentous bacteria

SM-Aud – somatomotor-auditory

SMD – Sensory Modulation Disorder

SM-SM – somatomotor-somatomotor

SM-Vis – somatomotor-visual

SNR – signal-to-noise ratio

SOR – sensory over-responsivity

SPD – Sensory Processing Disorder

SSPCA – sparse supervised principal component analysis

SUR – sensory under-responsivity

T1w – T1-weighted

T2w – T2-weighted

TE – echo time

Th17 – T helper 17 cell

TI – inversion time

TNF-α – tumor necrosis factor alpha

TR – repetition time

TREM2 – triggering receptor expressed on myeloid cells 2

USPIO – ultrasmall superparagmagnetic iron oxide

Vis-Aud – visual-auditory

Vis-Vis – visual-visual

VMH – ventromedial hypothalamic nucleus

WSD – Western-style Diet

ACKNOWLEDGMENTS

I would like to begin this section by acknowledging Dr. Damien Fair for his incredible support throughout my time in the lab. There will always be unexpected challenges that arise in research, but thanks to Damien's invaluable insights and unshakable attitude, these challenges never felt insurmountable. I left every meeting inspired and excited to continue my work. It is because of Damien's enthusiasm, expertise, and encouragement that I am able to present the dissertation that follows. I will always be grateful for his excellent mentorship and contributions to my growth as a scientist.

I would also like to acknowledge Dr. Elinor Sullivan for her constant guidance and support. I met Elinor through the ongoing collaboration between the Sullivan and DCAN labs, and I am grateful that we had the opportunity to work together. Elinor welcomed me into her lab and provided extensive mentorship as I worked on the experiments for Study 2. She has consistently gone above and beyond to help me succeed in my research, and I am grateful for the time and effort she has invested in me.

I am fortunate to have been part of a lab that fosters a culture of community and collaboration. I am indebted to all of the members of the DCAN Labs for their scientific discussions, generous guidance, and camaraderie. I would like to first extend my heartfelt thanks to those who have helped me think through my research questions and analyses. Thank you, Drs. Oscar Miranda-Dominguez, Eric Feczko, Alice Graham, Binyam Nardos, and Robert Hermosillo for your insights and patient guidance. Your mentorship was instrumental to my success as a researcher and has made a lasting impact on how I approach science. I would also like to thank the computing team for their support as I

conducted the image processing and analyses for these studies. The computing team developed many of the tools I used, even modifying them to suit the needs of my projects at times, and I am deeply grateful for their collaboration on these efforts. In addition to the aforementioned individuals, Eric Earl, Darrick Sturgeon, Anders Perrone, Jennifer Zhu, Anthony Galassi, Emma Schifsky, Olivia Doyle, Kathy Snider, Michael Anderson, Philip Robinson, and Greg Conan are among the many individuals who have helped me expand my computing capabilities. I would additionally like to thank the lab managers who regularly facilitated scientific advancement by connecting me to the right people, forms, tutorials, and procedures. Michaela Cordova, Nora Byington, and Dr. Amanda Rueter are among the people I have relied on to point me in the right direction, and I am grateful for all of the behind-the-scenes work these and other individuals do to ensure the lab is running smoothly. I would especially like to thank the graduate researchers in the lab who have taken on all of the previously mentioned roles and more. Drs. Bene Ramirez, Mollie Marr, Elina Thomas, and AJ Mitchell have each been incredible supports for me throughout my graduate education, and I am grateful to have shared my time in the lab with them.

I owe a huge debt of gratitude to the members of the Sullivan lab, as well. The Sullivan lab managed all operations relating to the non-human primate model, including setting up diet groups, conducting the neuroimaging, and piloting the immunofluorescence experiments. I am deeply appreciative of the constant support and resource sharing that occurred during our collaboration, as well as the thought-provoking discussions and excellent feedback. Jacqui Thompson, Geoff Dunn, and Matt Selby were among the members who helped me develop the experiments pursued in Study 2, and I

greatly appreciate their significant contributions. I would also like to acknowledge Geoff for conducting the amygdala staining experiment and sharing the Iba1-stained cell counts with me for an analysis in Study 1.

I would like to express my gratitude to my dissertation advisory committee for their support throughout my doctoral education. The valuable insights and advice from Drs. Stephen David, Ed Neuwelt, and John Williams have helped me to refine my research approach and have been instrumental in my development as a scientist. I am deeply appreciative of the time and energy that each member of the committee has taken to review my work and provide constructive feedback.

I would also like to thank the members of the Neuroscience Graduate Program and the Vollum Institute for enriching my graduate school experience. I have greatly appreciated the programmatic support and guidance I have received over the years from Dr. Kelly Monk, Dr. Marc Freeman, Dr. Gary Westbrook, Jessica Parks, and Liz Lawson-Weber. These individuals have always strongly advocated for students, and I am fortunate to have benefited from their contributions to the graduate program. I have additionally had the privilege of navigating graduate school with an impressive group of students across all of the graduate programs. Thank you for your incredible friendship and for making my time at OHSU a rewarding and enjoyable experience.

To all of the amazing individuals I have had the chance to work with outside of the lab, thank you for the shared experience of making OHSU a better place to work and learn. Thank you to all of the members of the Assessment Council, Graduate Student Organization, and All-Hill Student Council. I have the deepest respect for each of you, and I have appreciated your support and interest in my success. Thank you to my

Graduate Student Peer Network co-founders, Tavita Garrett, Dr. Rose Goueth, and Dr. Mollie Marr, for working tirelessly to launch a student mentoring program, and for being an excellent support system to me in the process. Lastly, I would like to acknowledge the members of the GRU Bargaining Team, Danielle Mathieson, Dr. Marc Meadows, and Rich Posert. It was an honor to work with you.

Finally, I would like to thank my incredible family for all of their continued love and support. Your sincere interest in my research has always been a source of joy for me. I would especially like to thank my wife, Lauren, for supporting me every step of the way. You have always celebrated my milestones, and I am grateful for everything you have done to make these years spectacular. Here's to our next chapter together.

ABSTRACT

Sensory processing disorder (SPD) is characterized by impairments in sensory processing, though the underlying neural correlates of these symptoms are largely unknown. Additionally, it is unclear what factors might lead to the development of SPD. Children with autism spectrum disorder (ASD) often report a SPD, so the two may share similar causes. Predictors of ASD include prenatal exposure to a Western-style diet (WSD), increased maternal adiposity, and increased maternal inflammation. These factors may contribute to ASD by stimulating neuroinflammation and thereby impacting microglia-mediated processes of neural circuit formation. However, these prenatal exposures and neuroinflammatory processes of circuit restructuring have not been sufficiently explored in SPD.

The goal of the present work is to advance what is known about the etiology of SPD. Japanese macaques were studied because their metabolic responses to a WSD, as well as their trajectory of brain development, better reflect those of humans than do rodent models. Study 1 characterized the functional connectivity of relevant sensory and emotional processing areas across development to expand upon prior connectivity studies. Functional connectivity was explored in relation to perinatal WSD exposure, prenatal exposure to maternal adiposity, and postnatal amygdala inflammation. The study also investigated the connectivity of these areas in humans with a subtype of SPD, sensory over-responsivity, to provide a baseline for comparison across species. Study 2 investigated whether neuroinflammation evident during the prenatal period persisted into the postnatal period to determine the timing of how neuroinflammation may impact

neural circuit formation. This study quantified microglia in the arcuate nucleus of the hypothalamus one year after birth.

Findings from both studies revealed that perinatal exposure to a WSD was associated with noticeable differences in functional connectivity and neuroinflammation during the prenatal and early postnatal periods, but adverse impacts were not found beyond 4 months of age. The strongest connectivity impacts were to intra-somatosensory connectivity at 4 months of age, consistent with reports that sensory over-responsivity is most common in the tactile domain. A slight decrease in microglial number was observed one year after birth, indicating that offspring exposed to a perinatal WSD may experience reduced neuroinflammation at this age. The consistency between studies demonstrates that heightened neuroinflammatory impacts occur during the same period as impacts to connectivity, suggesting a relationship between the two. Taken together, these results indicate that the earlier periods of development are more susceptible to the transient impacts of perinatal WSD exposure. Furthermore, no major differences in connectivity were found in the preadolescent human cohort, which aligns with the null findings in macaques.

The current work presents a coherent characterization of the impacts of perinatal WSD exposure in the context of SPD. This research advances what is known about a potential prenatal predictor of SPD, a potential mechanism by which neural circuits are altered, and the longitudinal functional connectivity patterns characteristic of SPD in relation to what is observed in humans. Future work can build from this foundation to develop a greater understanding of sensory processing and contribute to early detection methods and treatments.

CHAPTER 1. INTRODUCTION

1.1 Sensory Processing Disorder

Sensory processing disorder (SPD) is a neurological condition that affects how the brain processes sensory information. SPD encompasses a broad range of symptoms and behaviors that can be categorized into three main types: sensory modulation disorder (SMD), sensory discrimination disorder (SDD), and sensory-based motor disorder (SBMD). Each of these types can be further divided into subtypes (Mulligan et al., 2021; Miller et al., 2007).

SMD is characterized by demonstrated difficulties with noticing, reacting to, or adapting to ordinary sensory stimuli. The subtypes of SMD include sensory over-responsivity (SOR), sensory under-responsivity (SUR), and sensory craving (SC), which is sometimes referred to as sensory-seeking. SOR is distinguished by strong, negative emotional responses to sensory stimuli that most people are able to tolerate well. SUR involves a reduced response to sensory stimuli, which can include a lack of awareness of the sensory event, a delay before responding, or indifference. Individuals with SC behavior seek sensory stimulation, often in a way that is disruptive or disorganized.

SDD is an umbrella category of modality-specific disorders that involve difficulty detecting or interpreting the subtle qualities of, or differences between, sensory features. Individuals may experience a SDD within one or multiple sensory modalities.

SBMD is defined by difficulties with balance, motor coordination, and dexterity, and it can be categorized into two subtypes. The first subtype, postural disorder, is characterized by weaknesses in stability, motor strength, endurance, proprioception, and

coordination. The second subtype, dyspraxia, involves impairments in conceptualizing, planning, and executing skilled, new, or synchronized motor sequences.

Thus, SPD covers a wide range of symptoms that may have differing origins or neural correlates. For the purposes of this dissertation, SOR was selected as a primary research focus, as it is one of the more common subtypes of SPD (Ahn et al., 2004; Ben-Sasson et al., 2009). SPD is estimated to occur in as much as 14% of the general population of preschoolers (Ahn et al., 2004), and it is highly comorbid with other developmental disorders, occurring in approximately 95% of individuals with ASD (Tomchek and Dunn, 2007; Crane et al., 2009; Leekam et al., 2007), 69% of individuals with attention-deficit/hyperactivity disorder (ADHD; Parush et al. 2007), and 40% of individuals with Fragile X syndrome (Baranek et al., 2008). The incidence of SOR in particular, as determined by a 41-item assessment derived from the Sensory Over-Responsivity (SensOR) Scales (Schoen et al., 2008), was 16.5% in typically-developing school-aged children, indicating that the true incidence in the general population when including individuals with comorbid disorders may be higher. The study specifically assessed SOR in auditory and tactile modalities, and while 16.9% of children with SOR reported over-responsivity in both modalities, the vast majority only experienced tactile SOR (76.4%), further supporting the idea that even SPD subtypes may present as modality-specific and have potentially differing origins (Ben-Sasson et al., 2009).

Children with tactile SOR are often bothered by textures like clothing tags, which can usually be avoided, but an aversion to other sensations like washing one's face or receiving hugs can impede one's engagement in self-care, social participation, and other daily activities (Ben-Sasson et al., 2009). The same is true for children with auditory

SOR who are distracted or aggravated by the sounds of appliances, conversations, and crowds. The inability to habituate to these sounds can further undermine academic performance (Ben-Sasson et al., 2009). Beyond these direct experiences, SOR is also associated with anxiety, negative affect, poor sleep quality, and increased stress for both the child and caregivers (Carpenter et al., 2019; Bar-Shalita and Cermak, 2016; Ben-Sasson et al., 2009; Ben-Sasson et al., 2010; Carter et al., 2011; Critz et al., 2015; Gourley et al., 2013).

The symptoms of SOR can therefore negatively impact the individual's quality of life, as well as strain their relationships with family members and peers (Ben-Sasson et al., 2009). Thus, understanding the etiology of this disorder, including the factors that may cause, advance, or mitigate its symptoms, could increase support for the individuals who experience SPD and their families.

Critically, SPD is not yet recognized in the fifth edition of the Diagnostic and Statistical Manual of Mental Disorders (DSM-5; American Psychiatric Association, 2013a) as its own disorder. As the DSM-5 is regarded by health care professionals internationally as the authoritative guide to the diagnosis of mental disorders (American Psychiatric Association, 2013b), this demonstrates that there is not yet a consensus on risk factors and suitable treatments for SPD. Furthermore, it limits the ability of researchers to secure funding to study SPD and limits the ability of patients to receive insurance reimbursement for alternative treatment plans. Part of the reason why SPD is not yet recognized in the DSM-5 as an independent diagnostic entity is because researchers and clinicians have conflicting theories about whether the symptoms of SPD are a manifestation of other psychiatric conditions. For example, SOR may be a

behavioral manifestation of emotion dysregulation, which is common to many psychiatric disorders, or it may be a manifestation of ASD specifically, with SOR in nonautistic individuals being attributed to subthreshold autistic traits in those individuals (Schwarzlose et al., 2023). In fact, SOR was added to the diagnostic criteria for ASD in the DSM-5, but a common confound to this theory is that few SOR studies control for autistic traits or seek to understand the disorder outside of the context of ASD. Another theory suggests the opposite relationship between SOR and psychopathology, where neurological differences in sensory processing lead to the development of heightened anxiety and associated behaviors (Schwarzlose et al., 2023). Further research is needed to settle this debate and distinguish whether SOR is a contributor to, or an effect of, another psychiatric condition.

Studying the structure and function of brain regions using non-invasive approaches could help to identify differences specific to SPD and thereby elucidate the relationship between sensory symptoms and any overlapping neuronal correlates with other psychopathologies. While such studies are limited, several have begun to demonstrate differences unique to individuals with SPD. Fiber tractography conducted via diffusion tensor imaging (DTI) has characterized differences in the structural connectivity of white matter tracts in children with SPD compared to those with ASD and typically developing controls. The first study to explore fiber tracts in children with SPD compared twenty-four neurotypical males with sixteen males who were identified as having SPD via the Sensory Profile caregiver report questionnaire (Dunn and Westman, 1997) and who did not have an ASD diagnosis, all between the ages of 8 and 11 years old (Owen et al., 2013). There were no volumetric differences in gray or white matter

between groups, but the SPD group exhibited substantially decreased white matter microstructural integrity in primary sensory cerebral tracts and pathways involved in multisensory integration. These posterior cerebral tracts included the projection pathways and commissural tracts of the posterior corpus callosum, posterior corona radiata, and posterior thalamic radiations. Reductions to white matter connectivity may indicate impaired action potential propagation and lead to challenges with registering and integrating sensory input. Indeed, there were strong correlations between white matter connectivity and behavioral measures of auditory symptoms, multisensory integration, and inattention, indicating that the observed white matter pathology likely contributes to the behaviors commonly observed in SPD. A follow-up study compared fiber tracts between a similar cohort of neurotypical controls, individuals with SPD, and individuals with ASD (Chang et al., 2014). The SPD and ASD groups demonstrated reduced connectivity in the sensory processing regions of the dorsal visual stream and posterior corona radiata compared to controls, though the SPD group alone demonstrated reduced connectivity in the splenium of the corpus callosum. These studies demonstrate that while there is some overlap in the structural abnormalities that are present in SPD and ASD, there are also some differences that may serve to differentiate the two.

Resting-state functional connectivity magnetic resonance imaging (rs-fcMRI) is another method that may serve to characterize aberrant connectivity specific to SPD. One study compared children between the ages of 9 and 12 years old who were typically developing with those who scored strongly for SOR as determined by an item on the Short-Social Responsiveness Scale (Schwarzlose et al., 2023). When controlling for autistic traits, the children with SOR experienced reduced functional connectivity within

and between the sensorimotor networks, with no differences within or between other solely-sensory networks. This coincides with the aforementioned finding that most children with SOR tend to have difficulties solely with tactile processing (Ben-Sasson et al., 2009). There were other aberrant connections between the sensorimotor and visual networks and non-sensory areas, but no significant differences emerged for the auditory network. Additional connectivity findings indicated differences in stimulus-driven attention, determining stimulus salience, and sensory prediction. Taken together, these structural and functional findings indicate that SOR may be explained by sensory-specific neuronal underpinnings rather than manifest as an extension of emotion dysregulation or autism-associated traits.

Behavioral evidence further suggests that aberrant connections between sensory pathways and the amygdala may contribute to the presence of auditory SOR in adults with ASD. A strong connection to the amygdala, which is a brain region involved in the processing of negative emotions and fear-based memories, may explain the strong, negative emotional reactions and aversions to certain sounds in these individuals. Altered connectivity between the amygdala and auditory processing pathways is plausible considering that alterations in amygdala volume and functioning are already highly implicated in ASD (Andrews et al., 2022; Shen et al., 2022; Schumann et al., 2004; Schulkin et al., 2007). Specifically, behavioral studies propose that auditory SOR in adults with ASD may be due to a persistence of the non-classical auditory pathway (NCAP), which integrates direct connections to the amygdala (Møller et al., 2005; Møller and Rollins, 2002). The NCAP is the default hearing pathway in all children until age eight, at which point the classical pathway predominates. For context, the ascending

classical auditory pathway in adults relays information from the auditory nerve to the primary auditory cortex (AI) through the cochlear nuclei, the lateral lemniscus nuclei (LL), the central nucleus of the inferior colliculus (ICC), and the ventral portion of the medial geniculate body (MGB). The NCAP branches off the classical pathway at various levels and recruits separate neuronal populations. Neurons from the LL project to and receive input from the reticular formation, a region involved in awareness, detection, and attention to sensory stimulation. These returning inputs are forwarded from the LL to regions of the thalamus that are not involved with auditory sensory processing, the dorsal and medial MGB. These regions of the MGB bypass AI and project directly to secondary auditory cortices (AII) and auditory association cortices (AAC). The dorsal MGB and AAC also project to the lateral amygdala, which can only be reached in the classical pathway via a long chain of connections in the cerebral cortex and association cortices. Another unique feature of the NCAP is that it integrates ascending somatosensory information through a projection from the dorsal column nuclei to the exterior nucleus of the inferior colliculus (ICx), which relays information to the medial MGB (Lucker and Doman, 2015; Møller, 2006). This somatosensory connection is key to the proposed theory that the NCAP persists in adults with ASD.

A study by Møller's group demonstrated that neurotypical children will perceive a sound as becoming louder once stimulation to the vagus nerve along the wrist is applied (Møller and Rollins, 2002). Although the sound did not change in volume, the ascending somatosensory information from the wrist likely passed through the NCAP, impacted auditory processing, and altered the perception of the auditory stimulus. Neurotypical adults, however, did not perceive an increase in volume with tactile stimulation,

consistent with evidence that the NCAP is suppressed in these individuals. The authors repeated the experiment in adults with ASD and found that they were more likely to perceive an increase in loudness than control subjects (Møller et al., 2005). Given that somatosensory-auditory integration is established in the NCAP but not the classical pathway, the authors of this work suggest that the NCAP may persist in ASD (Musiek et al., 2011). If true, then this would suggest that direct connections to the amygdala may also persist in individuals with ASD who experience auditory SOR. Critically, there are non-classical ascending sensory pathways for visual and somatosensory input which engage a connection between the dorsal MGB and lateral amygdala, as well (Møller et al., 2005), indicating that aberrant amygdala connectivity may play a similar role in the other major sensory modalities of SOR. On the other hand, the posterior, multisensory area of the human superior temporal sulcus, or the superior temporal polysensory area in macaques, also integrates auditory and tactile stimulation, so it is possible that this or another multisensory area could underlie the observations seen by those authors (Beauchamp et al., 2008; Russo et al., 2010). Further research using neuroimaging methods like rs-fcMRI could follow up on these behavioral studies and investigate whether amygdala or NCAP connectivity is implicated in adults with SOR.

In addition to characterizing the brain changes common to individuals with SPD, it is also important to understand the biological processes that shape these changes and the mechanisms that can initiate them. While more research is needed to fully understand the factors that contribute to the progression of SPD, there is a wide body of research describing factors that can increase the incidence of highly comorbid disorders such as ASD. The prenatal environment in particular has been shown to have a significant

influence on the development of ASD. A well-documented environmental risk factor for ASD phenotype susceptibility in animal studies is prenatal exposure to a Western-style diet (WSD; Gawlińska et al., 2021; Fernandes et al., 2021). Inflammation likely mediates this association, as consumption of a WSD increases inflammation, and inflammation has the ability to impact fetal brain circuit formation (Bolton and Bilbo, 2014). Thus, prenatal exposure to a WSD and associated inflammatory impacts may mediate the changes to structural and functional brain connectivity that are typically observed in individuals with SPD.

1.2 Western-Style Diet Promotes Inflammation

A WSD, distinguished by high sugar and saturated fat content, is highly prevalent in the US (Hohos and Skaznik-Wikiel, 2017), and prenatal WSD exposure is associated with an increased incidence of the component behaviors of ASD, ADHD, and other neurodevelopmental disorders (Gawlińska et al., 2021; Howard et al., 2011; Fernandes et al., 2021). A potential mediator for how prenatal WSD exposure might impact offspring neurodevelopment is through maternal inflammation, which is also an independent prenatal risk factor for these neurodevelopmental disorders (May-Benson et al., 2009; Bolton and Bilbo, 2014; Scola and Duong, 2017; Anderson and Maes, 2014). WSD consumption elevates maternal inflammation in two major ways: directly in response to the circulating nutritional components, and indirectly by increasing maternal adipose tissue.

First, WSD consumption leads to an increased amount of fatty acids and sugars in the lumen of the small intestine. Intestinal epithelial cells (IECs) maintain a barrier

between the dietary components in the lumen and the lamina propria (LP), the layer of connective tissue that contains immune cells, blood vessels, and nerve fibers (Hunyady et al., 2000). One type of immune cell in the LP, the T helper 17 (Th17) cell, protects against diet-induced obesity and metabolic syndrome by regulating lipid intake (Kawano et al., 2022; Garidou et al., 2015; Hong et al., 2017). Th17 cells reduce lipid absorption by producing pro-inflammatory cytokine interleukin (IL)-17 which decreases IEC expression of the fatty acid transporter, CD36 (Kawano et al., 2022). Thus, Th17 cells ensure the overabundance of fatty acids from the WSD do not fully cross the IEC barrier and lead to metabolic disorders. However, the high presence of sugar from the WSD interferes with this protection by altering the intestinal microbiome. Sugars like sucrose expand the colonies of microbes like *Faecalibaculum rodentium* which in turn displace other members of the microbiota including segmented filamentous bacteria (SFB). SFB induces Th17 cell presence in the LP, so sugars indirectly reduce Th17 cell prevalence and lead to increased fatty acid absorption (Kawano et al., 2022).

Additionally, dietary fats instigate an inflammatory response in the intestine through multiple pathways. Free fatty acids can directly increase the production of pro-inflammatory cytokines such as IL-1β, IL-6, and tumor necrosis factor (TNF)-α in the intestine (Rohr et al., 2020; Kawano et al., 2016; Snodgrass et al., 2013; Duan et al., 2018; Yoshida et al., 2001; Fujiyama et al., 2007). These cytokines further stimulate inflammation by enhancing intestinal permeability to endotoxins such as lipopolysaccharides (LPS). Dietary fat also increases intestinal permeability by reducing the expression of tight junction proteins in the IEC layer (Suzuki and Hara, 2010), decreasing levels of barrier-forming cytokines (Rohr et al., 2020), and altering the

microbiome in ways that promote barrier disruption (Rohr et al., 2020; Kim et al., 2012). Once these fatty acids, pro-inflammatory cytokines, and LPS toxins pass through the IEC barrier and enter circulation, a systemic, low-grade inflammatory state ensues (Duan et al., 2018; Konrad and Wueest, 2014).

The second major way a WSD leads to inflammation is through increased adipose tissue. Circulating lipids accumulate in the adipose tissue and lead to tissue enlargement (hyperplasia) and increased adipocyte size (hypertrophy; Teng et al., 2014; Maury and Brichard, 2010; Jo et al., 2009; Ellulu et al., 2017; El Akoum et al., 2011; Funaki, 2009). This can promote hypoxia in adipose tissue and induce adipocyte cell death, macrophage infiltration, and increased expression of pro-inflammatory mediators including TNF-α, IL-6, and adipokines (Teng et al., 2014; Anghel and Wahli, 2007; Ellulu et al., 2017; Cinti et al., 2005; Karastergiou and Mohamed-Ali, 2010). Excess lipid accumulation additionally leads to ectopic lipid deposition in other tissues including the liver, pancreas, muscle, and blood vessels, which activates tissue leukocytes and further stimulates an inflammatory response (Duan et al., 2018; Lumeng and Saltiel, 2011). Thus, chronic consumption of a WSD can lead to a robust inflammatory state across many tissues and via a multitude of pathways.

1.3 Developmental Programming

During pregnancy, many of the fatty acids, sugars, and inflammatory mediators generated by the consumption of a WSD can impact the developing fetus by crossing through, or initiating a signaling cascade at, the placental barrier (Kabaran and Besler, 2015; Quraishi and Illsley, 1999; Joshi et al., 2022; Michelsen et al., 2019; Bolton and

Bilbo, 2014; Bordeleau et al., 2021; Denizli et al., 2022; Schepanski et al., 2018), which additionally experiences increased inflammation and reduced blood flow (Frias et al., 2011; Salati et al., 2019). Critically, this can lead to long-lasting outcomes through a phenomenon known as developmental programming. Developmental programming is the observation that the prenatal and early postnatal periods of rapid development are highly susceptible to epigenetic changes caused by environmental influences (Reynolds et al., 2010; Kwon and Kim, 2017; Entringer et al., 2015; Sutton et al., 2016; Heim et al., 2019). A prime example of this phenomenon occurred during the Dutch famine of 1944-1945, where children who were exposed to prenatal malnutrition exhibited differential DNA methylation at various regions across the genome in whole blood samples when compared to unexposed siblings. These epigenetic modifications included increased methylation of *INSR*, a gene involved in growth and insulin signaling, which was associated with greater birth weights. Exposed individuals additionally experienced a higher BMI, an altered glucose response, and elevated LDL and cholesterol levels in adulthood (Tobi et al., 2014). Epigenetic changes, gene-environment interactions, and other physiological impacts during massive developmental events like cellular differentiation, neurogenesis, neural migration, myelination, microglial proliferation, and synaptic pruning can result in substantial or lifelong changes to health, behavior, and disease risk (Sidman and Rakic, 1973; Toga et al., 2006; Knuesel et al., 2014; Nayak et al., 2014; Bale et al., 2010; Kwon and Kim, 2017; DeCapo et al., 2019; Entringer et al., 2015; Sutton et al., 2016).

In particular, prenatal exposure to maternal inflammation programs for long-term increases in offspring inflammation (Bilbo and Schwarz, 2009; Romero et al., 2007;

Denizli et al., 2022); alters structural and functional connectivity (Rasmussen et al., 2019; Graham et al., 2018; Rudolph et al., 2018; Spann et al., 2018); impacts working memory, cognition, and negative affect (Rudolph et al., 2018; Rasmussen et al., 2018; Gustafsson et al., 2018; Graham et al., 2018); and is associated with an increased incidence of neurodevelopmental disorders including ASD (Careaga et al., 2017; Parker-Athill and Tan, 2010; Guma et al., 2019), ADHD (Dunn et al., 2019), and schizophrenia (Guma et al., 2019; Scola and Duong, 2017).

The dietary components of a WSD may program offspring development in additive or alternative ways to the associated maternal inflammatory state. Like the vertical transfer of maternal immune cells and cytokines (Schepanski et al., 2018), fatty acids and glucose cross the placental barrier through diffusion and transport proteins to enter fetal circulation (DeCapo et al., 2019). Upon passing through the blood-brain barrier via similar active and passive transport pathways, these micronutrients impact neurodevelopment through impaired neurotransmission, reduced myelination, dendritic atrophy, and by further altering inflammatory cytokine levels in the brain (DeCapo et al., 2019).

Thus, the influx of maternal immune factors and dietary components to the developing fetus plays a major role in shaping the neurophysiological and behavioral outcomes of offspring. This indicates that factors from the maternal environment have significant effects on the brain. While it is a common misconception that the fetal blood-brain barrier (BBB) is underdeveloped and highly permeable *in utero*, recent reviews highlight evidence that suggests it is a robust barrier as early as twelve weeks into gestation (Saunders et al., 2014; Goasdoué et al., 2017). As such, it is not that the fetal

brain is more vulnerable to the infiltration of peripheral factors so much as its neurodevelopmental processes are especially susceptible to being impacted by the factors that reach the brain through usual routes. Of the myriad ways that inflammation may impact neurodevelopment, a major mediator may involve the actions of microglia, the resident immune cell of the brain.

1.4 Microglia Impact Neuronal Circuitry

Microglia are critical to the health of central nervous system (CNS) tissue. Constantly surveying the environment with their motile processes, microglia are the first responders to infections and injuries (Pons and Rivest, 2020; Shemer et al., 2015; Li and Barres, 2018). Microglia launch an immune response by secreting cytokines, recruiting additional cell types, migrating to sites of damage, and phagocytosing debris and dying cells (Smith et al., 2012; Rock et al., 2004; Miller et al., 2019; Tremblay et al., 2011). They also contribute to regenerative processes after injury, such as by releasing growth factors to promote neurogenesis and remyelination (Pons and Rivest, 2020). During homeostatic conditions, microglia continue to monitor the environment; phagocytose debris, dying cells, and myelin; control adult neurogenesis; modulate neuronal activity; and promote the survival of oligodendrocyte progenitor cells, among other tasks (Li and Barres, 2018). Despite only accounting for 5% to 15% of all adult brain cells, microglia clearly have a far-reaching impact (Pons and Rivest, 2020; Thion et al., 2018; Aguzzi et al., 2013). Crucially, this impact begins during early prenatal development, when microglia expand their roles to include the direct and substantial shaping of neuronal circuitry.

Microglia develop early, with microglial colonization of the human cerebrum beginning around the fourth gestational week—preceding BBB development, neurogenesis, neuronal migration, and myelination in many areas—and becoming more established by the twenty-fourth week (Menassa and Gomez-Nicola, 2018). This foundation allows microglia to participate in shaping neurodevelopment from the early stages.

Some of the neurodevelopmentally relevant processes that microglia engage in during the prenatal period include inducing neuronal cell death (Frade and Barde, 1998), limiting axonal outgrowth (Squarzoni et al., 2014), enhancing circuitry assembly by regulating the laminar positioning of cortical interneurons (Squarzoni et al., 2014), promoting axonal fasciculation to bind white matter tracts like the dorsal corpus callosum (Pont-Lezica et al., 2014), and fusing endothelial cells to increase vasculature network complexity (Li and Barres, 2018). During the perinatal and postnatal stages, microglia continue to remodel neural networks in pronounced ways: they regulate neurogenesis by phagocytosing neural precursor cells (Cunningham et al., 2013), and they conduct synaptic pruning.

Synaptic pruning is a process by which select synapses are eliminated. During the course of development and learning, “weaker” synapses are typically removed to refine circuit formation (Peet et al., 2020; Goda and Davis, 2003). Recent studies suggest that these “weaker” synaptic terminals display an “eat-me” signal that prompts microglia to phagocytose the synaptic spines and boutons. This “eat-me” signal, phosphatidylserine (PS), is a phospholipid that usually faces the cytoplasm. Once it is exposed on the surface, it is recognized by microglia expressing triggering receptor expressed on

myeloid cells 2 (TREM2) or G protein-coupled receptor 56 (GPR56, S4 splicing isoform) receptors (Peet et al., 2020; Scott-Hewitt et al., 2020; Li et al., 2020) and destines the synaptic element for microglial engulfment. Disrupted synaptic pruning may lead to neurodevelopmental disorders, including ASD, schizophrenia, and epilepsy (Neniskyte and Gross, 2017), demonstrating that microglia play a strong role in determining behavioral outcomes.

As a primary immune cell in the brain, microglia are necessarily sensitive to changes in the inflammatory state. Prenatal exposure to a WSD and the accompanying state of elevated inflammation stimulates an inflammatory response from the microglia in the fetal brain (Grayson et al., 2010). Immune activation may interfere with the ability of microglia to properly regulate the aforementioned neurodevelopmental processes, thereby leading to aberrant brain circuitry. Similarly, if inflammation persists into the early postnatal period, as is likely to occur due to the continued delivery of dietary components and maternal immune factors during lactation (Grant et al., 2011; DeCapo et al., 2019; Garofalo, 2010; Cabinian et al., 2016), then the microglial-dependent processes of neural precursor cell phagocytosis and synaptic pruning may also be impacted. Indeed, increased microglial activation and prevalence have been shown to increase neural precursor cell phagocytosis (Cunningham et al., 2013), and maternal immune activation in mice alters synaptic pruning and leads to social behavioral defects (Kim et al., 2017). Thus, microglia may serve as a potential mediator for the demonstrated relationship between prenatal exposure to WSD or inflammation and the aberrant brain connectivity implicated in neurodevelopmental disorders.

1.5 Resting-state Functional Connectivity MRI

Resting-state functional connectivity magnetic resonance imaging (rs-fcMRI) is a method that non-invasively measures the strength of connections across the brain. Two spatially distinct brain regions may be structurally connected by a series of adjoining neurons, but it can be difficult to determine whether this physical connection is functionally relevant based solely on the structural properties of the connection, such as fiber density or number of synapses. As long as a structural connection exists between brain regions of interest, it is possible to measure the degree to which that pathway is utilized to coordinate brain activity between the areas using rs-fcMRI.

This neuroimaging technique relies on the fact that the brain is always active, even when an individual is at rest. Brain regions emit spontaneous, low-frequency brain signals (Fox and Raichle, 2007; Raichle and Mintun, 2006; Logothetis and Wandell, 2004). If neurons in a particular region depolarize and fire an action potential, the electrical signal will travel down the axons and reach the post-synaptic targets on other neurons. This signal could continue through multiple synapses and evoke a synchronous response in a distal brain region. Rs-fcMRI compares the brain signals of two regions; if the brain signals are highly correlated, then the same spontaneous signal was found in both regions. This would indicate that a strong, structural connection capable of carrying the signal likely exists between them, and it would demonstrate that the two areas have a strong functional connection, meaning that the pathway is utilized often to purposefully coordinate neural activity (Fox and Raichle, 2007; Zhang et al., 2019a; Fox et al., 2005; Graham et al., 2015; Gao et al., 2017; Gao et al., 2015). The stronger the correlation strength, measured as a correlation coefficient, the more functionally connected two areas

are. A group of regions with correlated activity are often evaluated together as a resting-state brain network (Grayson and Fair, 2017).

In order to derive a correlation coefficient between areas, structural and functional brain scans must first be acquired. The process of acquiring the images is as follows. In simplified terms, MRI measures water content. The brain is roughly 75% water on average (Zhang et al., 2018; Mitchell et al., 1945), but water content varies across different tissue structures within the brain. Measuring water content elicits contrast between these different tissue structures, and those contrasting measurements can be converted into an image. The measurements are based on the magnetic properties of water. Water molecules contain hydrogen atoms. Each hydrogen atom has a proton that spins on its axis, generating a small magnetic field. Outside of the scanner, these protons are randomly positioned, but inside the scanner, the protons align with the direction of the scanner's magnetic field. A radio frequency excitation pulse deflects the protons out of alignment; when the pulse is over, the protons emit the radio frequency energy as they return to equilibrium. The emitted radio frequency signals undergo a Fourier transform and are converted to grayscale images. Changing the radiofrequency pulse sequences, such as by varying the time between successive pulses and the time between delivery of the pulse and receipt of the echo signal, can create different types of structural scans, such as T1-weighted and T2-weighted scans.

Functional images are collected in the same way as structural scans, but the contrast due to the hydrogen in the water molecules is impacted by the blood oxygen level dependent (BOLD) signal. Deoxygenated blood introduces inhomogeneities in the magnetic field, so the ratio between oxygenated and deoxygenated blood affects the

signal (Ogawa et al., 1990; Chavhan et al., 2009; Attwell and Iadecola, 2002). Neural activity increases blood flow, thereby recruiting more oxygenated blood to the active brain area, which results in a change in the ratio and a weaker signal (Malonek et al., 1997; Huettel et al., 2008). Thus, functional MRI scans measure changes in blood flow that are indicative of increased neural activity.

Once all of the structural and functional scans have been collected, the images are processed through a pipeline that corrects distortions, aligns brain structures to a standard, labelled atlas, and assigns the correct brain region label back to the functional signal. This image processing procedure is adapted from the Human Connectome Project (HCP) pipeline (Glasser et al., 2013). The output of this pipeline is a file that contains the functional time series data, or BOLD signal, for each labelled brain region. After quality checking and motion scrubbing steps are taken, a correlation matrix, where the correlation in signal between every combination of two brain regions, can be computed from this file and used for analyses.

Recent advances have made it possible to image non-human primates (NHPs) with rs-fcMRI in a similar manner as in humans (Ramirez, 2019; Miranda-Dominguez et al., 2014; Grayson et al., 2016; Robinson et al., 2014; Milham et al., 2018; Ramirez et al., 2020; Xu et al., 2018; Xu et al., 2020; Xu et al., 2019). Adaptations to the HCP preprocessing pipeline in particular have allowed NHP images to be processed using consistent methodology while overcoming species-related issues. For example, differentiating between head and brain tissue was a challenge, as larger orbital, neck, cheek, and forehead tissue in NHPs was previously mistaken for brain tissue due to similar image intensities (Ramirez, 2019). Advancements to image collection strategies

have additionally improved the quality of the data that are collected. One improvement used in this dissertation is in regards to the 15-channel knee coil that was adapted for use in macaques to accommodate their smaller head size. Use of this coil resulted in a reduced signal-to-noise ratio (SNR), so four structural images were acquired and averaged to improve the SNR. A challenge that continues to face the field is the use of anesthesia in NHP imaging procedures. While anesthesia is necessary to reduce the occurrence of motion artifacts in the scans (Fair et al., 2013; Power et al., 2012), it has a dampening effect on the functional BOLD signal strength. However, despite this potential limitation in signal strength, studies have validated that NHPs reproduce the same major functional networks that emerge in humans, such as all areas of the default mode network and primary motor network, thereby establishing reliable functional similarity between species (Miranda-Dominguez et al., 2014; Vincent et al., 2007; Van Essen and Glasser, 2018).

Being able to apply rs-fcMRI techniques to NHPs allows findings to be translated between species. This is achieved through the use of a cross-species brain map, specifically the Bezgin Regional Map parcellation, which can map the same labelled brain regions to human and macaque images based on aligned functional network topologies and cross-species landmarks (Bezgin et al., 2012; Robinson et al. 2014; Xu et al., 2020). Functional connectivity results in one species can now be directly compared to spatially-matched results in the other species.

Additionally, having a shared methodology between the two species can help relate non-MR findings. For example, while there is a growing body of research on the functional connectivity profiles of children with neurodevelopmental disorders like SPD,

some experimental manipulations that are related to SPD or that would be useful for understanding its etiology are unethical to perform in humans. These include directing pregnant individuals to consume an experimentally controlled WSD, due to its known associations with adverse offspring outcomes, and performing invasive procedures on offspring brain tissue to examine neuroinflammation. Dietary manipulations and brain sectioning are accepted procedures to perform in animal models presently, though it is not possible to ascribe an official behavioral diagnosis to animals as can be done in humans. Consequently, combining results from invasive procedures in animals with verified human diagnoses through shared functional connectivity profiles can bridge this cross-species gap and relate WSD- and neuroinflammation-specific findings to disorders like SPD.

1.6 Goals of the Dissertation

The goal of this dissertation is to advance the field of SPD research by characterizing the impacts of a potential risk factor for this disorder, prenatal WSD exposure. This work will leverage the advantages of a NHP model to explore these impacts in the context of human findings across two research aims. The model system and studies are summarized in Figure 1.1.

Study 1 explores the functional connectivity of areas that are contextually relevant to SPD. These areas include regions of interest in sensory and emotional processing networks; this selection derives from prior work in humans which demonstrate impacts to the functional connectivity of sensory areas in individuals with SOR (Schwarzlose et al., 2023) and suggest that non-classical sensory processing

pathways, which include direct connections to the amygdala, may be active in individuals with ASD (Møller et al., 2005; Møller and Rollins, 2002; Musiek et al., 2011). Functional connectivity will be examined in NHP offspring that were exposed to a WSD during the full duration of the prenatal period through weaning, hereafter referred to as the perinatal period, at five distinct developmental time points ranging from infancy through early adolescence. Functional connectivity research for SPD is often conducted in older children; examining functional connectivity across development will reveal the trajectory of changing connectivity and bridge the gap between birth and the more commonly studied time points. This study will use a machine learning model to determine whether differences in connectivity exist at each time point. For the ages at which a difference is found, these differences will be characterized in more depth to elucidate which connections are responsible for the greatest differences between diet groups. Furthermore, the impacts of two alternative contributors to altered neural circuitry, maternal adiposity and postnatal neuroinflammation, will be tested at the latest developmental time point to explore multiple predictors of long-term functional connectivity. To complement the NHP findings, the analysis will be repeated in a cohort of human children with SOR using the identical set of sensory and emotional connections labelled by the cross-species Bezgin parcellation. Comparing connectivity findings across species will determine whether perinatal WSD exposure is implicated in the development of the sensory connectivity profile characteristic of SPD.

Study 2 investigates a potential underlying mechanism of altered neural circuitry: postnatal neuroinflammation. Prior work in the NHP model used in this dissertation demonstrated an association between prenatal WSD exposure and elevated markers of

neuroinflammation *in utero*. These included increased levels of pro-inflammatory cytokines and increased microglial staining in the fetal hypothalamus (Grayson et al., 2010). Prenatal inflammation and microglial activation are associated with disruptions in neuronal proliferation, migration, and other aspects of circuit formation that may contribute to the progression of neurodevelopmental disorders (Vasistha et al., 2020; Dong et al., 2020; Denizli et al., 2022). However, postnatal neuroinflammation may continue to impact circuit formation by disrupting the microglia-mediated processes of synaptic pruning and the phagocytosis of neural precursor cells. Given that prenatal exposure to inflammation is associated with altered postnatal immune states in offspring (Denizli et al., 2022), and given that an estimated 69% - 100% of children with ASD experience heightened levels of neuroinflammation (Kern et al., 2016), it is likely that the WSD-induced microglial response demonstrated in the fetal study will persist postnatally and continue to disrupt neurodevelopmental processes. To explore this possibility, Study 2 probed for signs of postnatal neuroinflammation in one-year-old offspring who were exposed to a perinatal WSD. Neuroinflammation was assessed by counting the number of microglia and infiltrating macrophages present in the arcuate nucleus (ARC) of the hypothalamus, which is the same region that demonstrated increased microglial staining in the fetal study. ImageJ software (Fiji; Schindelin et al., 2012) was used to develop an automated procedure that would process the immunofluorescent images and measure the number of microglia and macrophage cells per image. A novel method of optimizing the parameters of the automated procedure was developed to ensure accurate cell counts when compared to a trained observer. A mixed effects model compared cell counts between diet groups and assessed the distribution of microglia and macrophages across

the rostral-caudal axis of the ARC; this is the first study to characterize the distribution in Japanese macaques and in juvenile NHPs more broadly. A further aim of this study tested whether maternal cytokine concentrations taken during the third trimester could predict offspring cell count. Results from these analyses elucidate the trajectory of neuroinflammation in response to perinatal WSD exposure and highlight the period when neural circuitry may be most affected by WSD-associated neuroinflammation.

These two studies characterize distinct facets of perinatal WSD exposure, but taken together, they can inform how brain connectivity relevant to SPD is impacted across development. By placing evidence from a highly controlled NHP model into the context of human findings, this dissertation advances insights into the etiology of SPD and reaffirms the powerful influence the prenatal environment can have on neurodevelopmental outcomes.

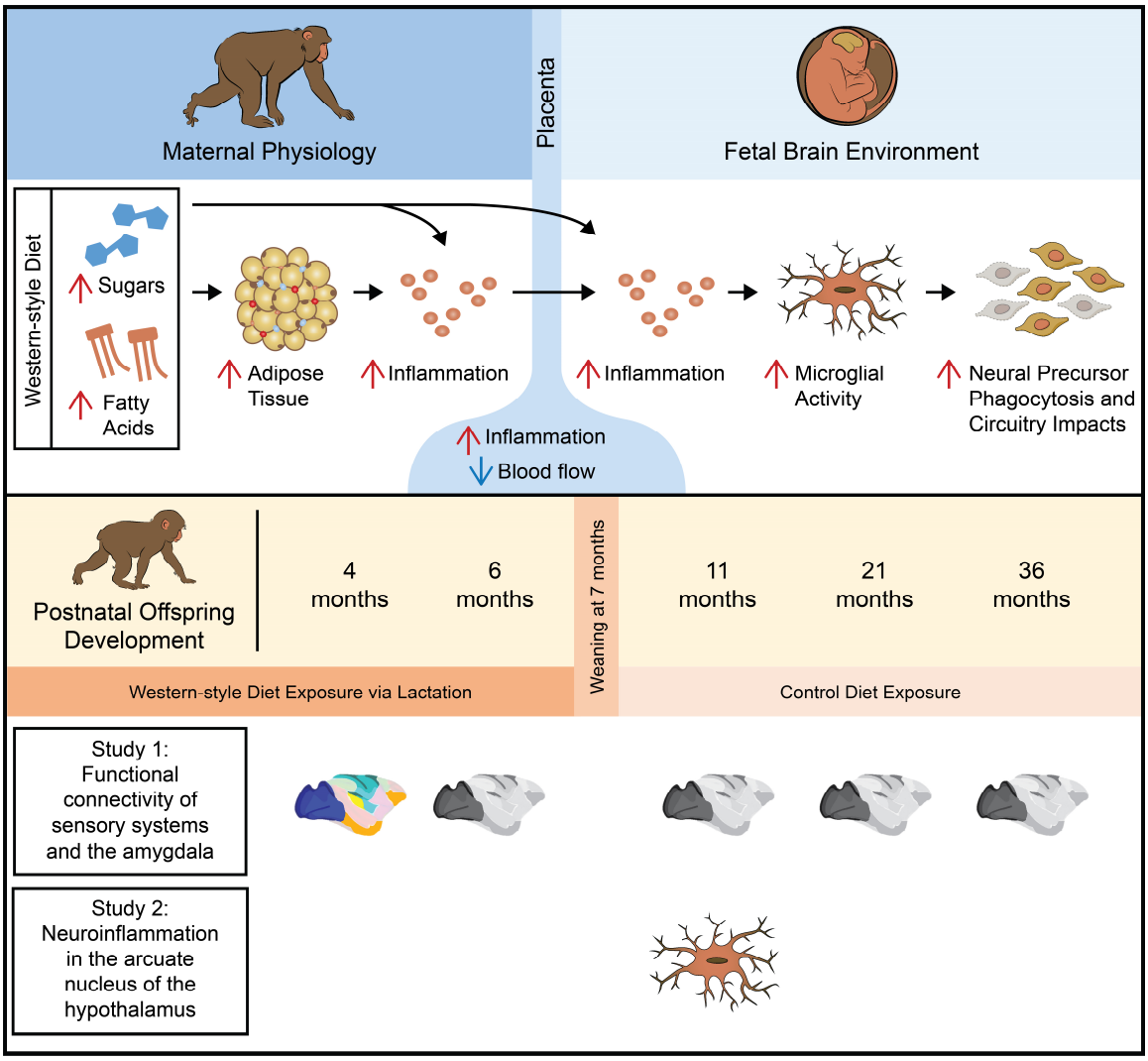

Figure 1.1. Summary of model system and dissertation studies.

This dissertation uses a non-human primate model of WSD-induced obesity to explore longitudinal impacts to functional connectivity and neuroinflammation in offspring. Consumption of a WSD elevates circulating levels of sugars and fatty acids, leading to increased adiposity and inflammation in the dams. The dietary components and inflammatory factors cross or act upon the placenta, which experiences increased inflammation and reduced blood flow, and enter or act upon the central nervous system of the developing fetus. Increased fetal neuroinflammation activates microglial cells and disrupts neural circuit formation through altered microglia-mediated processes such as

increased neural precursor cell phagocytosis. As WSD consumption additionally impacts breast milk composition, WSD exposure continues postnatally in offspring until weaning occurs at 7 months of age. This dissertation examines postnatal development at 4, 6, 11, 21, and 36 months of age across two studies. Study 1 explores the functional connectivity of sensory systems and the amygdala to characterize the longitudinal impacts of perinatal WSD exposure on connections relevant to SPD. Study 2 examines microglia prevalence in the arcuate nucleus of the hypothalamus at the one year time point to assess whether neuroinflammation persists and serves as a potential mediator of altered connectivity findings. Full-color brain and microglia icons for Studies 1 and 2 indicate an analysis that yielded a statistically significant finding; grayscale brains for Study 1 indicate non-significant results at those time points (6, 11, 21, and 36 months). Red up arrows indicate an increased effect; the blue down arrow indicates a reduced effect.

CHAPTER 2. PERINATAL WESTERN-STYLE DIET EXPOSURE ASSOCIATED WITH ALTERED SENSORY FUNCTIONAL CONNECTIVITY IN INFANT JAPANESE MACAQUES

2.1. Abstract

Sensory processing disorder (SPD) is a neurological condition characterized by impaired sensory processing, but its causes and neural correlates remain poorly understood. The maternal environment is strongly implicated in the progression of neurodevelopmental disorders, and one environmental factor that is hypothesized to promote the development of SPD is prenatal Western-style diet (WSD) exposure. This study examined the effects of perinatal WSD exposure on functional connectivity in macaques to characterize impacts to the proposed neural correlates of SPD. Impacts were examined across development to explore longitudinal changes in the connectivity of sensory and emotional processing areas. The functional connectivity of children with sensory over-responsivity (SOR), a subtype of SPD, was additionally examined to allow for findings to be compared across species; this approach investigated whether perinatal WSD exposure could be associated with the functional connectivity patterns of SOR. A machine learning model was used to predict perinatal diet group or SOR based on differences in functional connectivity. Differences in the connectivity of sensory networks and the amygdala were only found in macaques at the earliest time point tested, 4 months of age. Intra-somatomotor, visual-auditory, somatomotor-auditory, somatomotor-visual, and intra-visual network connections demonstrated the greatest differences between perinatal diet groups at 4 months of age, with impacts to the

connectivity of the primary motor cortex being the most pronounced. While the same set of sensory and amygdala connections were unable to predict SOR in children, this result is consistent with the poor model performance in macaques at the same developmental time point. These findings provide insight into the longitudinal impacts to functional connectivity in the context of SPD, and they suggest that impacts from perinatal WSD exposure are transiently present during early infancy.

2.2. Introduction

Sensory processing disorders (SPD) impact roughly 14% of children in the US (Ahn et al., 2004), yet the etiology of this condition remains poorly understood. Although many children with SPD do not have a comorbid psychiatric diagnosis, approximately 95% of children with autism spectrum disorder (ASD) report a SPD (Tomchek and Dunn, 2007; Crane et al., 2009; Leekam et al., 2007), indicating that there may be some overlap between the conditions that lead to ASD and those that lead to SPD. Many genetic and environmental factors have been linked to the development of ASD, though a particularly strong predictor involves the state of the maternal environment during gestation. Three highly correlated maternal factors have been shown to increase the incidence of ASD behaviors in offspring: the consumption of a Western-style diet (WSD), obesity, and an elevated inflammatory state (Gawlińska et al., 2021; Fernandes et al., 2021; Howard et al., 2011; DeCapo et al., 2019; Careaga et al., 2017; Parker-Athill and Tan, 2010; Guma et al., 2019). Animal studies commonly use a WSD to induce obesity and the associated inflammatory state in dams in order to study impacts to offspring neurodevelopment that are characteristic of the behaviors and phenotypes of many neurodevelopmental

disorders, including ASD (Sullivan et al., 2010; Peleg-Raibstein et al., 2012). However, more research is needed to determine whether prenatal WSD exposure is associated with SPD symptoms, as well.

SPD is a broad umbrella for conditions that affect sensory processing, including sensory modulation disorder (SMD), sensory discrimination disorder (SDD), and sensory-based motor disorder (SBMD; Mulligan et al., 2021; Miller et al., 2007). An important first step to understanding how these behaviors arise is to identify which areas of the brain may have altered functioning. A handful of studies to date have explored neural connectivity at the structural and functional level. A diffusion tensor imaging (DTI) study demonstrated substantially decreased white matter microstructural integrity in primary sensory cerebral tracts and pathways involved in multisensory integration (Owen et al., 2013). Another study identified several networks that had altered functional connectivity in children with sensory over-responsivity (SOR), a subtype of SPD, between the ages of 9 and 12 years old (Schwarzlose et al., 2023). These areas included sensorimotor and visual networks, as well as connections to non-sensory areas including the hippocampus and amygdala, among others. A behavioral study by Møller's group (2005) further suggested that aberrant connections from sensory processing pathways to the amygdala may be implicated in individuals with ASD, potentially explaining the negative emotions that are part of SOR (Møller et al., 2005). These findings illustrate that sensory and amygdala connectivity may be altered in children with SPD, but it is still unclear what prenatal factors may increase the likelihood of these outcomes. Additionally, these limited studies have only revealed differences at a few ages around the preadolescent period. A comprehensive exploration of connectivity changes across

development could help identify markers for early detection of SPD and contribute to the understanding of how brain networks are remodeled over time.

The present study bridges these gaps by comparing longitudinal functional connectivity findings from non-human primates (NHPs) exposed to a perinatal WSD to humans with SOR. A set of connections between the sensory networks and the amygdala were selected to probe for differences specifically in the areas that are hypothesized to be involved in SPD and SOR. Differences in connectivity trained a machine learning model to classify NHP subjects by perinatal diet group at the distinct ages of 4, 6, 11, 21, and 36 months of age. The model successfully classified subjects at 4 months of age, so the connections that contributed the most to accurate model prediction were evaluated to identify the brain connections that were most impacted by perinatal WSD exposure. Additionally, differences in connectivity at the latest time point in NHPs, 36 months of age, were used to predict two other measures. First, connectivity was used to predict maternal adiposity in an effort to determine whether increased adiposity would have a separate impact from perinatal WSD exposure. Second, connectivity was used to predict a measure of neuroinflammation in offspring: the number of microglia and macrophages within the amygdala at the same time point. Microglia actively shape neural circuitry through processes like synaptic pruning. This analysis therefore probed for an association between altered connectivity and a potential mediator of altered connectivity within individuals. Neither of these measures were successfully predicted from connectivity, indicating no long-term impacts associated with maternal adiposity or postnatal neuroinflammation. Finally, a translational brain map was applied to the human functional connectivity data to allow for direct comparisons between species. The

machine learning model used the same set of sensory and amygdala connections to predict a measure of SOR in 9- and 10-year-old children. Like the findings from the NHPs at the same developmental age (36 months), this model was unable to successfully classify the children. These findings provide a longitudinal characterization of the connectivity of sensory and emotional processing areas across species and indicate that impacts are transiently present during early infancy.

2.3. Materials and Methods

2.3.1. Animal Model

A well-established NHP model of WSD-induced obesity was chosen for this study (Sullivan et al., 2010; Sullivan et al., 2012). In this model, dams were fed either a WSD or a control diet (CTR). A larger proportion of dams on the WSD developed obesity, defined as greater than 19.6% body fat pre-pregnancy, though some dams on the CTR diet spontaneously developed obesity as well (McCurdy et al., 2009); as these macaques demonstrate the full range of human metabolism, this natural variation in weight gain is consistent with what is observed in humans (Thompson et al., 2018).

Importantly, the offspring of dams that consumed a WSD have demonstrated the component behaviors of multiple neurodevelopmental disorders, including ASD. These behaviors include increased anxiety and aggression (Sullivan et al., 2010; Thompson et al., 2017), decreased social engagement, and increased idiosyncratic behaviors consisting of abnormal movement, abnormal posture, increased head tossing, and repetitive stereotypy (Mitchell et al., 2022b).

Additional maternal and offspring phenotypes from this model, including inflammatory profiles and neuronal impacts, have been characterized in earlier reports (Dunn et al., 2022; Mitchell et al., 2022b; Sullivan et al., 2010; Grayson et al., 2010; Ramirez et al., 2020; Ramirez et al., 2021; Thompson et al., 2018; McCurdy et al., 2009; Sullivan et al., 2017; Comstock et al., 2012).

The MRI scans were collected and made available by the Sullivan lab. Image processing was performed in conjunction with other members of the Developmental Cognition and Neuroimaging (DCAN) Labs. All animal procedures were in accordance with National Institutes of Health guidelines on the ethical use of animals and were approved by the Oregon National Primate Research Center (ONPRC) Institutional Animal Care and Use Committee.

2.3.1.1 Adult Female Macaques

Adult Japanese macaques (*Macaca fuscata*) were housed in indoor/outdoor pens containing 4–12 individuals each (male/female group ratio of 1-2/3-10). Animals were given *ad libitum* access to food and water. Breeding groups were assigned to either the experimental control (CTR) diet or Western-style diet (WSD) and were provided with fruits and vegetables for daily nutritional enrichment. Experimental diet compositions are described below. Females consumed their assigned experimental diet for at least fourteen months prior to offspring birth. Females were sedated two to three times during pregnancy for fetal dating and third trimester measures. Pregnant females gave birth naturally in their social groups. Maternal age at offspring birth (mean $\pm$ SEM) was 10.81 $\pm$ 0.55 years for the CTR group and 8.52 $\pm$ 0.41 years for the WSD group in the present

study. Maternal pre-pregnancy weight (mean ± SEM) was 9.92 ± 0.32 kg for the CTR group and 9.96 ± 0.37 kg for the WSD group in the present study, with one missing value for one of the WSD offspring.

2.3.1.2 Macaque Juvenile Offspring

The juvenile subjects in the present study were born over the course of seven consecutive years, with no offspring born during the third year included for analysis. While offspring began consuming the maternal diet at 4 months of age, it became their primary food source by 6 months. This continued exposure to the same diet from gestation through lactation is therefore considered to be a perinatal rather than a purely prenatal dietary exposure. At a mean age of 7.22 ± 0.32 months for the CTR group and 7.50 ± 0.20 months for the WSD group (mean ± SEM; 7 and 3 missing values for the CTR and WSD groups, respectively), the offspring were weaned and relocated to group-housing with 6-10 similarly aged juveniles and 1-2 unrelated adult females. While the majority of juvenile subjects consumed the CTR diet after weaning, 14 subjects consumed a post-weaning WSD. This study included maternal siblings, (43 of the 69 included subjects had at least one sibling in the study, with all 43 born from a total of 17 dams), though paternal identification was unknown.

A total of 81 juveniles were recruited and scanned for this study. Twelve subjects were excluded from analysis due to a variety of reasons, including medical issues, poor quality scans at every available age point, and a change in maternal diet partway through gestation. Of the 69 juveniles who remained in the study, 48 of them contributed acceptable-quality scans at more than one time point. Of these, 37 had quality scans at

three or more time points. This study sought to include a roughly equal number of subjects from each experimental perinatal diet group and balance for offspring sex (N = 69; Perinatal CTR n = 33; Female n = 34). However, to increase the sample size, this study included offspring who consumed a post-weaning WSD (n = 14, Female n = 8) and combined scans that were collected under two separate acquisition parameter settings (Table 2.1). These two factors were not accounted for as covariates in the classification analyses of this study. While this presents a limitation, prior work in this model has established that post-weaning diet group does not have a significant effect on amygdala volume growth across the time points included in this study (Ramirez et al., 2020), and the scan acquisition protocol does not have a significant effect on mean cortical thickness across these same time points (Ramirez et al., 2021).

2.3.1.3 Macaque Dietary Information

Regarding energy sources, the CTR diet (Monkey Diet no. 5000, Purina Mills) provided approximately 14.7% of calories from fat, 58.5% from carbohydrates, and 26.8% from protein. The WSD (TAD Primate Diet no. 5L0P, Test Diet, Purina Mills) provided approximately 36.6% of calories from fat, 45.0% from carbohydrates, and 18.4% from protein. Representative of a typical Western-style diet, the chemical composition of the experimental WSD contained a larger proportion of fats and sugars compared to the CTR diet. Saturated fat comprised approximately 0.9% of the CTR diet formulation and 5.4% of the WSD. Monounsaturated and polyunsaturated fats comprised 4.4% of the CTR diet and 9.0% of the WSD. Sugars (primarily fructose and sucrose) comprised approximately 3.1% of the CTR diet and 18.9% of the WSD. The animals that

were fed the WSD were also provided with calorically dense treats (35.7% of calories from fat, 56.2% from carbohydrates, and 8.1% from protein) once per day. Macronutrient composition was obtained from diet specification sheets and is previously described (Thompson et al., 2017).

2.3.2. Macaque Subject Demographics

MRI scans were acquired in offspring at roughly 4, 6, 11, 21, and 36 months of age. The demographic composition of each age group is summarized in Table 2.1. A total of 39 offspring, aged 4.39 $\pm$ 0.03 months (mean $\pm$ SEM), contributed scans for the 4-month age group (Female n = 19; Perinatal CTR n = 22; Post-weaning WSD n = 2; Scan Protocol #1 n = 21). A total of 25 offspring, aged 6.59 $\pm$ 0.04 months, contributed scans for the 6-month age group (Female n = 12; Perinatal CTR n = 16; Post-weaning WSD n = 2; Scan Protocol #1 n = 9). A total of 37 offspring, aged 11.06 $\pm$ 0.03 months, contributed scans for the 11-month age group (Female n = 17; Perinatal CTR n = 19; Post-weaning WSD n = 8; Scan Protocol #1 n = 19). A total of 32 offspring, aged 21.13 $\pm$ 0.04 months, contributed scans for the 21-month age group (Female n = 14; Perinatal CTR n = 13; Post-weaning WSD n = 7; Scan Protocol #1 n = 21). A total of 35 offspring, aged 36.56 $\pm$ 0.07 months, contributed scans for the 36-month age group (Female n = 19; Perinatal CTR n = 14; Post-weaning WSD n = 10; Scan Protocol #1 n = 24).

Table 2.1. Demographic composition of macaque subjects at each age time point.

Subjects in 4-month Group								
Scan Protocol	#1				#2			
Perinatal Diet	CTR		WSD		CTR		WSD	
Post-weaning Diet	CTR	WSD	CTR	WSD	CTR	WSD	CTR	WSD
Male	3	0	9	0	3	0	5	0
Female	7	0	2	0	7	2	1	0
Total	39							
Subjects in 6-month Group								
Scan Protocol	#1				#2			
Perinatal Diet	CTR		WSD		CTR		WSD	
Post-weaning Diet	CTR	WSD	CTR	WSD	CTR	WSD	CTR	WSD
Male	1	0	5	0	3	0	4	0
Female	3	0	0	0	7	2	0	0
Total	25							
Subjects in 11-month Group								
Scan Protocol	#1				#2			
Perinatal Diet	CTR		WSD		CTR		WSD	
Post-weaning Diet	CTR	WSD	CTR	WSD	CTR	WSD	CTR	WSD
Male	1	1	6	2	3	0	7	0
Female	4	2	1	2	7	1	0	0
Total	37							
Subjects in 21-month Group								
Scan Protocol	#1				#2			
Perinatal Diet	CTR		WSD		CTR		WSD	
Post-weaning Diet	CTR	WSD	CTR	WSD	CTR	WSD	CTR	WSD
Male	1	1	6	2	2	0	6	0
Female	4	2	3	2	3	0	0	0
Total	32							
Subjects in 36-month Group								
Scan Protocol	#1				#2			
Perinatal Diet	CTR		WSD		CTR		WSD	
Post-weaning Diet	CTR	WSD	CTR	WSD	CTR	WSD	CTR	WSD
Male	2	3	5	1	1	0	4	0
Female	2	2	5	4	4	0	2	0
Total	35							

2.3.3. Macaque MRI Acquisition

The MRI acquisition protocols used in this dissertation have been previously described in prior publications from the research group (Ramirez et al., 2020; Ramirez et al., 2021; Ramirez, 2019).

Imaging was obtained in a single session for each macaque subject at each time point. MRI scans were acquired on a Siemens TIM Trio 3.0 Tesla scanner. A 15-channel knee coil was modified to scan the heads of the macaque offspring. Ketamine (10-15 mg/kg) was administered to allow for intubation, and macaques were maintained on <1.5% isoflurane anesthesia for the duration of the scan. Macaques were continuously monitored for irregularities in heart rate, respiration, and peripheral oxygen saturation.

The scan acquisition protocol was updated partway through the study to optimize future outputs. Importantly, the acquisition parameters for the resting-state functional scan were not changed. The acquisition parameters for protocols #1 and #2 are as follows. Both protocols acquired a total of four T1-weighted (T1w) anatomical images (Scan Protocol #1: TE= 3.86 ms, TR= 2500 ms, TI= 1100 ms, flip angle= 12°, 0.5 mm isotropic voxel; Scan Protocol #2: TE= 3.33 ms, TR= 2600 ms, TI=900 ms, flip angle= 8°, 0.5 mm isotropic voxel), which were averaged to improve the signal-to-noise ratio. Both protocols acquired one T2-weighted (T2w) anatomical image (Scan Protocol #1: TE= 95 ms, TR= 10240 ms, flip angle=150°, 0.5 mm isotropic voxel; Scan Protocol #2: TE= 407 ms, TR= 3200 ms, 0.5 mm isotropic voxel). Both protocols acquired a 30-minute resting-state blood oxygen level dependent (BOLD) scan using the same acquisition settings. This scan was acquired 45 minutes after the initial ketamine injection and utilized a gradient echoplanar imaging (EPI) sequence (TR = 2070 ms, TE = 25 ms,

FA = 90°, 1.5 mm^3 voxels, 32 slices with interleaved acquisition, FOV = 96 × 96 mm). For distortion correction purposes, Scan Protocol #1 acquired field map images (TR = 450 ms, TE = 5.19 ms/7.65 ms, FA = 60°, 1.25 × 1.25 × 2 mm^3 voxels, 40 slices, FOV = 120 × 120 mm), and Scan Protocol #2 acquired a reverse EPI sequence.

2.3.4. Macaque MRI Preprocessing

MRI preprocessing steps are detailed in prior publications from the research group (Ramirez et al., 2020; Ramirez, 2019; Xu et al., 2018; Xu et al., 2019) and follow the standards for human data and the Adolescent Brain Cognitive Development (ABCD) project (Ramirez, 2019). Briefly, preprocessing was accomplished by modifying the Human Connectome Project (HCP) minimal preprocessing pipeline (Glasser et al., 2013) for use in macaques. Study-specific templates were created from averaged T1w images for each age group (Scott et al., 2016). During structural preprocessing, the age-matched study-specific template was registered and warped to each subject's averaged T1w image using tools from the FMRIB Software Library (FSL) (Smith et al., 2004; Woolrich et al., 2009; Jenkinson et al., 2012; Andersson et al., 2003) and Advanced Normalization Tools (ANTs) packages (version 1.9; ANTs, 2022). White and gray matter structures, as well as subcortical regions, were segmented after applying the affine transformations and warps from this registration to the template mask. Segmented and masked structural images were then processed through modified versions of the PreFreeSurfer, FreeSurfer, and PostFreeSurfer stages of the modified HCP pipeline using the FreeSurfer image analysis suite (FreeSurfer, 2022; Dale et al., 1999; Fischl et al., 1999). Subjects were aligned to the Yerkes19 macaque surface-based atlas (Donahue et al., 2016) for normalized

registrations. Functional preprocessing was accomplished in the fMRIVolume and fMRISurface stages of the modified HCP pipeline. These stages included distortion corrections, motion correction, alignments of functional EPI to structural T1w data, resampling, smoothing, and mapping the volumetric data to the standard Connectivity Informatics Technology Initiative (CIFTI) grayordinates space. This grayordinates space consisted of the 56,522 surface anchor points of the Yerkes19 standard space. The final output from this pipeline was a single matrix that contained the cortical surface timeseries and subcortical volume timeseries.

After the MRI data had been processed through the pipeline, trained raters performed a rigorous quality control assessment on the outputs. Raters evaluated the data on a scale of 1 to 3, with 1 indicating good quality and 3 indicating poor quality. A score of 2 required a second trained rater to assess the image; the two raters conferred and agreed on whether to include or exclude the subject. Artifacts that merited a subject for exclusion from the study included poor delineations of white and gray matter, brain warping, excessive blurriness, ringing artifacts from motion in the scanner, and in the case of functional data, poor registration to the T1w image or signal dropout over a large area.

Motion censoring was conducted by measuring the total framewise displacement (FD), calculated as the sum of the absolute values of the backward-difference for all translation and rotation measures, across a 30 mm brain radius. Frames with FD > 0.3 mm were excluded, as well as any isolated frames that came from a group of fewer than five contiguous frames below this threshold, and exactly 20 minutes of data was extracted from the remainder by selecting frames for inclusion at random. Prior studies have

validated this motion correction protocol (Fair et al., 2013; Power et al., 2012; Power et al., 2014).

Once the functional timeseries data had been quality checked and motion censored, the Bezgin Regional Map parcellation (Bezgin et al., 2012) was applied to assign labelled, monkey-specific, brain regions of interest (ROIs) to the data. This yielded 82 ROIs belonging to seven functional networks defined in monkeys (Grayson et al., 2016). The correlation between the timeseries signals for every pair of ROIs was calculated using the Pearson product-moment coefficient and saved as a functional connectivity matrix of correlation coefficients (Feczko et al., 2018). The subset of correlation coefficients selected for this analysis consisted exclusively of the correlation coefficients for any pair of ROIs that belonged to either the Auditory, Somatomotor, or Visual networks; the correlation coefficients for any pair that included an ROI from the aforementioned networks and one of the two ROIs that represented the amygdala (one for each brain hemisphere); and the single correlation coefficient denoting the connectivity strength between the pair of amygdala ROIs. In total, this resulted in correlation coefficients for 378 functional connections within and between all of the sensory networks and the amygdala. Specifically, this included connections within and between the 4 ROIs of the Auditory network, the 14 ROIs of the Somatomotor network, the 8 ROIs of the Visual network, and the 2 ROIs from the Limbic network that denote the left- and right-hemisphere amygdala.

2.3.5. Statistical Analysis of Macaque Data

The Functional Random Forest (FRF; Github, 2022b) is a machine learning algorithm that constructs a series of decision trees to predict an outcome. For this classification analysis, the input predictors were the 378 correlation coefficients for the set of sensory and amygdala connections, and the outcome measure was the perinatal diet group of the juvenile subject. A separate FRF model was created for each age group. Each model constructed a series of 1000 decision trees. Each tree trained on a random selection of 90% of the data and tested classification prediction on the remaining 10% of the data. During training, a bootstrapped dataset was randomly selected from a subset of the training data for each tree. A random subset of input features was evaluated at each node where a tree would split; the feature that provided the greatest reduction in classification error was retained in the constructed decision tree. The maximum variable importance, or greatest amount of error reduction, provided by each of the 378 features across model repetitions was exported to identify the features that contributed the most to perinatal diet group distinction. During testing, a random subset of testing data was used to evaluate the accuracy of the model. This was accomplished through 6 repetitions of 5-fold cross-validation. The perinatal diet group for each test subject was predicted by each of the 1000 trees in the model, and the final classification was determined by majority vote from the 1000 trees. In addition to predicting correctly-labelled data, the model was also used to predict null data, wherein the diet group label had been randomly permuted across subjects. Distributions of overall accuracy, specificity (accurate identification of true negatives when classifying perinatal CTR subjects), and sensitivity (accurate identification of true positives when classifying perinatal WSD subjects) were

constructed from the predictions of the observed and null models. A Wilcoxon rank sum test was used to evaluate the significance of these three performance metrics. If all three metrics were significantly better for the observed models than for the null models, then the FRF model was considered valid for predicting perinatal diet group from the set of connectivity features. Further details regarding the implementation of the FRF have been previously described (Feczko et al., 2018; Cordova et al., 2020; Feczko et al., 2019).

The performance metrics were tested separately for each age-specific FRF model. If the age-specific model was deemed valid, then the variable importance of the features were evaluated to identify the connections that drove accurate model prediction. To assess how these features differed between groups, boxplots were generated to inform visual trends; however, further statistical testing for significant differences in the feature distributions was not performed as the features were already identified by a statistically significant analytical model. The most important features were further grouped by the networks to which the component ROIs belonged; intra- and inter-network representation was evaluated to characterize the types of connections that were most important to model performance.

2.3.6. Human Participants and MRI Processing

Data were obtained from the ABCD Study at the baseline time point (year 1 arm 1) when participants were between the ages of 9 and 10 years old (108-131 months). The ABCD Study has been described previously (Garavan et al., 2018; Heeringa and Berglund, 2020; Collection 3165, 2022a). Participants were included in the present study if they met the following criteria: 1) MRI scans passed quality control; 2) functional data

passed motion quality thresholds; 3) the number of frames in the motion and CIFTI files matched; 4) the participant had an SOR score. This yielded a total of 6,806 participants. Details on these four criteria follow.

1) MRI scans were collected at 21 sites across the United States and uploaded to the National Institute of Mental Health (NIMH) Data Archive (NDA; NIMH Data Archive, 2022). Imaging data from this shared repository was included in the present study only if it had passed the quality control standards set by the ABCD Data Analytics and Informatics Core (DAIC), also known as the Data Analysis, Informatics & Resource Center (DAIRC; Collection 3165, 2022a; Saragosa-Harris et al., 2022; Hagler et al., 2019; ABCD Study, 2022). Imaging data were processed using a modified version of the HCP Pipeline by the Developmental Cognition and Neuroimaging (DCAN) Labs (Collection 3165, 2022b; Sturgeon et al., 2022). The Bezgin Regional Map parcellation (Bezgin et al., 2012), which identifies functional network parcellations in macaques, was deformed and registered into human space using a previously described method of joint-embedding to align cortical surfaces across species (Ramirez, 2019; Xu et al., 2020). This human-aligned Bezgin parcellation was applied to the functional outputs to label the human brain in the same way as the macaque brain and allow for cross-species ROI-based comparisons.

2) Motion censoring was performed in the same way as described for the macaque imaging data. Frames with FD > 0.2 mm were excluded, as well as the first five frames and any isolated frames that came from a group of fewer than five contiguous frames below this threshold. Exactly 8 minutes of data that passed this motion threshold was extracted. Participants with fewer than 8 minutes of motion-censored data were excluded.

3) The Brain Imaging Connectivity Extraction Program Solution (BICEPS), a MATLAB-based tool (MATLAB, 2022) developed by the DCAN Labs, was used to perform motion censoring (Github, 2022a; GUI_environments, 2022). After motion censoring, the software extracted the correct number of frames and created a connectivity matrix, or a file that recorded the correlation between the time series signals for every pair of ROIs identified by the Bezgin parcellation. During this process, the number of frames found in the motion numbers file was compared to the number of frames found in the CIFTI parcellated time series file. A mismatch in the number of frames could lead to the inclusion of frames that did not pass the motion quality threshold. Three subjects were excluded due to a mismatched number of frames.

4) The 11-item Short-Social Responsiveness Scale was administered when participants were 10 to 11 years of age. One of the items stated that the participant "Seems overly sensitive to sounds, textures, or smells." Parents responded to this item with "Not True", "Sometimes True," "Often True," or "Almost Always True." These responses were converted to an ordinal variable with the levels 1, 2, 3, and 4 respectively. This item was considered to be a measure of SOR and was used as the outcome variable for the analysis. Subjects that did not have an SOR score were excluded.

Of the final set of 6,806 subjects, 5,670 had an SOR score of 1; 805 had a score of 2; 229 had a score of 3; and 102 had a score of 4.

2.3.7. Statistical Analysis of Human Data

The analysis method used for the macaque data was repeated with the human data to better allow for direct cross-species comparisons. Three separate FRF models were

constructed to assess the data in slightly different ways. The first was a regression model, where the four possible SOR scores were treated as a continuous variable for the full set of 6,806 subjects. The second was a classification model where the subjects were grouped into two categories: those with an SOR score of 1 (n = 5,670), and those with an SOR score of 2, 3, or 4 (n = 1,136). Unlike for regression, it is useful to have balanced group sizes for classification, so the algorithm randomly selected 1,136 subjects from each of the two categories when constructing the model. The third model was also a classification model, but it excluded subjects that had an SOR score of 2. As a result, subjects with a score of 1 (n = 5,670) were compared to subjects with a score of 3 or 4 (n = 331). While this model trained with the smallest number of subjects (random selection of 331 per group), it is possible that connectivity differences between subjects on distal ends of the SOR scale would be pronounced enough to overcome this limitation.

The input predictors for all models consisted of the same 378 features used in the macaque models, and the outcome measure was the SOR score of the human subject. A random selection of 80% of the data was used for training, and the remaining 20% was reserved for testing. Models were tested using three repetitions of 10-fold cross-validation. The regression model was constructed with 1,000 trees, whereas the two classification models were constructed with 2,000 trees each. Model performance for the regression model was determined by improvements to three measures: the mean absolute error (MAE) in predicting the SOR score, the correlation between subjects' observed and predicted SOR scores, and the intraclass-correlation coefficient (ICC). Model performance for the classification models was determined by assessing the distributions

of overall accuracy, specificity, and sensitivity between the observed and null models, as described previously for the macaque analysis.

2.4. Results

2.4.1. Sensory connections accurately predicted perinatal diet exposure at 4 months of age

FRF model performance metrics for each age group are shown in Figure 2.1. The FRF model used 378 functional connectivity features between sensory networks and the amygdala to classify offspring by perinatal diet group with a mean overall accuracy of 73.9% at 4 months of age. A Wilcoxon rank sum test revealed that this model was significantly more accurate than the permuted model which achieved 51.1% overall accuracy ($p < 0.001$). The specificity and sensitivity of the model at the 4-month old time point was also significantly greater than those metrics for the permuted models. The model had a specificity of 78.3% when classifying offspring exposed to a perinatal CTR diet, indicating the ability of the model to correctly identify true negatives, and a Wilcoxon rank sum test determined that this was significantly more accurate than the permutation specificity of 64.1% ($p = 0.050$). The model had a sensitivity of 66.9% when classifying offspring exposed to a perinatal WSD, indicating the ability of the model to correctly identify true positives, and a Wilcoxon rank sum test determined that this was significantly more accurate than the permutation sensitivity of 37.6% ($p < 0.001$). Given that these three metrics were significantly improved in the model with correctly-labelled, observed data, this indicates that the FRF model is valid for predicting perinatal diet group from the set of connectivity features. Perinatal exposure to a WSD alters the set of

sensory and amygdala connectivity strengths at 4 months of age to the extent that they can be used to predict the perinatal diet exposure for any given subject.

The FRF model did not achieve significance across all three performance metrics at any other age point. Thus, the model is not valid for predicting perinatal diet exposure at the later developmental time points. While there may still be discrete differences in connectivity between perinatal diet groups at these age points, this result indicates that there is not a strong enough pattern of differences in sensory and amygdala connectivity to differentiate between groups.

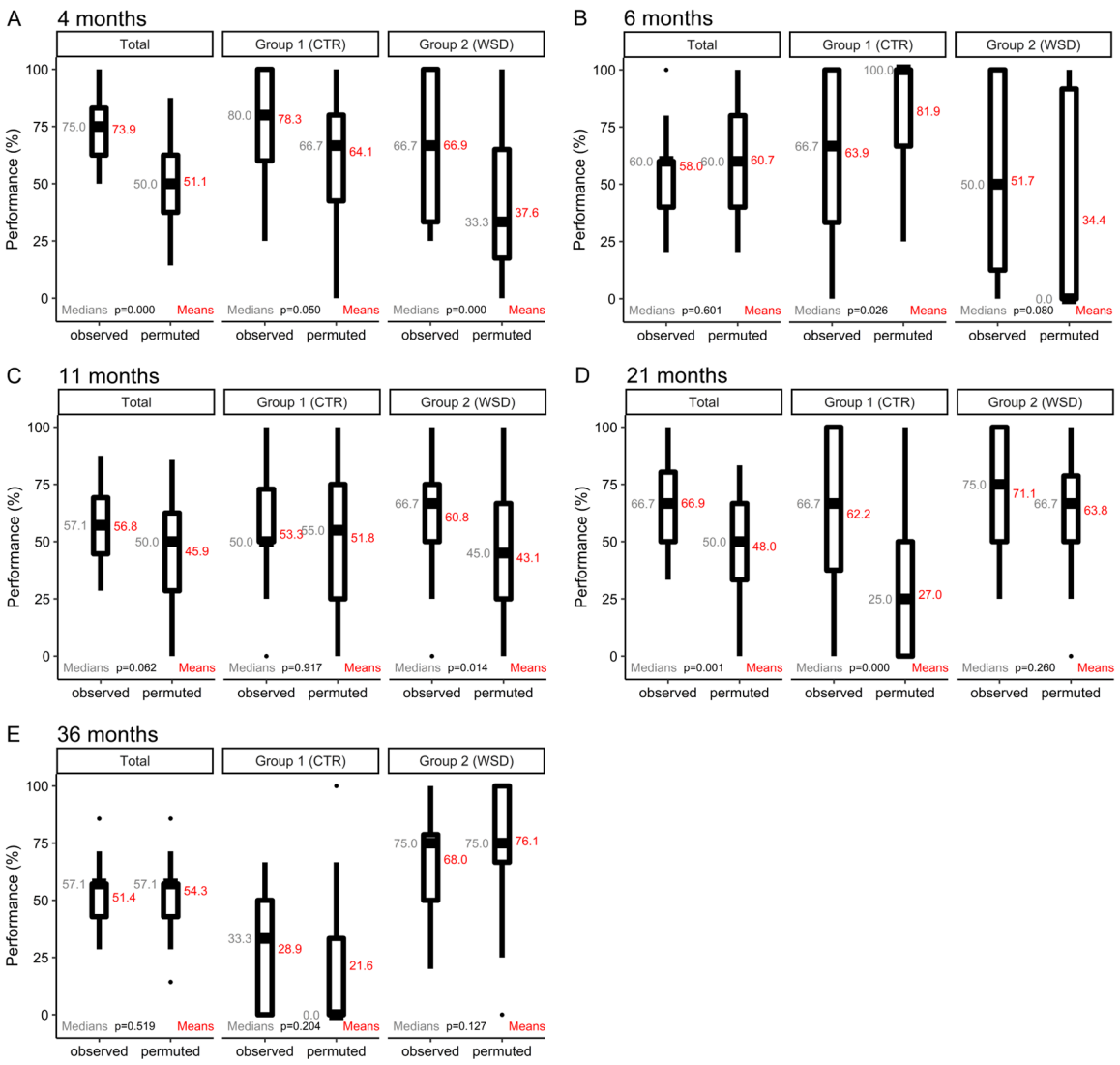

Figure 2.1. Performance metrics for each age-specific FRF model.

The functional connectivity of 378 connections within and between all sensory network regions and the amygdala were used to predict perinatal diet exposure at 4 **(A)**, 6 **(B)**, 11 **(C)**, 21 **(D)**, and 36 **(E)** months of age. Overall accuracy is measured in the left-most panels entitled, "Total." Specificity is measured in the center panels entitled, "Group 1 (CTR)." Sensitivity is measured in the right-most panels entitled, "Group 2 (WSD)." The performance accuracy scores of the model repetitions with labelled data ("observed") were compared to those of the repetitions that used permuted data ("permuted"). Wide

bars refer to the 25th/75th percentiles; thinner bars refer to the 2.5th/97.5th percentiles. Significance was determined by a Wilcoxon rank sum test.

2.4.2. Intra-Somatomotor and Visual-Auditory network connections disproportionately aided model prediction at 4 months of age

The FRF model accurately classified subjects at 4 months of age based on 378 functional connectivity input features. Features that differed more between groups likely played a more prominent role in helping the decision tree distinguish between groups. One way to measure the importance of a feature to a model is by calculating the variable importance, or the sum of the decrease in error when a decision tree is split by that feature. The variable importance of each of the 378 features was calculated for each of the six model repetitions that were run. The maximum variable importance that each feature achieved across the six repetitions was selected.

The maximum variable importance values for the 378 features ranged from -0.032 to 0.193 (Figure 2.2A), where a more positive value denoted a greater reduction in error and, therefore, a more important feature. The midpoint of this range is 0.080; thus, a maximum variable importance value of 0.080 or above denoted an importance to the model that was greater than at least half of all possible importance values. Only 8% of features, or a total of 30 features, achieved a maximum variable importance value that was in the upper half of the demonstrated range.

Each feature represents a functional connection between two ROIs. Each ROI belongs to a functional network. The 30 most important features were grouped by the networks represented by each ROI in the connection pair. For example, the most

important feature with a maximum variable importance of 0.193 belonged to the functional connection between the primary motor cortex ROI of the left hemisphere and the medial premotor cortex ROI of the left hemisphere. Each ROI was a member of the somatomotor network, so the network grouping for this connection would be the "somatomotor-somatomotor" or "intra-somatomotor" group. For clarity, any grouping that included a connection to the amygdala included the term "amygdala" in the grouping name rather than its functional network, "limbic."

The 30 most important features belonged to five network groups, with the greatest proportion of features, at 43%, deriving from the somatomotor-somatomotor network group (Figure 2.2B). Another 30% of features were connections between the somatomotor and visual networks, 17% were visual-auditory connections, 7% were somatomotor-auditory connections, and 3% were visual-visual connections.

These proportions were not representative of the overall distribution of network groupings across the full set of 378 connections (Figure 2.2C). For example, somatomotor-somatomotor network connections comprised just 24% of all 378 connections, yet they comprised 43% of the 30 most important features, indicating that they were over-represented in the set of features that drove model performance. Visual-auditory connections were also over-represented, encompassing 17% of the 30 most important features when only an 8% representation was expected by chance. On the other hand, the somatomotor-auditory group, visual-visual group, and the combined groups of features that contained any connection to the amygdala were all underrepresented in the set of 30 most important features. Two groups, the somatomotor-visual and auditory-

auditory features, were included in the set of 30 most important features in proportions that were representative of their respective shares among all 378 features.

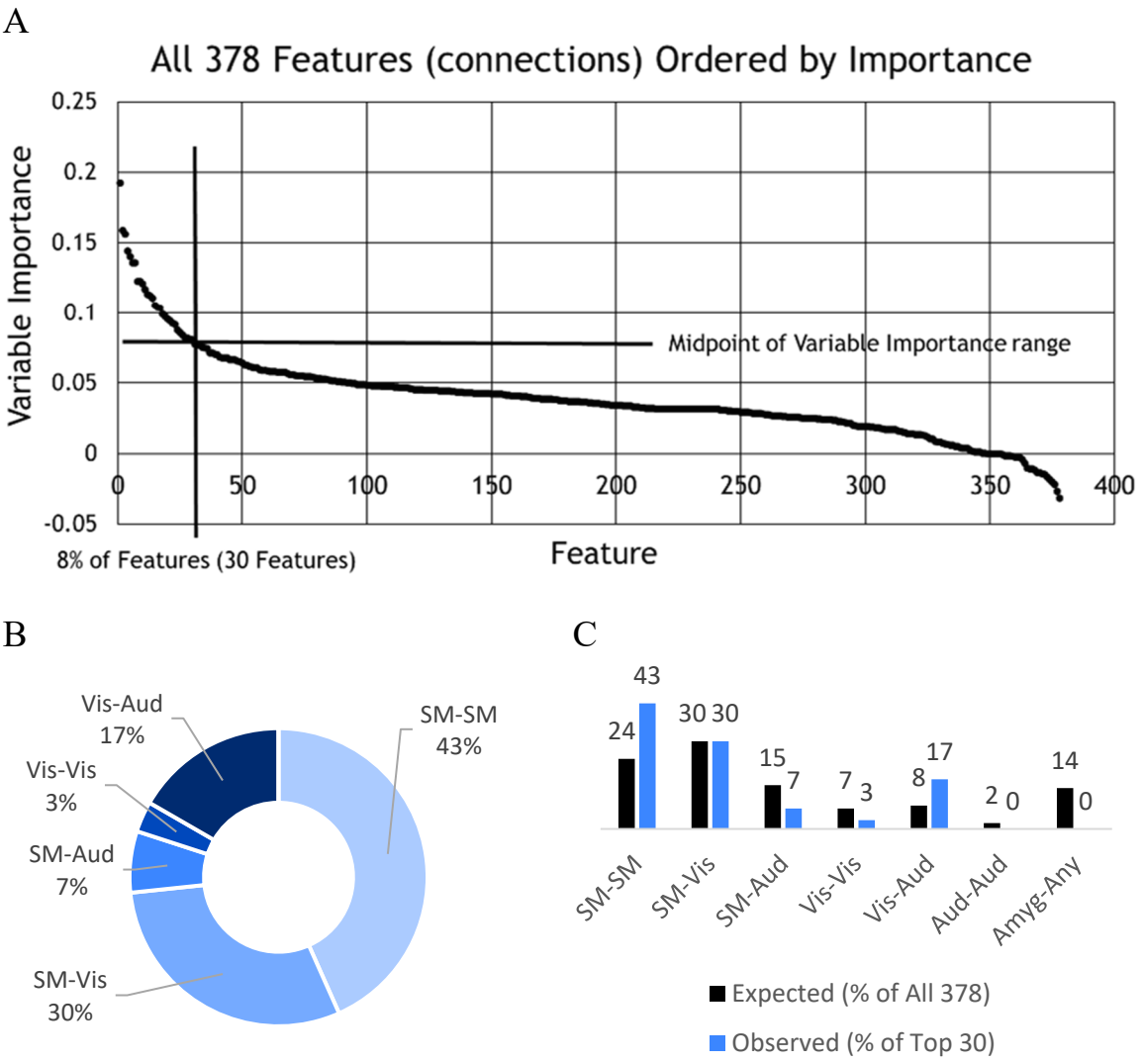

Figure 2.2. Top 30 features most important to 4 month model performance.

(A) The maximum variable importance value for each of the 378 functional connectivity features is displayed. The 378 features are ordered along the x-axis from highest to lowest maximum variable importance value. The midpoint of the range of variable importance values is marked with a horizontal line at 0.080. A vertical line at position 30 along the x-axis visually separates the 30 features that achieved a maximum variable importance value greater than the midpoint of the range of values from the remaining features. **(B)** Chart displaying the percentage of the 30 most important features that

belong to each of the represented network groupings. **(C)** Comparison of network grouping representation. Dark blue bars, on the left side of each pair, display the percentage of all 378 features that belong to the respective network grouping. Lighter blue bars, on the right side of each pair, display the percentage of the 30 most important features that belong to the respective network grouping. Abbreviations from **(B)** and **(C)**: Amyg-Any, amygdala-any network; Aud-Aud, auditory-auditory; SM-Aud, somatomotor-auditory; SM-SM, somatomotor-somatomotor; SM-Vis, somatomotor-visual; Vis-Aud, visual-auditory; Vis-Vis, visual-visual.

The 30 most important features are listed in Table 2.2. Notably, many individual ROIs appear more than once. Table 2.3 summarizes the ROIs that appeared in at least three of the 30 most important features. The right primary motor cortex and left primary somatosensory cortex were the two connections that appeared the most, appearing in 7 and 5 features respectively. Both of these ROIs are part of the somatomotor network, demonstrating again that differences in somatomotor network connectivity were strong drivers of model performance.

Table 2.2. The 30 features with maximum variable importance values in the upper half of the observed range of values.

Abbreviations: Hemi, brain hemisphere; ROI, region of interest (Bezgin et al., 2012).

		ROI 1			ROI 2		
Order of Importance	Maximum Variable Importance	Network	Hemi.	ROI Name	Network	Hemi.	ROI Name
1	0.1925	Somatomotor	Left	Primary Motor Cortex	Somatomotor	Left	Medial Premotor Cortex
2	0.1588	Somatomotor	Left	Secondary Somatosensory Cortex	Somatomotor	Right	Primary Motor Cortex
3	0.1560	Visual	Right	Visual Anterior Cortex, Dorsal Part	Somatomotor	Right	Medial Premotor Cortex
4	0.1441	Visual	Left	Visual Anterior Cortex, Ventral Part	Somatomotor	Right	Secondary Somatosensory Cortex
5	0.1404	Somatomotor	Left	Anterior Cingulate Gyrus	Somatomotor	Right	Primary Motor Cortex
6	0.1360	Auditory	Right	Secondary Auditory Cortex	Somatomotor	Right	Primary Somatosensory Cortex
7	0.1359	Visual	Left	Visual Area 2	Visual	Right	Visual Area 1
8	0.1226	Somatomotor	Left	Secondary Somatosensory Cortex	Somatomotor	Right	Medial Premotor Cortex
9	0.1226	Somatomotor	Left	Primary Somatosensory Cortex	Somatomotor	Right	Primary Motor Cortex
10	0.1210	Visual	Right	Visual Area 1	Somatomotor	Left	Secondary Somatosensory Cortex
11	0.1166	Somatomotor	Left	Primary Somatosensory Cortex	Somatomotor	Left	Medial Premotor Cortex
12	0.1134	Visual	Right	Visual Anterior Cortex, Ventral Part	Somatomotor	Right	Primary Motor Cortex
13	0.1124	Somatomotor	Left	Primary Somatosensory Cortex	Somatomotor	Left	Primary Motor Cortex

14	0.1106	Visual	Right	Visual Anterior Cortex, Dorsal Part	Auditory	Right	Secondary Auditory Cortex
15	0.1053	Visual	Left	Visual Anterior Cortex, Ventral Part	Somatomotor	Left	Primary Somatosensory Cortex
16	0.1042	Visual	Right	Visual Area 1	Somatomotor	Right	Posterior Insula
17	0.1036	Visual	Right	Visual Area 2	Auditory	Left	Primary Auditory Cortex
18	0.0994	Visual	Right	Visual Area 2	Somatomotor	Right	Posterior Insula
19	0.0974	Somatomotor	Right	Posterior Insula	Somatomotor	Right	Primary Somatosensory Cortex
20	0.0957	Visual	Left	Visual Anterior Cortex, Dorsal Part	Auditory	Left	Primary Auditory Cortex
21	0.0942	Visual	Right	Visual Anterior Cortex, Dorsal Part	Somatomotor	Right	Posterior Insula
22	0.0926	Visual	Left	Visual Area 1	Somatomotor	Left	Medial Premotor Cortex
23	0.0919	Somatomotor	Left	Anterior Cingulate Gyrus	Somatomotor	Right	Medial Premotor Cortex
24	0.0879	Somatomotor	Left	Medial Premotor Cortex	Somatomotor	Right	Primary Motor Cortex
25	0.0859	Visual	Left	Visual Area 1	Auditory	Left	Primary Auditory Cortex
26	0.0841	Somatomotor	Right	Primary Motor Cortex	Somatomotor	Right	Medial Premotor Cortex
27	0.0823	Somatomotor	Right	Secondary Somatosensory Cortex	Somatomotor	Right	Primary Motor Cortex
28	0.0821	Somatomotor	Left	Primary Somatosensory Cortex	Somatomotor	Right	Superior Parietal Cortex
29	0.0811	Visual	Left	Visual Area 2	Auditory	Right	Primary Auditory Cortex
30	0.0804	Auditory	Left	Primary Auditory Cortex	Somatomotor	Left	Secondary Somatosensory Cortex

Table 2.3. ROIs that were included in at least three of the 30 features with the greatest maximum variable importance.

The table is ordered first by the number of times an ROI appears in a feature, and then alphabetically by network and ROI name.

Network	Hemisphere	ROI Name	Number of Instances
Somatomotor	Right	Primary Motor Cortex	7
Somatomotor	Left	Primary Somatosensory Cortex	5
Auditory	Left	Primary Auditory Cortex	4
Somatomotor	Left	Medial Premotor Cortex	4
Somatomotor	Right	Medial Premotor Cortex	4
Somatomotor	Right	Posterior Insula	4
Somatomotor	Left	Secondary Somatosensory Cortex	4
Visual	Right	Visual Anterior Cortex, Dorsal Part	3
Visual	Right	Visual Area 1	3

2.4.3. Perinatal WSD exposure was associated with consistent, network-specific changes in connectivity strength at 4 months of age

Each of the thirty features that achieved the greatest maximum variable importance in the FRF model constructed on the 4 month old offspring data was assessed for differences between perinatal diet groups. The distribution of connectivity strengths, measured as correlation coefficients, among offspring exposed to a perinatal WSD and CTR were compared for each feature (Figure 2.3). For example, the feature that contributed the most to accurate model performance was the connection between the left primary motor cortex and left medial premotor cortex. Offspring that were perinatally exposed to a WSD showed decreased connectivity in that feature (0.057 ± 0.010, mean $\pm$ SEM) compared to controls (0.158 ± 0.030) at four months of age.

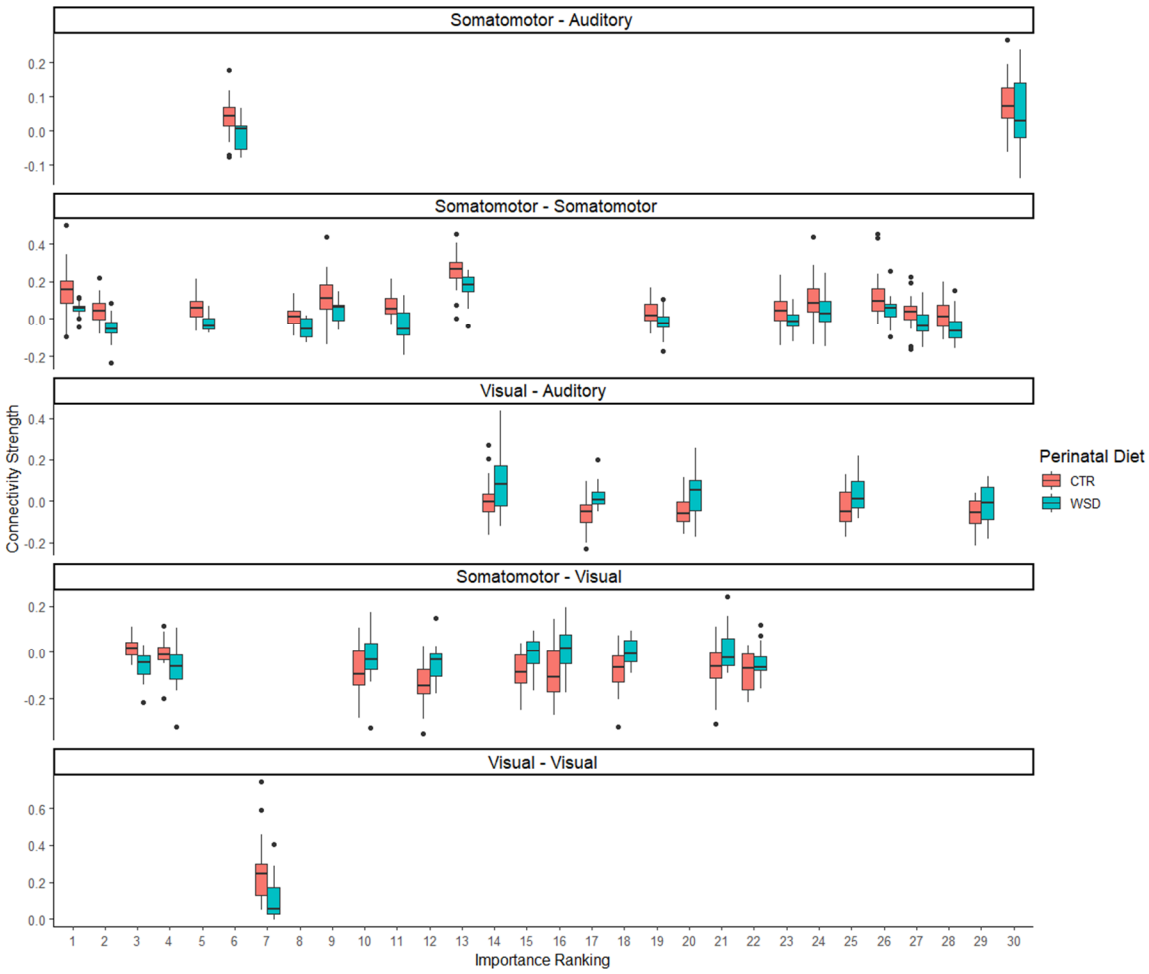

Figure 2.3. Distribution of connectivity strengths between perinatal diet groups for each of the 30 features with the greatest maximum variable importance.

The 30 features are ordered along the x-axis from highest to lowest maximum variable importance value. Boxplots are clustered by network group. Pink boxplots, on the left side of each pair, represent the distribution for the perinatal CTR diet offspring. Blue boxplots, on the right side of each pair, represent the distribution for the perinatal WSD offspring. Wide bars refer to the 25th/75th percentiles; thinner bars refer to the 2.5th/97.5th percentiles.

All of the features that belonged to the two network groupings that were over-represented in the 30 most important features followed a consistent pattern of altered connectivity (Figure 2.3). The perinatal WSD offspring displayed weaker connectivity across all 13 connections in the somatomotor-somatomotor network group, and they displayed stronger connectivity across all 5 connections in the visual-auditory network group. The two connections in the somatomotor-auditory network group were also consistent, with decreased connectivity in the perinatal WSD group. Differences in connectivity strength were mixed for the somatomotor-visual network group. While perinatal WSD offspring displayed trends toward decreased connectivity for the first two connections in the network group, the remaining seven connections were characterized by trends toward increased connectivity. The only connection for the visual-visual network group demonstrated decreased connectivity for the perinatal WSD group. Significance testing was not performed on these distributions as they were already identified as being important for a statistically significant model prediction.

2.4.4. Amygdala-Somatomotor connectivity weakly contributed to model performance at 4 months of age

Connections to the amygdala were not present in the 30 most important features. However, amygdala connectivity may still be a weak driver of accurate model performance. While amygdala connections were not present in the 30 most important features, or the top 8% of all 378 features, four amygdala connections were present in the top 15% of all features, or within the 56 most important features. These four connections were between the amygdala and somatomotor network (Table 2.4), and they ranked at 44,

47, 49, and 50 when all features were ordered by maximum variable importance. The maximum variable importance values for these connections ranged from 0.068 to 0.064 (highest to lowest). A maximum variable importance of 0.064 is greater than 46% of the values in the range exhibited by the model. This suggests that amygdala-somatomotor connectivity may still provide valuable information to the model as it learns to distinguish between diet groups.

The distributions of amygdala connectivity strengths were characterized by weak differences between diet groups (Figure 2.4). Additionally, when looking across the amygdala connections that were present within the upper 50% of most important features (or the 189 most important features), a consistent pattern of altered connectivity did not emerge in any network grouping. Thus, amygdala-somatomotor connectivity, while constituting the most important amygdala connections, may have only weakly contributed to accurate model performance at 4 months of age.

Table 2.4. The 27 amygdala connections within the upper half of most important features.

Abbreviations: Hemi, brain hemisphere; ROI, region of interest (Bezgin et al., 2012).

		ROI 1			ROI 2		
Order of Importance	Maximum Variable Importance	Network	Hemi.	ROI Name	Network	Hemi.	ROI Name
44	0.0678	Somatomotor	Left	Anterior Cingulate Gyrus	Limbic	Right	Amygdala
47	0.0663	Somatomotor	Right	Posterior Insula	Limbic	Left	Amygdala
49	0.0653	Somatomotor	Right	Medial Premotor Cortex	Limbic	Right	Amygdala
50	0.0641	Somatomotor	Left	Posterior Insula	Limbic	Right	Amygdala
58	0.0592	Somatomotor	Left	Primary Motor Cortex	Limbic	Left	Amygdala
61	0.0583	Somatomotor	Left	Posterior Insula	Limbic	Left	Amygdala
62	0.0583	Visual	Right	Visual Anterior Cortex, Ventral Part	Limbic	Right	Amygdala
69	0.0561	Visual	Right	Visual Anterior Cortex, Dorsal Part	Limbic	Right	Amygdala
85	0.0519	Visual	Right	Visual Area 1	Limbic	Right	Amygdala
86	0.0516	Somatomotor	Right	Primary Somatosensory Cortex	Limbic	Left	Amygdala
96	0.0491	Visual	Right	Visual Area 2	Limbic	Left	Amygdala
109	0.0474	Somatomotor	Left	Secondary Somatosensory Cortex	Limbic	Right	Amygdala
119	0.0455	Somatomotor	Right	Primary Motor Cortex	Limbic	Right	Amygdala
121	0.0454	Somatomotor	Right	Primary Motor Cortex	Limbic	Left	Amygdala
124	0.0451	Somatomotor	Right	Anterior Cingulate Gyrus	Limbic	Right	Amygdala

138	0.0434	Auditory	Left	Primary Auditory Cortex	Limbic	Right	Amygdala
140	0.0430	Somatomotor	Right	Anterior Cingulate Gyrus	Limbic	Left	Amygdala
141	0.0430	Somatomotor	Left	Primary Somatosensory Cortex	Limbic	Left	Amygdala
146	0.0427	Auditory	Right	Secondary Auditory Cortex	Limbic	Right	Amygdala
147	0.0427	Visual	Left	Visual Anterior Cortex, Dorsal Part	Limbic	Left	Amygdala
148	0.0426	Somatomotor	Right	Superior Parietal Cortex	Limbic	Right	Amygdala
150	0.0424	Auditory	Right	Primary Auditory Cortex	Limbic	Left	Amygdala
152	0.0422	Visual	Left	Visual Area 1	Limbic	Right	Amygdala
155	0.0418	Somatomotor	Right	Superior Parietal Cortex	Limbic	Left	Amygdala
157	0.0413	Somatomotor	Left	Primary Motor Cortex	Limbic	Right	Amygdala
160	0.0409	Visual	Left	Visual Anterior Cortex, Ventral Part	Limbic	Left	Amygdala
184	0.0369	Somatomotor	Left	Anterior Cingulate Gyrus	Limbic	Left	Amygdala

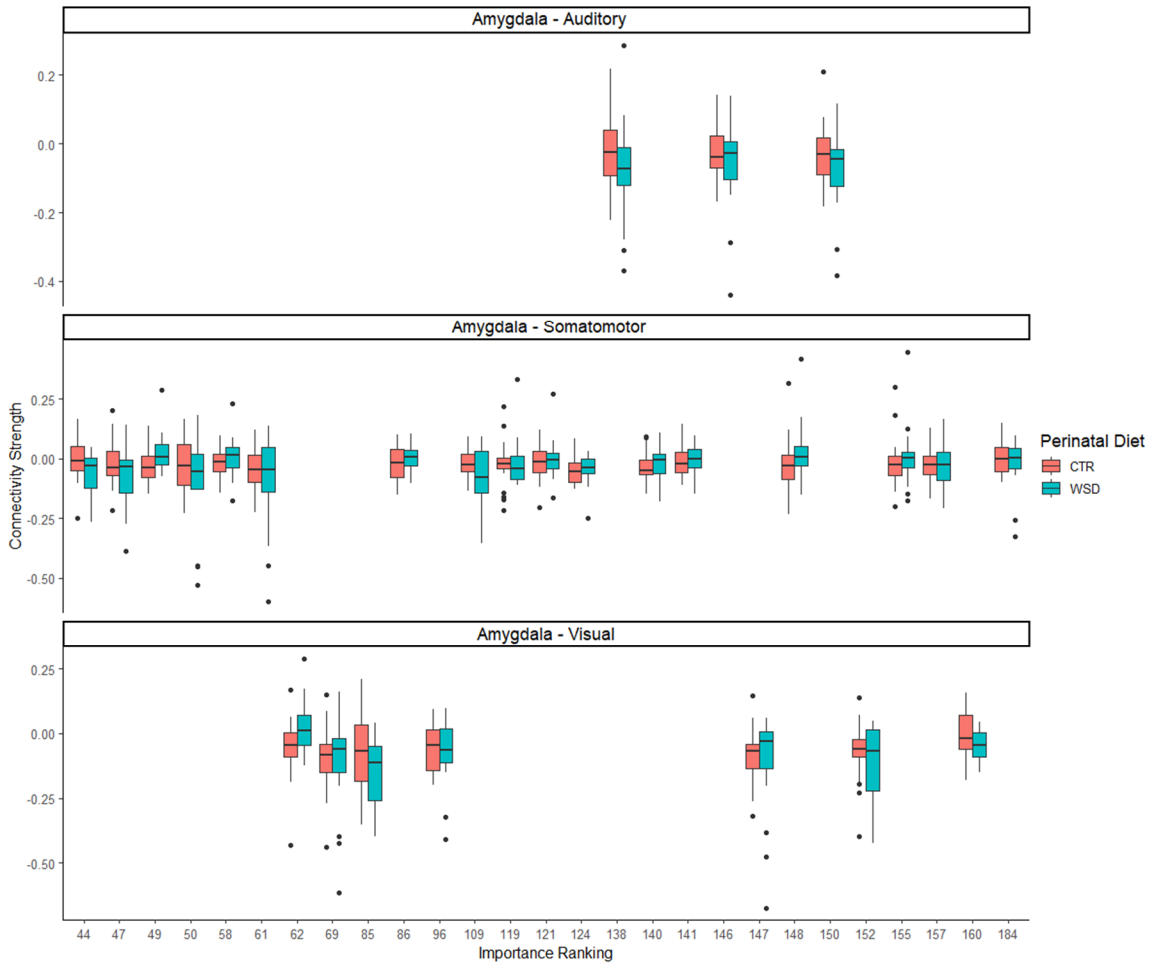

Figure 2.4. Distribution of connectivity strengths between perinatal diet groups for amygdala connections within the upper 50% of features with the greatest maximum variable importance.

The amygdala features are ordered along the x-axis from highest to lowest maximum variable importance value, with the x-axis position denoting the variable importance order among all 378 connections. Boxplots are clustered by network group. Pink boxplots, on the left side of each pair, represent the distribution for the perinatal CTR diet offspring. Blue boxplots, on the right side of each pair, represent the distribution for the perinatal WSD offspring. Wide bars refer to the 25th/75th percentiles; thinner bars refer to the 2.5th/97.5th percentiles.

2.4.5. SOR score in children was not predicted by differences in sensory and amygdala connectivity

Three FRF models were run on slightly different subsets of human imaging data from the ABCD study. None of the models demonstrated significant predictive capabilities (Table 2.5, Figure 2.5). Thus, these models are not valid for predicting a child's SOR score from the functional connectivity within and between their sensory networks and the amygdala.

Table 2.5. Performance metrics for the human SOR regression model.

Performance metrics for the FRF regression model were not significantly different between the observed and null (permuted data) models ($p > 0.05$ for each metric). Values displayed are the means across three model repetitions. Abbreviations: ICC, intraclass-correlation coefficient; MAE, mean absolute error; R, Pearson's correlation coefficient; SOR, sensory over-responsivity.

Model	**R**		**ICC**		**MAE**	
	Observed	Permuted	Observed	Permuted	Observed	Permuted
Regression	0.0187	0.0010	0.5171	0.5140	0.3946	0.3968

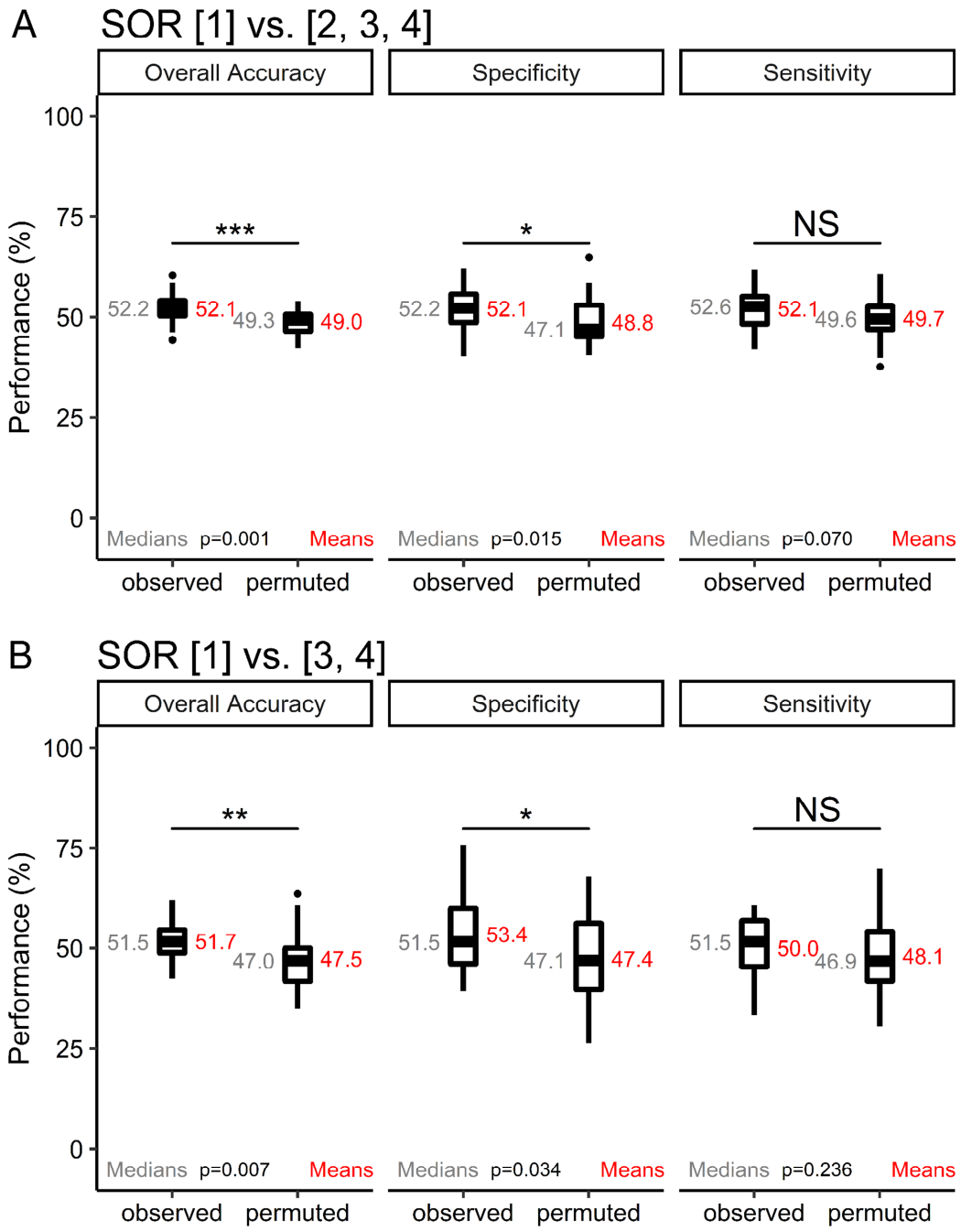

Figure 2.5. Performance metrics for the human SOR classification models.

The functional connectivity of 378 connections within and between all sensory network regions and the amygdala were used to predict SOR score in children. **(A)** This classification model predicted two classes of SOR score: one class was defined by a score of "1," and the other was defined by a score of "2," "3," or "4." **(B)** This classification

model predicted two classes of SOR score: one class was defined by a score of "1," and the other was defined by a score of "3" or "4." Specificity is the prediction accuracy for the group of subjects with an SOR score of 1. Sensitivity is the prediction accuracy for the group of subjects with an SOR score of 2, 3, or 4 in **(A)**, and an SOR score of 3 or 4 in **(B)**. The performance accuracy scores of the model repetitions with labelled data ("observed") were compared to those of the repetitions that used permuted data ("permuted"). Wide bars refer to the 25th/75th percentiles; thinner bars refer to the 2.5th/97.5th percentiles. Significance was determined by a Wilcoxon rank sum test. *p < 0.05; **p < 0.01; ***p < 0.001; NS = non-significant.

2.5. Discussion

There are several conflicting theories about the origins of the symptoms of SPD. While some evidence suggests SPD may be a manifestation of other root psychiatric conditions, other data supports the hypothesis that SPD may stem from direct disruptions to sensory processing, in some cases leading to the emotional dysregulation seen in psychiatric conditions as a consequence of the experience of living with the symptoms of SPD. This study took the position of the latter theory and explored the connectivity of a subset of brain regions that represent the primary cortical areas for processing sensory input. Prior evidence suggested that connections to the amygdala may be a strong component of ascending sensory processing pathways, especially in non-classical sensory pathways that may persist in adults with ASD (Møller et al., 2005; Møller and Rollins, 2002; Musiek et al., 2011), so the amygdala was included in the ROI subset, as well. The amygdala is intrinsic to the processing of negative emotions, so even if purely-sensory

connectivity was not found to be disrupted, alterations to amygdala connectivity could support the hypothesis that emotional dysregulation is a driving factor behind the symptoms of SPD.

While the juvenile macaques used in this study were not tested explicitly for symptoms of SPD, prior work in this animal model established that the offspring who were exposed to a WSD during the perinatal period displayed the component behaviors of ASD, including sensorimotor behaviors that involved abnormal movements, posture, and increased head tossing and pacing (Mitchell et al., 2022b). Prenatal exposure to a WSD is associated with an increased incidence of ASD, but that does not mean that every subject in the perinatal WSD group would develop the component behaviors of ASD. However, given that an estimated 95% of children with ASD experience a SPD (Tomchek and Dunn, 2007; Crane et al., 2009; Leekam et al., 2007), it is likely that the perinatal WSD offspring that did develop the behaviors typical of ASD would also experience a SPD and the underlying brain circuitry responsible for the symptoms. Following this logic, it was expected that the perinatal WSD group would include an increased proportion of subjects that displayed altered circuitry representative of disruptions to sensory or emotional processing.

This expectation was supported when offspring were 4 months of age, but the machine learning algorithm was unable to successfully predict perinatal diet group at the later time points of 6, 11, 21, and 36 months of age. A follow-up characterization of the 4 month model results revealed that differences in intra-somatomotor, visual-auditory, somatomotor-auditory, somatomotor-visual, and intra-visual network connections were the most distinct between perinatal diet groups, with the first two network groupings

being over-represented in the set of the 30 features that contributed the most to improving model prediction. Connectivity was impacted in the same direction for each network grouping except the somatomotor-visual group, demonstrating a largely consistent impact of perinatal WSD exposure on network-wide connectivity. Impacts to the connectivity of the primary motor cortex seemed to be the most pronounced, as the ROI was part of the connection that was identified as being the most important to the model, and it appeared in seven of the 30 most important features, more than any other ROI. Amygdala connectivity was not found to be a strong contributor to model performance, though weak differences in connectivity may have still improved the model. Amygdala-somatomotor connections, in an inconsistent pattern within the network grouping, displayed a maximum variable importance greater than 46% of the other values in the demonstrated range from the model, placing these connections within the top 15% of connections when ordered by importance. While the same set of sensory and amygdala connections were unable to predict a measure of SOR in a cohort of 9 and 10 year old children, this finding is consistent with the poor model performance in macaques at the same developmental time point.

2.5.1. Functional connectivity may be more susceptible to WSD-associated disruptions during prenatal and early postnatal development

Perinatal WSD exposure in macaques was associated with differences in the functional connectivity of sensory systems and the amygdala at 4 months of age but not at 6, 11, 21, or 36 months of age. This suggests that neural circuitry is impacted during

prenatal and early postnatal development, but once the perinatal dietary exposure is removed, these functional circuits recover and become indistinguishable from the connectivity patterns present in control subjects.

Importantly, there may be a further distinction between prenatal and perinatal WSD exposure. Integral to this distinction is the observation that the juvenile offspring were exposed to their perinatal diet through lactation and solid food consumption until weaning at 7.22 ± 0.32 (mean ± SEM) months of age for the CTR group and 7.50 ± 0.20 months of age for the WSD group. Thus, the exposure from the *in utero* environment matched the dietary exposure at both the 4 and 6 month old time points, yet differences in functional connectivity were only strong enough to drive model prediction at 4 months of age. If prolonged postnatal WSD exposure had the ability to impact connectivity strongly, then differences should have been greater after an additional two months of exposure at 6 months of age. Additionally, the 11 month time point was fewer than four months after weaning; if significant results were present four months after birth, it is surprising that strong results were not found four months after weaning, despite a longer exposure to the WSD by that point.

These findings can be interpreted in multiple ways. First, it is possible that the maternal environment associated with WSD consumption may lead to *in utero* impacts that differ from the impacts of postnatal WSD exposure. For example, it is well-established that WSD consumption during pregnancy can lead to an elevated inflammatory state (Grayson et al., 2010). It is also known that the immune system is still developing in neonates and infants (Basha et al., 2014; Christensen et al., 2014). Thus, the inflammatory response to WSD consumption generated in the dam may differ

significantly from the response generated in the offspring during postnatal WSD exposure. Neuroinflammation may impact neural circuit formation, so a difference in neuroinflammatory influences between the prenatal and postnatal periods may explain the lack of continued impacts at 6 and 11 months of age despite current and recent WSD exposure.

Another interpretation is that neurodevelopment proceeds through different stages and may be more susceptible to disruptions at different times. The third trimester in particular is a highly dynamic period characterized by rapid cortical maturation and dramatically increased neuronal connectivity (Marr, 2020; Tau and Peterson, 2010; Andescavage et al., 2017; van den Heuvel et al., 2015; Thomason et al., 2015). Prenatal inflammatory influences like elevated maternal immune activation, increased maternal IL-6 concentrations, and infection with SARS-CoV-2 during the third trimester are all associated with impacts to offspring neurodevelopment: these impacts consisted of altered neonatal functional connectivity within the salience network, reduced working memory at two years of age, and an increased incidence of neurodevelopmental disorder diagnosis at one year of age compared to infection during the first or second trimester, respectively (Spann et al., 2018; Rudolph et al., 2018; Edlow et al., 2022). Rapid synaptogenesis continues through the first year of life, and synaptic pruning does not outpace synapse formation until later in childhood (Eltokhi et al., 2020; Levitt, 2003). It therefore makes sense that impacts during the third trimester and first year of life, when cerebral connectivity is undergoing its greatest period of development, would be more pronounced than effects that occur at other time points. When comparing developmental stages across species, a 4 month old macaque (rhesus) is roughly the equivalent of an 8

month old human, 6 months in macaques is roughly equivalent to 15 months in humans, and 11 months in macaques is roughly equivalent to 36 months in humans (Workman et al., 2013; Translating Time, 2022). Only the 4 month old time point falls within the first year of comparable human development. Thus, if the 4 month time point is the only one in which connections are undergoing dramatic construction, then this increased susceptibility to perturbations in circuit remodeling would explain why the perinatal WSD exposure is associated with an impact at 4 months but not 6 or 11 months.

A combination of the above two interpretations would suggest that prenatal WSD exposure may play a greater role in altering circuitry than postnatal WSD exposure due to the direct impacts of the inflammatory maternal environment during the most dynamic, and therefore most vulnerable, period of connectome development. Even if separation from the maternal environment removes the most impactful exposure, the 4 month time point may be near enough to the point of separation that effects can still be detected by the FRF model. Six months would appear to be enough time for the trajectory of functional connectivity to recover and assume a pattern similar to that of control subjects, even in the face of postnatal WSD exposure.

Regardless of which of the three proposed interpretations holds the most weight, the long-term outcome is shared: the functional connectivity of the sensory systems and the amygdala is plastic and robust against long-lasting impacts from earlier periods of WSD exposure. Future research could explore what mechanistic changes allow the pronounced differences at earlier time points to rapidly resolve and revert to the typical connectivity patterns of the control group.

2.5.2. Impacts to functional connectivity at later ages may be too weak to drive model performance

Although the present findings only indicate strong impacts to functional connectivity at the 4 month time point, the null model findings at the later time points do not necessarily rule out the possibility of altered connectivity at these ages. For example, it is possible that only a subset of the WSD offspring developed the characteristics of ASD and SPD, and the remaining WSD offspring may have displayed behavior and functional connectivity that was more similar to that of the control subjects. Thus, the differences in connectivity driven by the most impacted WSD offspring at 4 months of age may have subsided slightly at later time points such that the entire group's connectivity profile—which would include the connectivity of subjects who did not experience the component behaviors of ASD or SPD despite exposure to the perinatal risk factor—was no longer substantially different from that of the control subjects. This would erode the ability of the machine learning model to distinguish between groups, but it does not confirm that the most impacted WSD offspring no longer experienced differences in functional connectivity. Repeating the FRF with the exclusion of subjects in the WSD group that did not display the component behaviors of ASD could improve group-wide consistency and increase model performance, as long as a large enough sample size was retained. Alternatively, the FRF could be replaced with a more detailed analysis of each connection to test for discrete differences between groups without the effect being diluted or overpowered by a majority of connections that were not significantly different between groups.

Another major limitation to the analysis is the limited sample sizes, which can lead to insufficient model training. The 4 month sample had the greatest number of subjects (N = 39), and it was also the time point with the greatest consistency in life experiences among the five ages. Thus, the significant predictive ability of the model may be due to congruent connectivity patterns within each group that differed in a consistent way between groups. This consistency may have diminished over time as offspring experienced a natural variation in neurodevelopmental trajectories. Thus, it is possible that the null findings at these later time points were not due to the WSD offspring developing the same connectivity pattern as seen in the controls, but they may instead indicate that the variety of connectivity patterns within the WSD group was highly variable, inconsistent, and partially overlapping with connectivity patterns seen in the CTR group, thereby leading to an inability to accurately classify these subjects against permuted data. Greatly increasing the sample sizes may reduce group variance and allow the models to learn to detect the various connectivity patterns that characterize the WSD group and distinguish them from the patterns typical of the CTR group.

An additional consideration is that diet exposures were only consistent during the 4 and 6 month old time points. At the later time points, a roughly equal proportion of subjects from each perinatal diet group consumed a post-weaning WSD (11 months: 21.1% of perinatal CTR and 22.2% of perinatal WSD offspring consumed a post-weaning WSD; 21 months: 23.1% perinatal CTR and 21.1% perinatal WSD; 36 months: 35.7% perinatal CTR and 23.8% perinatal WSD). Thus, any impacts from post-weaning WSD exposure were equally distributed across the two groups, such that the model would not be able to distinguish between groups based on any differences in functional connectivity

inherent to the impacts of a post-weaning WSD. However, this also meant that there was less differentiation in diet exposures between groups at later ages. For example, at 4 months of age, 100% of the perinatal CTR group had never been exposed to a WSD, and 100% of the perinatal WSD had been exposed to the WSD since conception. At 11 months of age, those proportions dropped to roughly 78.9% and 22.2% respectively. This drop was the result of a deliberate effort to ensure the majority of subjects consumed a post-weaning CTR diet so as to predominantly test the effects of the perinatal exposure. However, it also meant that 21.1% and 77.8% of the perinatal CTR and WSD groups, respectively, had a similar experience of exposure to a WSD at some point in their lives. While it is unlikely that WSD exposures at different time points would lead to the same, indistinguishable connectivity patterns at 11 months of age, it may be a potential contributor to poor model prediction, especially in light of the small sample sizes.

2.5.3. Functional connectivity outcomes are consistent between macaque and human cohorts

The FRF analysis performed in macaques was repeated in humans using highly conserved methodology to reduce potential confounds and variance. This included the use of the same minimal MRI preprocessing standards via similar pipelines, the same brain parcellation to label ROIs, the same set of 378 connections within and between sensory areas and the amygdala, and the same FRF algorithm for analysis. Major differences included a much larger sample size in humans (up to 6,806 subjects), higher motion censoring standards in humans (8 min at FD < 0.2 mm instead of 20 minutes at FD < 0.3 mm), and different outcome measures.

The predicted outcome measure in humans was an SOR score that ranged from no observed issues with seeming overly sensitive to sensory stimuli (a score of "1") to sometimes ("2"), often ("3"), and almost always seeming overly sensitive ("4"). This SOR score was condensed into a binary variable that separated the subjects with a score of 1 from subjects who scored either a 2, 3, or 4 for one classification model, and those who scored either a 3 or 4 for another classification model. In all cases, these group separations were meant to mimic the grouping variable for the macaque data. Given that a prenatal WSD is a known predictor of the behavioral phenotypes of ASD—a neurodevelopmental disorder which is highly comorbid with SPD—and given that the WSD offspring displayed the component behaviors of ASD, the following hypothesis was made: the children with an SOR score of 1 were hypothesized to have functional connectivity similar to macaques with perinatal CTR diet exposure, and children with a score of 2, 3, or 4 were hypothesized to show connectivity patterns consistent with the perinatal WSD macaque cohort. If the FRF model that trained on the human data was valid for predicting SOR score from the set of functional connections, then the model could have been applied to the macaque data. The cross-species brain parcellation would enable the identical set of functional connections in macaques to be processed through the human-based decision trees. Each macaque would have been assigned an SOR score or binary SOR class, and a follow-up analysis could have determined whether the perinatal WSD group was assigned a higher SOR score. This would have indicated that the functional connectivity patterns seen in WSD macaques were similar to those of children with SOR, thereby implicating perinatal WSD exposure in the development of SOR. This analytical exploration could not be conducted, however, because none of the

variations of the human FRF model achieved significance across all three performance metrics.

Instead, poor model performance indicates that the functional connectivity of the sensory systems and the amygdala did not differ substantially between children with different SOR scores. This result is consistent with what was demonstrated in macaques. Macaques at 36 months of age are at roughly the equivalent developmental time point as the 9 and 10 year old children in the human cohort used for this analysis. Neither the children nor the 36 month old macaques displayed enough differences in functional connectivity to accurately predict the respective SPD-related outcome measure. While a concrete relationship cannot be established between null results for the macaque and human analyses, this at least demonstrates a consistent absence of distributed, SPD-related impacts to functional connectivity in late childhood. Alternatively, it is also possible that fewer or weaker connectivity differences existed in the human cohort but were not pronounced enough to train the FRF model, or that the SOR score was an unreliable measure of the intended SPD symptom. Further analyses would be required to test whether functional connectivity patterns and impacts to discrete connections correspond across species.

In fact, a recent study has identified differences in discrete connections using the same human cohort as in the present study. Schwarzlose and colleagues (2023) examined connectivity in children from the ABCD study at the 9-10 year old time point and at 12 years of age (Schwarzlose et al., 2023). Image processing methods were largely conserved, though there were some differences in motion censoring, and a different brain parcellation was used to map ROIs—the Gordon parcellation (Gordon et al., 2016).

Connectivity strengths of connections within a shared network grouping were averaged; these single averages for each network grouping were tested separately for differences between groups using linear mixed-effects models. The two subject groups consisted of subjects with an SOR score of 1 and subjects with an SOR score of 3 or 4. This study tested connections in the same general network groupings as explored in the present study and only found a significant difference for one grouping: decreased intra-somatomotor network connectivity in children with an SOR of 3 or 4. The study did not indicate effect size, so it is unclear whether this difference was substantial in addition to being significant. There were no other significant connections within or between the other sensory networks and the amygdala. These findings are roughly consistent with the present finding: if differences in functional connectivity between SOR groups were limited to the set of intra-somatomotor connections as demonstrated by Schwarzlose and colleagues (2023), then this might not have constituted a robust enough difference to drive accurate model performance. Thus, this consistency further supports the interpretation that perinatal WSD and SOR are not characterized by altered sensory connectivity at the preadolescent developmental time point, save for differences in intra-somatomotor connectivity in humans. While this coherence between three studies might seem to suggest that the symptoms of SPD and SOR arise from other cognitive areas rather than purely sensory areas, Schwarzlose and colleagues (2023) demonstrated impacts to others connections that are still in line with a sensory-specific account of SOR. These areas included connections between the cingulo-opercular network and amygdala, which might account for atypical error detection and not just-right sensory experiences,

as well as connections between the hippocampus and sensory networks (sensorimotor and visual networks), which might explain impaired sensory prediction.

Additionally, it is promising that the only sensory-specific difference found by Schwarzlose and colleagues (2023) was decreased intra-somatomotor connectivity. Results from the 4 month old macaque data indicated that decreased intra-somatomotor connectivity was the strongest driver of model performance as evidenced by over-representation in the set of the 30 most important features as well as by occupying the top two spots in the feature set. The consistent direction of decreased connectivity in the perinatal WSD and highly-symptomatic SOR groups hints at a link between the dietary exposure and the behavioral outcome. It also suggests a plausible trajectory where the strongest differences at 4 months of age may persist and present as some of the only remaining differences in sensory connectivity at a later age. Altered intra-somatomotor connectivity is also in line with behavioral findings that show that most children with SOR experience over-responsivity in the somatosensory domain (Ben-Sasson et al., 2009).

Taken together, the present human analysis and the human study by Schwarzlose and colleagues (2023) provide outcomes that are consistent with the results demonstrated in the macaque analyses, encouraging further investigation into the relationship between perinatal WSD exposure and altered functional connectivity.

2.5.4. Maternal obesity and inflammation may be additive or alternative factors to maternal diet regarding impacts to functional connectivity

This study found an association between perinatal WSD and altered functional connectivity at 4 months of age, but it is possible that alternative, related factors may have had a different impact. For example, a WSD often induces an increase in adiposity, and it is possible that the increased adiposity is the downstream mechanism that impacts offspring functional connectivity. Thus, the higher incidence of increased adiposity in the WSD group would be the factor that drives group-level differences that are generally attributed to diet in this scenario. However, there is metabolic variability within the human and macaque populations, such that some individuals on a WSD remain lean and some individuals on a "control" diet develop obesity. Grouping by perinatal diet exposure therefore mixes subjects from different maternal adiposity exposures and dilutes any impact of adiposity. Grouping explicitly by maternal adiposity could instead lead to greater differences in functional connectivity between groups if adiposity is truly the downstream mechanism that impacts functional connectivity. Alternatively, maternal adiposity might not be the underlying mediator of dietary impacts but rather a separate factor that leads to different outcomes. Grouping explicitly by maternal adiposity could still reveal important information about whether these two factors act on neural circuitry in the same way or through different mechanisms. To explore these possibilities, the FRF analysis in 36 month old macaques was repeated using the same subjects and functional connections but a different predicted outcome measure: maternal adiposity (see Supplementary Material). Roughly half of the subjects from each perinatal diet group were exposed to a high level of maternal adiposity, so the two prenatal factors led to

distinct groupings. Maternal adiposity was measured as the percent body fat of the dam prior to pregnancy with the subject. However, both a regression model predicting percent body fat and a classification model comparing binary categories of maternal adiposity were unable to achieve significant performance metrics (Figure 2.7). This indicates that neither perinatal WSD exposure nor maternal adiposity were associated with altered functional connectivity of sensory and emotional processing areas at 36 months of age. This result adds confidence to the conclusion that the neural circuitry of the selected areas is relatively robust against long-term environmental impacts from the prenatal period.

Another potential mediator of altered circuitry related to WSD exposure is neuroinflammation. As mentioned previously, prenatal exposure to maternal inflammation may impact circuit formation *in utero*, but it is also possible for prenatal inflammation to program for long-term postnatal inflammation (Bilbo and Schwarz, 2009; Romero et al., 2007; Denizli et al., 2022). Postnatal inflammation, either deriving from prenatal WSD exposure or other life experiences, could continue to impact circuit formation through the process of synaptic pruning. Synaptic pruning is the process of removing weak connections between neurons. It is conducted by microglia, which are the resident immune cells of the brain. In a state of heightened neuroinflammation, microglia become activated. Research demonstrates that microglial activation can lead to dramatic differences in synaptic pruning activity, which impacts neural circuit formation and behavioral outcomes (Kim et al., 2017; Cowan and Petri, 2018; Kleinhans et al., 2016; Huang et al., 2016; Ypma et al., 2016). Thus, if differences in functional connectivity are able to predict a marker of increased neuroinflammation, then this would suggest that disruption to a microglial-mediated process like synaptic pruning may be responsible for

the alterations in circuitry. To explore this possibility, the FRF analysis in 36 month old macaques was repeated using a subset of subjects that had undergone a procedure for measuring neuroinflammation in the amygdala (see Supplementary Material). Increased neuroinflammation can lead to increased microglial proliferation and migration (Sarlus and Heneka, 2017; Belhocine et al., 2022; Lively and Schlichter, 2013), so the number of microglia in the amygdala was quantified for ten subjects from the 36 month imaging group. A subset of 53 connections between the amygdala and all ROIs within the sensory networks was used to predict microglial count with an FRF regression model. The model was unable to achieve significant performance metrics, however, so an association between amygdala connectivity and neuroinflammation could not be drawn (Figure 2.8). This finding is limited by the small sample size, so further research should seek to expand the analysis to a larger sample. Additionally, it would be interesting to repeat this analysis at the 4 month age point to see whether increased neuroinflammation leads to the same changes in functional connectivity as seen with perinatal WSD exposure. If both factors are associated with similar changes, and if there is high overlap between the perinatal WSD group and the subjects with increased neuroinflammation, this would suggest that perinatal WSD exposure may impact neural circuitry through increased neuroinflammation. Further research could identify whether microglia in particular mediate that relationship.

2.5.5. Limitations and Future Directions

The FRF is a powerful tool for predicting an outcome measure from a large set of independent and dependent features, but there are limitations to its capabilities. A

primary limitation is the reliance on widespread differences across many features between groups, or at least dramatic differences if restricted to a smaller subset of features. The FRF is not as effective at identifying differences in isolated features, as it is designed to learn patterns associated with each group rather than test for significant differences for each feature. Analyses that implement other approaches could be useful in identifying more subtle differences in connectivity associated with WSD exposure or a higher SOR score.

Several other analyses were attempted on the macaque and human data sets, but they did not reach significance. A latent growth curve analysis was performed on the macaque data to explore changes in connectivity strengths over time. This analysis models the trajectory of an outcome measure across the five time points, fits a line (linear, quadratic, or cubic) to the data, and reports the intercept and slope of the best-fitting line. The outcome measure could consist of a single connection, such as the connectivity strength between the amygdala and primary visual cortex at each time point, or it could consist of a latent variable measure derived from all connections within a network grouping, such as all amygdala-visual network connections. Once a best-fitting line was modeled across the data from all subjects, known as the "unconditional model," predictor variables like perinatal WSD exposure could be applied in a "conditional model" to examine whether the predictor resulted in a change in the trajectory. A significant difference in intercept between perinatal CTR and WSD subjects would indicate that the functional connectivity of the outcome connection was different prior to the 4 month time point, and a significant difference in slope would indicate that perinatal WSD exposure impacted the rate of change in the strength of the connection over time.

This analysis would have been useful for characterizing how connectivity changes across development with perinatal WSD exposure. However, the model was unable to fit an unconditional model for any single connection between the amygdala and any of the sensory ROIs used in the present study, and it was unable to fit an unconditional model for any latent variables derived from any network grouping that included the amygdala. Sensory-only connections and network groupings, which did not include a connection to the amygdala, were not tested in this analysis, as the goal was to test for altered connectivity to the amygdala as a potential explanation for SOR behaviors that are characterized by negative emotional responses to sensory stimuli. The latent growth curve model was unable to fit the data because there was high variance in connectivity strengths across subjects. For example, some subjects would start with a positive correlation for a given connection at 4 months of age, drop to a negative correlation by 11 months, and return to a positive correlation by 36 months of age, while other subjects would display the opposite trajectory. The resulting average from these data points would be a flat line around a correlation of 0, and the high variance across subjects would yield poor model fit metrics, meaning the model was not valid for fitting the data. Given that a coherent trajectory could not be modeled for any connection, it was determined that evaluating connections at each time point separately would be necessary. The strength of the FRF is that it can evaluate the entire set of connections, including sensory-only connections, in the same model, and the variability across subjects and connections would be beneficial as it would add information to the model. A future direction for the macaque data would be to apply another type of analysis that might be more sensitive at detecting focal differences between groups. The sparse supervised principal component

analysis (SSPCA) is one such analysis that is better equipped to identify focal differences across a wide set of features and may be better suited to the macaque data.

The human data similarly was unable to train the FRF, so several other analytical methods were pursued to attempt to better characterize the data. A partial least squares regression (PLSR) was performed to see whether the network groupings of the 378 features would form sub-groups, or components, that were associated with the SOR score outcome measure. This analysis yielded poor performance and could not be used to assess the data. Similarly, a repeated measures ANOVA demonstrated that there was no significant interaction between network grouping and SOR score; this was the same when using 4 SOR scores as when using 2, with the scores of "2," "3," and "4" aggregated into a group together. This analysis was adapted from a previously described method (Miranda-Dominguez et al., 2022). Lastly, an iterative SSPCA (Github, 2023) was run to attempt to identify focal differences across the set of 378 connections between the 4 SOR groups. The analysis implements a sparsity penalty that reduces the contributions of features with small effects so as to reduce their propensity to act as noise within the data set. This analysis was run with 3 principal components, using the delta kernel for the SOR output variable, with the sparsity penalty set to either 10 (a relatively low value) or the square root of 300 (relatively high, as the maximum value is the square root of 378, the number of features). However, the misclassification error rate never deviated significantly from chance, indicating that the set of 378 connections could not be used to reliably predict the SOR score in children, even when adjusting for noise.

Another major limitation to this study was the small sample sizes for the macaque data. Increased sample sizes may have reduced the variability in the connectivity patterns

observed within each group, which would have aided FRF model prediction. Additionally, even if perinatal WSD exposure was not associated with differences in connectivity at later time points, it would be interesting to see whether differences would emerge if only subjects from the perinatal WSD group that displayed the component behaviors of ASD were retained. A greater number of subjects would likely have been needed to pursue this analysis. Future studies could test for behaviors common to SOR in this cohort to assess whether there is an association between perinatal WSD exposure, SOR behavior, and differences in the functional connectivity of sensory processing areas at 4 months of age.

Similarly, the SOR score in humans may have been a poor outcome measure since it was a single item that relied on parental reporting of a subjective behavior. A more detailed series of questions or tests for SOR may have improved classification. While such a sample was obtained for this study—the functional connectivity strengths of children from the Autism Brain Imaging Data Exchange (ABIDE) who had received a valid diagnosis of ASD were acquired (ABIDE, 2017)—too few subjects had imaging data that passed the motion quality control standards set for this study, so the larger cohort from the ABCD study was selected instead. Future directions for this line of research could ensure larger samples of subjects with detailed behavioral data are acquired to reduce variability in imaging outcomes.

Another future direction for this study includes collecting imaging data in children across development. Since strong differences were found at the 4 month old age point in macaques, it is possible that distinct differences would be found in human infants, as well. This could be true for many neurodevelopmental disorders and brain

connections. Characterizing functional connectivity profiles at these early time points may lead to the development of a diagnostic tool that helps clinicians identify, validate, or predict neurodevelopmental outcomes. Early detection and intervention could allow caregivers to better support and accommodate these individuals. Additionally, a cross-species comparison of functional connectivity in 1 year old humans with SOR symptoms, or who later develop SOR symptoms, to the 4 month old macaques in this study could test for a relationship between perinatal WSD exposure and SOR, increasing what is known about perinatal risk factors for SPD.

2.5.6. Conclusions

Perinatal WSD exposure was associated with altered connectivity in sensory and emotional processing areas at 4 months of age but not at 6, 11, 21, or 36 months of age in macaques. These impacts are characterized primarily by decreased connectivity within the somatomotor network, within the visual network, and between the somatomotor and auditory networks; increased connectivity between the auditory and visual networks; and mixed effects between the somatomotor and visual networks. Connections to the amygdala were only weakly impacted. These results suggest that a prenatal risk factor for ASD, which is a disorder that is highly comorbid with SPD, may disrupt sensory connectivity during infancy, supporting the theory that altered sensory processing may serve as an origin for the symptoms of SPD. Interestingly, the continuation of postnatal WSD consumption was not sufficient to generate strong connectivity differences at 6 months of age, suggesting that the period of rapid synaptogenesis during the third trimester and first few months of life may be more susceptible to the impacts of WSD

exposure. The functional connectivity patterns of these same ROIs in preadolescent children with SOR were also unable to train an FRF model, as was the case in the developmentally comparable 36 month old macaques, demonstrating a consistency in null results across species. Taken together, these results suggest that the functional connectivity of sensory networks and the amygdala are largely robust against the influences of perinatal WSD exposure with age. However, the nature of the FRF analysis and the limitations of small sample sizes in the macaque cohort mean that nuanced differences in these or other sensory connections across the brain at later ages cannot be ruled out. Follow-up analyses could probe for focal differences in specific connections to ascertain whether any sensory-specific impacts remain at the later time points. Further research is needed to understand the remodeling mechanisms that alter brain circuitry by 4 months of age and the processes that mitigate differences at later ages. Lastly, additional cross-species comparisons are encouraged to better determine whether perinatal WSD exposure is a prenatal risk factor for SPD.

2.6. Supplementary Materials

2.6.1. Methods and Materials

2.6.1.1 Macaque Adiposity Measurements and Statistical Analysis

The imaging results from the 36-month age group were additionally used to predict the pre-pregnancy adiposity of each subject's mother. Adiposity could not be predicted at the other ages due to missing adiposity data. Adiposity was measured with dual-energy X-ray absorptiometry scans as previously described (Dunn et al., 2022). The percent body fat of each dam prior to the pregnancy with the subject was used as the predicted value for the regression analysis. This measure was divided into two categories to additionally create a binary classification measure. Dams with a percent body fat less than or equal to 19.6% were classified as "low adiposity," and those with greater than 19.6% body fat were classified as "high adiposity." This cut-off was chosen as it roughly corresponds to a body mass index (BMI) of 30 in humans, where values above 30 are considered "obese." Maternal pre-pregnancy percent body fat (mean $\pm$ SEM) was 19.25 $\pm$ 2.25% for the perinatal CTR group and 21.37 $\pm$ 2.25% for the perinatal WSD group in the present study. The number of subjects classified as being exposed to low and high maternal adiposity across the other demographic groups is represented in Table 2.6.

A regression FRF model was run on the 36-month old subjects using the 378 functional connections to predict percent body fat. A separate classification FRF model was run on the same subjects and connections to predict maternal adiposity group. Both models implemented 5-fold cross-validation with 6 repetitions, 1000 trees, and 90% of the data reserved for the training set, consistent with the parameters of the models used for the longitudinal analysis of perinatal WSD exposure.

Table 2.6. Demographic composition of macaque subjects at the 36 month time point that were exposed to maternal low or high adiposity.

Subjects in 36-month Group Classified by Maternal Adiposity Exposure (Low, High Adiposity)								
Scan Protocol	#1				#2			
Perinatal Diet	CTR		WSD		CTR		WSD	
Post-weaning Diet	CTR	WSD	CTR	WSD	CTR	WSD	CTR	WSD
Male	2, 0	2, 1	5, 0	1, 0	0, 1	0, 0	0, 4	0, 0
Female	2, 0	2, 0	1, 4	4, 0	0, 4	0, 0	0, 2	0, 0
Total	35							

2.6.1.2 Macaque Amygdala Marker of Neuroinflammation and Statistical Analysis

The imaging results from the 36-month age group were additionally used to predict the number of microglia and macrophages in the amygdala of each subject. This neuroinflammatory measure was collected for only a subset of subjects at 36 months of age following neuroimaging, so the analysis could not be conducted at other time points. As only 10 subjects had functional connectivity and amygdala staining data, results should be considered preliminary.

Following imaging, the number of microglia and macrophages, identified by immunofluorescent staining of ionized calcium-binding adaptor protein-1 (Iba1), was quantified as previously described (Dunn et al., 2022). Images were collected across 7 subregions of the amygdala. The average number of Iba1-stained cells per standard-sized image was calculated across all images collected at each subregion for each subject. Every subject had images from at least five of the seven amygdala subregions. This yielded between five and seven average counts per subject. The average of these average counts was calculated. This final value was considered the average number of Iba1-stained cells across the entire amygdala for that subject. All amygdala staining and cell

counting procedures were conducted by members of the Sullivan lab; Iba1-stained cell counts averaged across the amygdala for each subject were shared for use in the current analysis.

The demographic composition of the subjects included in this analysis is represented in Table 2.7. Offspring that were exposed to a perinatal WSD had a slightly greater number of Iba1-stained cells across the amygdala (Figure 2.6), with a group average of 23.6 cells compared to 21.3 cells for controls (not statistically significant).

Table 2.7. Demographic composition of macaque subjects at the 36 month time point that were included in the amygdala staining analysis.

Subjects in 36-month Group with the Amygdala Neuroinflammatory Measure								
Scan Protocol	#1				#2			
Perinatal Diet	CTR		WSD		CTR		WSD	
Post-weaning Diet	CTR	WSD	CTR	WSD	CTR	WSD	CTR	WSD
Male	1	0	1	0	1	0	1	0
Female	2	0	1	0	1	0	2	0
Total	10							

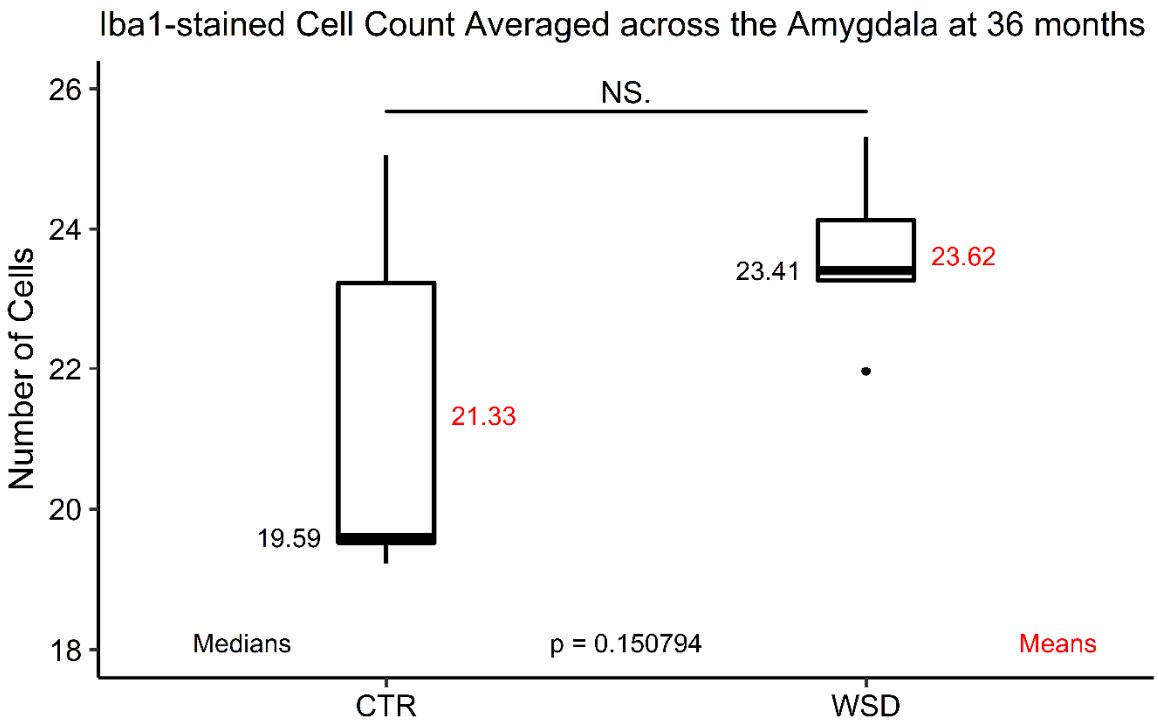

Figure 2.6. Iba1-stained cell count in the amygdala at 36 months.

The distribution of the number of Iba1-stained microglia and macrophages per image averaged across the amygdala trended slightly higher for offspring exposed to a perinatal WSD (n = 5) compared to controls exposed to a perinatal CTR diet (n = 5) at 36 months of age ($p > 0.05$, Wilcoxon rank sum test). Wide bars refer to the 25th/75th percentiles; thinner bars refer to the 2.5th/97.5th percentiles. Abbreviations: NS, non-significant.

All connections strictly between the amygdala and the sensory networks, totaling 53 connections including the connection between both hemispheres of the amygdala, were selected as training features for an FRF regression model. The model implemented 6-fold cross-validation with 5 repetitions, 3000 trees, and 90% of the data reserved for the training set. These parameters differed from those used in the longitudinal analysis of

perinatal WSD exposure with the goal of mitigating the high variance from the smaller sample size.

Additionally, all connections between and within the sensory areas and the amygdala, totaling 378 connections, were used to predict the average Iba1-stained cell count across the amygdala using a PLSR.

2.6.2. Results

2.6.2.1 Connections between sensory networks and the amygdala do not predict maternal adiposity at 36 months of age

Maternal adiposity, represented as percent body fat in a regression model and as binary categories in a classification model, was not predicted by the 378 connections between sensory networks and the amygdala at 36 months of age. Performance metrics for the FRF regression model, including the R, ICC, and MAE, were not significantly different between the observed and null (permuted data) models ($p > 0.05$ for each metric). Figure 2.7 demonstrates the weak, negative correlation between observed and predicted maternal body fat percentages for each subject, indicating the inability of the model to accurately predict maternal adiposity. Performance metrics for the FRF classification model were similarly poor, with the average overall accuracy, specificity, and sensitivity of the model lower for the observed model than for the null model (data not shown). As neither model demonstrated significant predictive capabilities, these models are not valid for predicting a subject's exposure to maternal adiposity from the functional connectivity within and between their sensory networks and the amygdala.

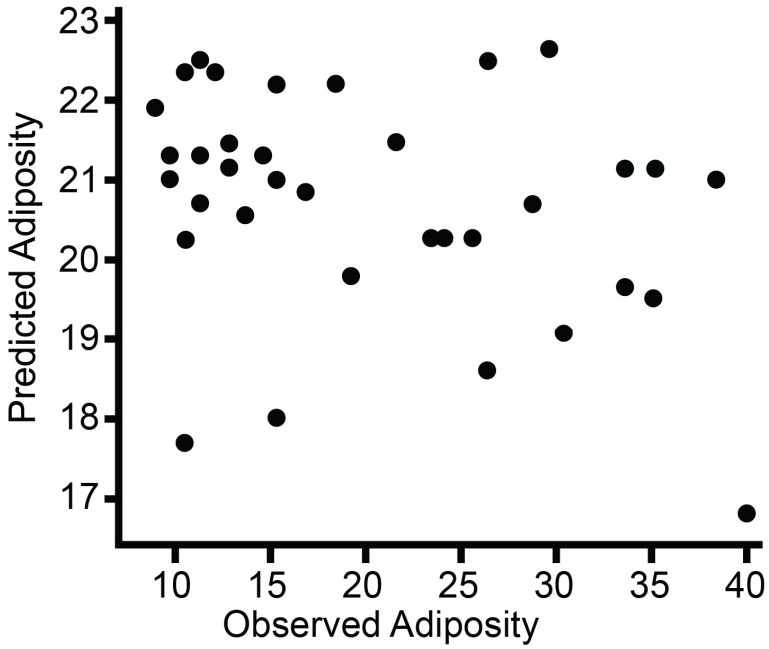

Figure 2.7. Adiposity predictions from the 36 month regression model.

A weak, negative correlation is demonstrated between the observed and predicted maternal pre-pregnancy adiposity values for each subject at 36 months of age. Adiposity is represented as percent body fat. Performance metrics for the FRF regression model, including the R, ICC, and MAE, were not significantly different between the observed and null (permuted data) models ($p > 0.05$ for each metric). Abbreviations: ICC, intraclass-correlation coefficient; MAE, mean absolute error; R, Pearson's correlation coefficient.

2.6.2.2 Amygdala connectivity does not predict amygdala neuroinflammation at 36 months of age

Measures of amygdala connectivity and neuroinflammation were collected in juvenile macaques at 36 months of age ($N = 10$) to explore a potential relationship between neuroinflammation and altered neural circuitry in a region implicated in SPD. The connectivity strengths of the 53 connections between the amygdala and all ROIs within the sensory networks (Bezgin et al., 2012) were used to train FRF model prediction. The predicted outcome variable was the average number of Iba1-stained microglia and macrophages across the amygdala of each subject. A strong, positive correlation between observed and predicted Iba1-stained cell counts would have demonstrated model accuracy, but this was not achieved by the model (Figure 2.8). Performance metrics for the FRF regression model, including the R, ICC, and MAE, were not significantly different between the observed and null (permuted data) models ($p > 0.05$ for each metric). Thus, the model was unable to use amygdala connectivity to predict a measure of neuroinflammation in the amygdala of offspring.

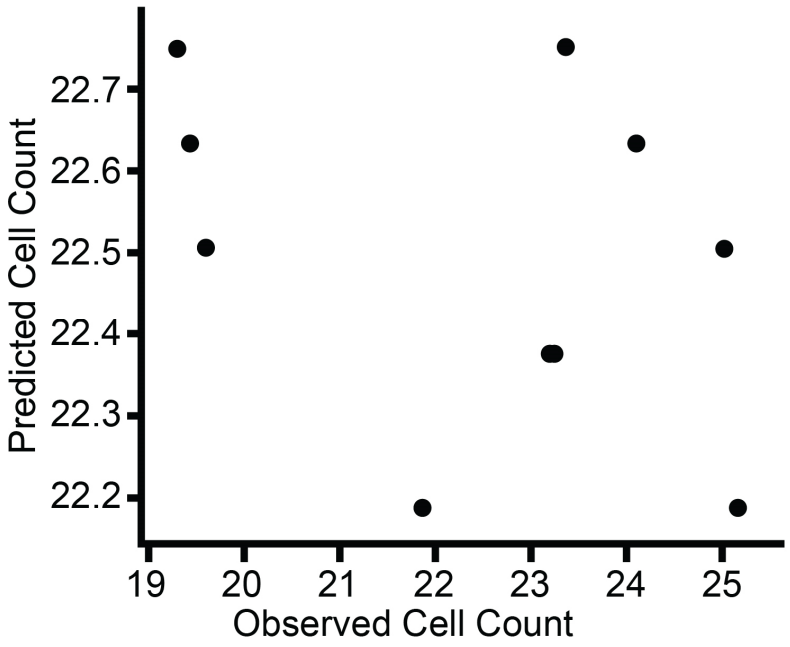

Figure 2.8. Amygdala Iba1-stained cell count predictions from the 36 month regression model.

The predicted number of Iba1-stained microglia and macrophages across the amygdala is compared to the observed number for each subject at 36 months of age (N = 10). The weak, negative correlation between observed and predicted Iba1-stained cell count demonstrates the inability of the model to accurately predict a marker of amygdala neuroinflammation from amygdala connectivity strengths. Performance metrics for the FRF regression model, including the R, ICC, and MAE, were not significantly different between the observed and null (permuted data) models ($p > 0.05$ for each metric). Abbreviations: ICC, intraclass-correlation coefficient; MAE, mean absolute error; R, Pearson's correlation coefficient.

Additionally, a PLSR was used to determine whether network groupings within the broader set of 378 connections between and within the sensory areas and the amygdala could predict average amygdala Iba1-stained cell count. As only 10 subjects were available for this analysis, a within-sample approach was used to maximize the available data. This approach revealed that several network groupings were able to predict cell count, as determined by a strong correlation between observed and predicted cell count. The network groupings with an r of 1.0 included somatomotor-auditory connections (8 components, $p < 0.01$), somatomotor-somatomotor connections (5 components, $p < 0.01$), amygdala-somatomotor connections (6 components, $p < 0.01$), and somatomotor-visual connections (5 components, $p < 0.01$), indicating that these connections were the most predictive of cell count. The connectivity within the visual-visual and visual-auditory network groupings similarly generated models that strongly predicted cell count with r values of 0.88 and 0.86 respectively (2 components and $p < 0.01$ for each). The auditory-auditory, amygdala-visual, and amygdala-auditory network groupings, however, were less predictive of cell count ($r = 0.62$, 0.61, and 0.59, respectively, for 2, 1, and 1 component, respectively, with $p < 0.05$ for all), indicating that there was more noise leading to weaker associations within the samples.

The PLSR was repeated using an out-of-sample approach to determine whether these findings were generalizable. Of the 10 subjects, 9 were used to train a model, and the amygdala cell count of the 10^{th} subject was predicted using its functional connectivity. This prediction was repeated once for each subject, yielding 10 model runs per network grouping. The distribution of the mean absolute error of these predictions was compared to that of 1,000 null models wherein the data were randomly permuted.

Using this approach, no network grouping achieved a significant or strong *r* value above 0.07 for any number of components. Additionally, the effect size (Cohen's *d*) between the two distributions of mean absolute error was small for each network grouping, indicating that the ability of the network connections to predict cell count in a novel sample is not meaningfully better than chance. This approach was similarly repeated with the cell count data normalized by a Box-Cox transformation rather than by z-scores, and was repeated while leaving 3 subjects out instead of 1, with similar non-significant findings. Thus, although the connectivity of certain network groupings was able to predict cell count in a data set that had been used to train the model, no network grouping was able to adequately predict cell count in a novel sample, demonstrating that the observed relationship between connectivity and cell count was not generalizable. The number of microglia in the amygdala likely does not have any strong bearing on the connectivity of sensory areas and the amygdala, though a larger sample size would be useful in confirming this finding.

CHAPTER 3. PERINATAL WESTERN-STYLE DIET EXPOSURE ASSOCIATED WITH DECREASED MICROGLIAL COUNTS THROUGHOUT THE ARCUATE NUCLEUS OF THE HYPOTHALAMUS IN JAPANESE MACAQUES

3.1 Abstract

Perinatal exposure to a high-fat, high-sugar, Western-style diet (WSD) is associated with multiple neurodevelopmental disorders, including autism spectrum disorders and attention-deficit hyperactivity disorder. This association may have an underlying inflammatory component, as consumption of a WSD during pregnancy can lead to an elevated inflammatory environment. Indeed, our group has previously shown that prenatal WSD exposure is associated with increased markers of inflammation in the placenta and fetal hypothalamus in non-human primates. In this follow-up study, we sought to determine whether this heightened inflammatory state persisted into the postnatal period, as prenatal exposure to inflammation has been shown to reprogram offspring immune function, and long-term neuroinflammation would present a potential means for prolonged disruptions to neurodevelopment. Neuroinflammation was assessed in one-year-old offspring by counting microglia and macrophages in the region of the hypothalamus examined in the fetal study, the arcuate nucleus (ARC). The ARC was chosen as it is sensitive to circulating immune factors due to its highly permeable blood-brain barrier. Resident microglia and peripherally-derived macrophages were immunofluorescently stained with their shared marker, ionized calcium-binding adaptor

protein-1 (Iba1), and quantified in eleven regions along the rostral-caudal axis of the ARC. A mixed effects model revealed main effects of perinatal diet ($p = 0.011$) and spatial location ($p = 0.003$) on Iba1-stained cell count. Perinatal WSD exposure was associated with a slight decrease in the number of Iba1-stained cells, and cells were more densely located in the center of the ARC. These findings suggest that the heightened inflammatory state experienced *in utero* does not persist postnatally. This inflammatory response trajectory could have important implications for understanding how neurodevelopmental disorders progress.

3.2 Introduction

A Western-style diet (WSD), which is calorically dense and typically high in saturated fats and sugar, is a prenatal predictor of behaviors common to multiple neurodevelopmental disorders including autism spectrum disorders and attention-deficit hyperactivity disorder (Gawlińska et al., 2021; Fernandes et al., 2021; Howard et al., 2011). Animal studies have similarly demonstrated an association between prenatal WSD exposure and increased anxiety-like behaviors (Sullivan et al., 2010; Peleg-Raibstein et al., 2012). This may have far-reaching impacts, as the consumption of a WSD is highly prevalent among individuals in the US (Hohos and Skaznik-Wikiel, 2017).

A potential mediator for how prenatal diet might impact offspring neurodevelopment is through maternal inflammation. Circulating inflammatory signals resulting from WSD consumption can impact the developing fetus by crossing or acting on the placental barrier, leading to increased exposure to *in utero* inflammation (Bolton and Bilbo, 2014; Bordeleau et al., 2021; Denizli et al., 2022).

Using a non-human primate (NHP) model of WSD-induced obesity, our group has previously shown that a prenatal WSD is associated with increased levels of inflammatory cytokines in the placenta and fetal hypothalamus, as well as increased microglial staining in the fetal arcuate nucleus (ARC) of the hypothalamus (Grayson et al., 2010). These results are characteristic of a heightened inflammatory state. Prenatal inflammation has been shown to disrupt neuronal proliferation, migration, and other aspects of circuit formation that may contribute to the progression of neurodevelopmental disorders (Vasistha et al., 2020; Dong et al., 2020; Denizli et al., 2022). Postnatal inflammation, and especially microglial activation, may similarly impact neurodevelopment by altering synaptic pruning and other processes. Given that prenatal exposure to inflammation is associated with altered postnatal immune states in offspring (Denizli et al., 2022), we hypothesized that the WSD-induced microglial response found in the fetal offspring would persist postnatally and continue to disrupt neurodevelopmental processes. To explore this possibility, the present study assessed neuroinflammation in the ARC of one-year-old offspring who were exposed to a perinatal WSD.

The hypothalamus is an ideal region to probe for neuroinflammation because it is located in a periventricular area of the brain where the blood-brain barrier (BBB) is generally more permeable to cytokines and other infiltrating inflammatory factors like macrophages (Rijnsburger et al., 2017; Haddad-Tóvolli et al., 2017). Exposure to these factors could induce microglial activation, which is associated with increased microglial proliferation (Sarlus and Heneka, 2017; Belhocine et al., 2022) and migration (Lively and Schlichter, 2013). It is therefore expected that individuals with inflammation that persists

from the perinatal exposure to WSD would have a greater number of microglia and macrophages present in the ARC. To assess this, microglia and macrophages in ARC tissue were stained with their shared protein marker, ionized calcium-binding protein-1 (Iba1), imaged via fluorescent microscopy, and counted. Cell counts were quantified at eleven regions along the rostral-caudal axis of the ARC to further determine whether a perinatal WSD is associated with region-specific differences. Considering that functionally distinct neuronal populations are distributed unevenly throughout the ARC, spatially-dependent impacts to microglial density could have specific functional repercussions. However, the distribution of microglia within the ARC under control conditions has not been sufficiently characterized in NHPs. This study addressed that gap by assessing counts across the full length of the ARC.

Our study revealed two main findings. First, perinatal WSD was associated with a slight but significant decrease in the number of Iba1-stained cells across the full ARC, which is opposite of the effect seen in fetal tissue. Consistent with other findings, this may elucidate a trajectory where prenatal WSD exposure induces a heightened neuroinflammatory response *in utero* that resolves when WSD is discontinued after weaning, distinguished by a potentially compensatory decrease in microglial proliferation and macrophage infiltration over time. Second, we found that Iba1-stained cells were more densely located in the center of the ARC compared to the rostral and caudal ends, independent of perinatal diet. Thus, periods of elevated inflammation and microglial activation may disproportionately impact centrally-located subpopulations of the ARC, such as those responsible for feeding. Taken together, these findings could inform previously demonstrated associations between WSD exposure, neuronal impacts in the

ARC, and decreased feeding behaviors in our NHP model. More broadly, these findings could have important implications for understanding how perinatal WSD exposure impacts neural circuit formation and leads to neurodevelopmental disorders.

3.3 Materials and Methods

3.3.1. Animal Model

This study used the same animal model as in Study 1, though different sets of subjects were included in the sample. Information about the animal model is repeated here with updated demographic information specific to the samples used in the present study.

All animal procedures were in accordance with National Institutes of Health guidelines on the ethical use of animals and were approved by the Oregon National Primate Research Center (ONPRC) Institutional Animal Care and Use Committee.

3.3.1.1 Adult Female Animals

Adult Japanese macaques (*Macaca fuscata*) were housed in indoor/outdoor pens containing 4–12 individuals each (male/female group ratio of 1-2/3-10). Animals were given *ad libitum* access to food and water. Breeding groups were assigned to either the experimental control (CTR) diet or Western-style diet (WSD) and were provided with fruits and vegetables for daily nutritional enrichment. Experimental diet compositions are described below. Females consumed their assigned experimental diet for at least fourteen months prior to offspring birth. Females were sedated two to three times during pregnancy for fetal dating and third trimester measures. Pregnant females gave birth

naturally in their social groups. Maternal age at offspring birth (mean ± SEM) was 7.96 ± 0.53 years for the CTR group and 9.91 ± 0.68 years for the WSD group in the present study. Maternal pre-pregnancy weight (mean ± SEM) was 8.61 ± 0.72 kg for the CTR group and 10.83 ± 0.88 kg for the WSD group in the present study.

3.3.1.2 Juvenile Offspring

The juvenile subjects in the present study were born over the course of four consecutive years. While offspring began consuming the maternal diet at 4 months of age, it became their primary food source by 6 months. This continued exposure to the same diet from gestation through lactation is therefore considered to be a perinatal rather than a purely prenatal dietary exposure. At a mean age of 8.00 ± 0.22 months for the CTR group and 8.82 ± 0.27 months for the WSD group (mean ± SEM), the offspring were weaned and relocated to group-housing with 6-10 similarly aged juveniles and 1-2 unrelated adult females. All juvenile subjects consumed the CTR diet after weaning. Necropsy occurred at a mean age of 12.80 ± 0.20 months for the CTR group and 13.70 ± 0.25 months for the WSD group (mean ± SEM).

A total of 16 juvenile subjects were selected for this study with groups balanced evenly for perinatal diet and sex. However, two female subjects were not included in the final analysis due to poor tissue staining. Of the remaining 14 subjects included in the analysis (CTR $n = 7$), each diet group had 3 female offspring. No maternal siblings were included; paternal identification was unknown.

3.3.1.3 Dietary Information

Regarding energy sources, the CTR diet (Monkey Diet no. 5000, Purina Mills) provided approximately 14.7% of calories from fat, 58.5% from carbohydrates, and 26.8% from protein. The WSD (TAD Primate Diet no. 5L0P, Test Diet, Purina Mills) provided approximately 36.6% of calories from fat, 45.0% from carbohydrates, and 18.4% from protein. Representative of a typical Western-style diet, the chemical composition of the experimental WSD contained a larger proportion of fats and sugars compared to the CTR diet. Saturated fat comprised approximately 0.9% of the CTR diet formulation and 5.4% of the WSD. Monounsaturated and polyunsaturated fats comprised 4.4% of the CTR diet and 9.0% of the WSD. Sugars (primarily fructose and sucrose) comprised approximately 3.1% of the CTR diet and 18.9% of the WSD. The animals that were fed the WSD were also provided with calorically dense treats (35.7% of calories from fat, 56.2% from carbohydrates, and 8.1% from protein) once per day. Macronutrient composition was obtained from diet specification sheets and is previously described (Thompson et al., 2017).

3.3.2. Tissue Collection

Juvenile brain tissue was obtained from the Obese Resource tissue bank. The tissue was collected as previously described (Thompson et al., 2017; Sullivan et al., 2010; Grayson et al., 2006; Rivera et al., 2015). Euthanasia adhered to the AVMA Guidelines on Euthanasia in Animals and standard operating procedures set by ONPRC. ONPRC Necropsy staff sedated the animals with Ketamine (15-25 mg/kg i.m.) before transportation to the necropsy room. Animals were deeply anesthetized with sodium

pentobarbital (25-35 mg/kg i.v.). After confirming anesthetic depth via loss of palpebral, corneal, pain, and pharyngeal reflex, the abdomen was incised and terminal blood samples were collected from the aorta or caudal vena cava. Exsanguination was completed via aorta severance. Brains were perfused by flushing the carotid artery with 0.9% heparinized saline (0.5-1 l) followed by 4% paraformaldehyde (PF, approximately 1-2 l) buffered with sodium phosphate ($NaPO_4$, pH 7.4) until fixed. Brains were partitioned into blocks and underwent the following applications: 24 hours at 4°C in 4% PF, 24 hours in 10% glycerol buffered with $NaPO_4$, 72 hours in 20% glycerol solution, frozen in -50°C 2-methylbutane, and stored at -80°C until sectioning. Coronal sections of the hypothalamus were collected in 1:24 series at a thickness of 25 μm using a freezing microtome as previously described (Grayson et al., 2006). Sections were stored at -80°C in cryoprotectant until staining.

3.3.3. Immunofluorescence for Iba1

Ten coronal brain sections, representing as much of the full rostral-caudal length of the ARC as available, were selected per subject. These sections were then grouped into two replicate samples of five sections each, with each replicate representing a roughly matched representation of the ARC. Replicates underwent the staining protocol four weeks apart. Slides were imaged within two to three weeks of staining. Order of staining, slide mounting, and imaging were balanced for perinatal diet and offspring sex and randomized as much as possible. The person performing the procedures was blinded to animal group and demographics.

Tissue sections were washed in potassium phosphate buffered saline (KPBS) and then blocked in 5% non-sterile donkey serum (NDS; Lot #3112604 and #3140992; Catalog #S30-100ML; Sigma-Aldrich) in 0.4% Triton-X into KPBS for 60 minutes at room temperature. The primary antibodies consisted of rabbit anti-Iba1 (Lot #PTK1381 and #PTG5394; Catalog #019-19741; 1:1,500; Wako Chemicals USA), for microglia and macrophage identification, and mouse anti-NeuN (Lot #GR3247200-1; Catalog #ab104224, 1:1000; Abcam) for identification of neuronal somas. The primary antibodies were diluted in 2% NDS into KPBS and applied to tissue sections for 60 minutes at room temperature followed by 22 hours at 4°C. Tissue sections were then washed in KPBS. The secondary antibodies for Iba1 (Donkey anti-Rabbit Alexa Fluor 488; Lot #2045215; Catalog #A21206; 1:1,000; Invitrogen) and NeuN (Donkey anti-Mouse Alexa Fluor 568; Lot #GR3238496; Catalog #ab175700-2; 1:500; Abcam) were diluted in 2% NDS into KPBS and were applied for 60 minutes at room temperature. Sections were washed again in KPBS and then counterstained using DAPI (Lot #2016420; Catalog #D3571; Molecular Probes) at a concentration of 3 μM in KPBS for 3 minutes at room temperature. After a final set of washes in KPBS, sections were mounted on gelatin subbed slides and coverslipped with ProLong Gold Antifade Mountant (Lot #2001971; Catalog #P36930; Invitrogen). Slides were stored at 4°C.

3.3.4. Image Collection

Images were captured using fluorescent microscopy on an Olympus VS110-S5 virtual slide scanner (Olympus America Inc., Center Valley, PA, USA). The microscope employed a BrightLine Sedat filter set (Semrock, Inc., Rochester, NY, USA) which

offered filters for 405 nm, 488 nm, and 561 nm optimized for DAPI, Alexa Fluor 488, and Alexa Fluor 568 respectively. The imaging plane was determined by manually focusing on DAPI staining. The fluorescent excitation was applied sequentially with an exposure time of 100 ms, 250 ms, and 175 ms for the 405 nm, 488 nm, and 561 nm filters respectively. One large area encompassing the ARC and surrounding regions was imaged per hemisphere at 20x for a total of twenty hemisphere images per subject (Figure 3.1C,D). Each hemisphere image was anatomically matched to one of eleven coronal locations containing the ARC as defined in the Paxinos Stereotaxic Atlas (Paxinos et al., 2009). Atlas-matched locations ranged between an interaural position of 17.45 mm (most rostral position) and 12.90 mm (most caudal position) rostral to ear-bar zero (EBZ), which corresponds to Bregma -04.50 mm and -09.00 mm (Figure 3.1A).

The size of the ARC varied across atlas-matched locations. To ensure cell counts were standardized for total ARC area across atlas-matched locations, the ARC was subdivided into standard-sized boxes. First, the perimeter of the ARC was determined based on structural landmarks. For example, in most sections located at an interaural position between 14.70 and 16.95 mm, the ventromedial hypothalamus was characterized by a high density of neurons stained brightly with NeuN, and the median eminence was characterized by a relative lack of NeuN-stained cells, allowing for the area of the ARC to exist between those two easily-identified structures. Then, square boxes of 1125 x 1125 pixels in size (approximately 360 x 360 μm) were arranged in a configuration that maximized the number of boxes that could fit within the confines of the ARC (Figure 3.1D). Each hemisphere image was then cropped in accordance with the placement of the

boxes. Each hemisphere image generated between one and seven cropped box images. A total of 837 cropped box images were collected from the 14 juvenile subjects.

Cropped box images, henceforward referred to as "images," were evaluated for focus quality. Images that were completely out-of-focus or were otherwise too blurry to be accurately counted, manually or automatically, were excluded from analysis. Poor quality images were found in generally equal proportions across all diet and sex groups. After excluding 130 images, a total of 707 images were included for the final analysis.

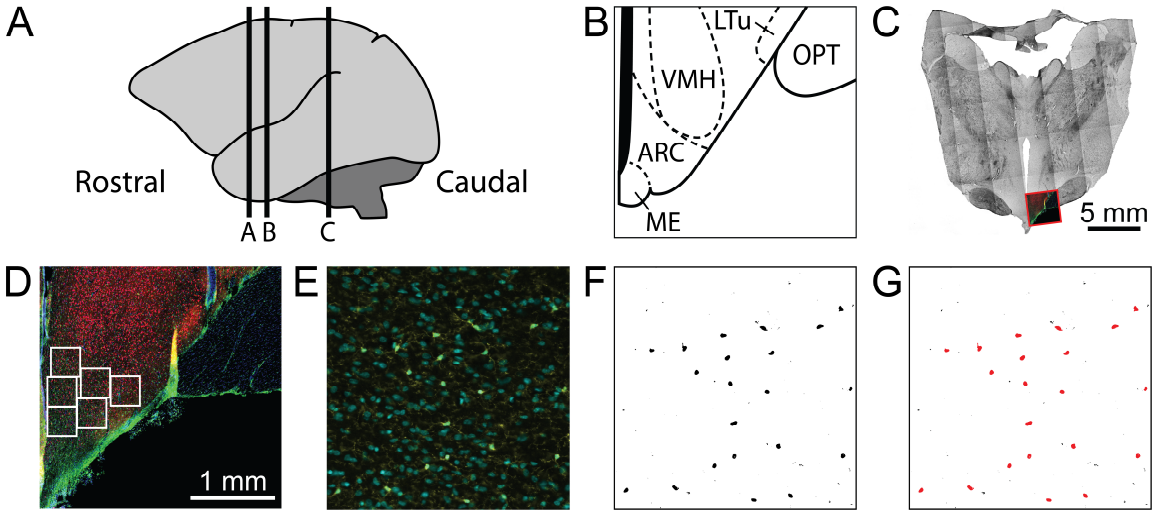

Figure 3.1. Image collection protocol.

After identifying the location of a slice within the ARC, immunofluorescent images were processed and cells were counted using ImageJ. **(A)** The ARC is located 17.45 mm (position A) to 12.90 mm (position B) rostral to ear bar zero (EBZ; position C). **(B)** Atlas reference for 15.15 mm rostral to EBZ. Section position was determined based on structural landmarks apparent in the fluorescent image including observation of the median eminence and shape of the ventromedial hypothalamus. **(C)** Brightfield overview image at 10x magnification of a coronal section 15.15 mm rostral to EBZ. ARC is located

at the base of the brain alongside the third ventricle. Box overlay denotes the area that was fluorescently imaged. **(D)** Immunofluorescent image from the box overlay area in **(C)**. Immunofluorescent images were acquired on a slide scanner at 20x. Blue = DAPI, Green = Iba1, Red = NeuN. Standard-sized boxes (white) of 1125 x 1125 pixels (approximately 360 x 360 μm) were placed over the ARC to maximize coverage of the area without overlapping neighboring regions. These boxes were used to crop the immunofluorescent image into standard-sized ARC images that were processed and underwent cell counting. **(E)** One of the cropped ARC images from the source image in **(D)**. ARC images were processed in ImageJ to display the DAPI channel in cyan and the Iba1 channel in yellow, allowing for the cell bodies of interest to appear teal in color. The automated color thresholding method, Maximum Entropy, was optimized to recognize the teal color ranging between 50 and 109 (hue display limits) and produce the binary image shown in **(F)**. **(F)** Binary images derived from the overlap of DAPI and Iba1 staining were used in the automated counting algorithm. **(G)** Red areas denote which cell objects from the binary image in **(F)** were counted by the automated counting algorithm optimized for objects larger than 110 square pixels in area. This image shows that all cells visible in **(E)** were successfully counted. Brain illustrations in **(A)** and **(B)** were adapted with significant changes from the Paxinos Stereotaxic Atlas (Paxinos et al., 2009). Abbreviations from **(B)**: ARC, arcuate nucleus; ME, median eminence; OPT, optic tract; LTu, lateral tuberal nucleus; VMH, ventromedial hypothalamic nucleus.

3.3.5. Automated Cell Counting

ImageJ software (Fiji; Schindelin et al., 2012) was used to develop an automated procedure that would process the images and measure the number of Iba1-stained cells per image. Before these image processing and cell counting parameters were fully optimized, thresholding strategies were evaluated. First, the channel-specific images from the Iba1 and DAPI channels were pseudocolored yellow and cyan respectively and merged to form an image that displayed the overlap of Iba1 staining and cell nuclei (Figure 3.1E). This highlighted microglia and macrophage cell bodies in teal and distinguished them from any soma-shaped processes and artifacts in yellow. The resulting images were considered "raw" as their intensity values had not been manipulated. Preliminary testing revealed that applying ImageJ's color threshold to the merged images led to a substantially more accurate cell count than applying a grayscale intensity threshold to single-channel Iba1-only images. The color threshold was based on adjusting the display limits, or pixel values ranging from 0 to 255, of the hue component of the Hue, Saturation, and Brightness (HSB) settings. The merged images and promising hue display limit options were therefore chosen for use in the optimization analysis. To determine the full set of optimal parameter settings that would generate automated cell counts with the greatest accuracy, a train-then-test approach was utilized (Figure 3.2).

Two independent sets of twenty images each were selected for the train-then-test approach. These image sets were matched across a range of image quality characteristics, such as acceptable variations in staining intensity and focus, and balanced for experimental diet group and sex. Six images from each set were derived from offspring that had been exposed to a perinatal WSD and post-weaning WSD; however, these

subjects and their images were not included in the final analysis due to their incongruent post-weaning diet. One image set was exposed to the full range of parameter settings to assess the accuracy of each combination ("Train Set"), and the other set was reserved for validating the combination that achieved the greatest accuracy ("Test Set"). The number of Iba1-stained cells per image were manually counted for each image in each set by two blinded, trained observers. The counts were similar enough that a single observer's counts were recorded for every image rather than deriving an average count.

The procedure for determining the optimal parameters settings that would lead to the most accurate automated count included the following steps. 1) The color-merged images underwent one of four processing methods to better distinguish cell bodies from the background. 2) The processed images underwent a color threshold which isolated the teal-colored cell bodies by adjusting the lower and upper hue display limits, and a thresholding method was applied to pixels in the narrowed color range. 3) The color-thresholded, binary images underwent an object size threshold where the "Analyze Particles" function was used to generate a count of any object that covered an area greater than a set minimum size. 4) The automated count was compared to the manual count to assess the accuracy of each parameter combination. A more detailed explanation of these four steps can be found in the Supplementary Material.

An ImageJ macro was created to automatically run the full Train Set of twenty images through the four steps, described above. This macro determined the accuracy of 7500 combinations of processing, color thresholding, and object size thresholding parameter options. Combination 8 had the greatest accuracy score of 90.4% and consisted of the following parameter settings. Processing method: Raw. Color Threshold

Algorithm: Maximum Entropy. Color Threshold Hue Display Limits: 50-109. Minimum Object Size: 110 square pixels.

The combination with the greatest accuracy in the Train Set, Combination 8, was validated on the Test Set. The parameter settings were applied to all twenty images of the Test Set, and the resulting final accuracy score was 85.3%, surpassing the minimum acceptable accuracy score of 80% (Xing and Yang, 2016; Lunde and Glover, 2020).

A final step in validating the accuracy score was undertaken. It was important to ensure that the automated method was counting the same Iba1-stained cells identified by the trained observer, rather than simply counting the same number of non-cell objects and artifacts. To ensure the automated and manual methods counted the same target objects, an error rate was calculated for each combination. A more detailed explanation of the error rate can be found in the Supplementary Material, but briefly, the error rate is the sum of the automated method's missed cells and false positives divided by the total number of manually counted cells. When applied to the Train Set, Combination 8 yielded an error rate of 0.286. Only 360 of the other 7499 parameter combinations yielded a better error rate, with the lowest error rate recorded as 0.216. When applied to the Test Set, Combination 8 yielded an error rate of 0.221. These error rates indicated that the reported accuracy of the automated counting method, Combination 8, was highly valid. Thus, Combination 8 was used with the full data set of 707 images. A separate ImageJ macro was used to apply the parameter settings of Combination 8 and automatically count the Iba1-stained cells for each image in the full data set. Cell counts were saved to a csv file.

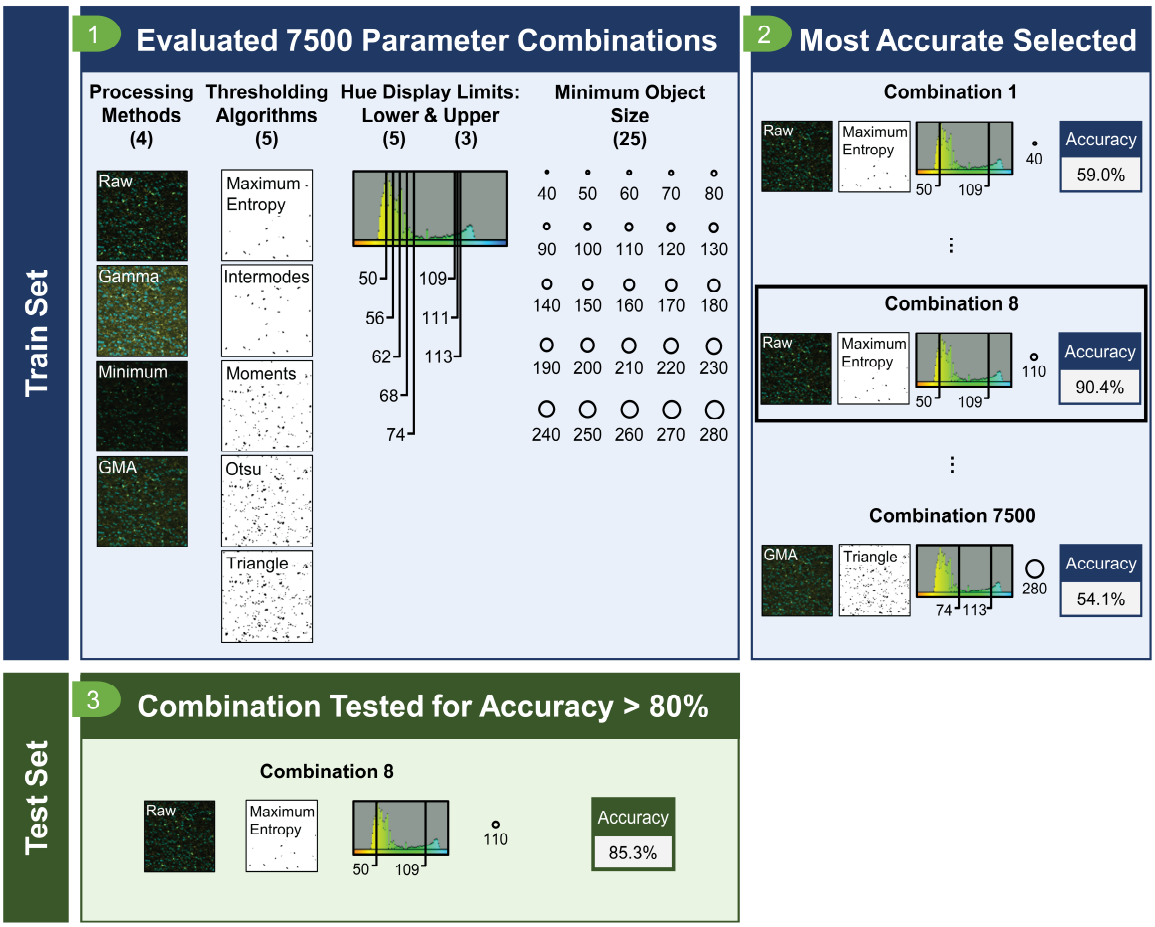

Figure 3.2. Optimizing the parameter settings for the automated counting procedure.

Two independent sets of twenty ARC images each were selected for the purpose of optimizing the procedure used to automatically count cells. One set was used for the parameter optimization ("Train Set"), and the other set was reserved for validating the optimized method ("Test Set"). Step 1: A total of 7500 parameter combinations (consisting of four processing options, five thresholding algorithms, five lower and three upper values for the hue display limits, and twenty-five minimum object sizes) were applied to each image in the Train Set. The example binary images in the Thresholding Algorithms column were derived from the Raw image thresholded within a color range of

50-109 (hue display limits). The object size circles are illustrative and are not actual size or shape. Step 2: The combination with the highest accuracy score was selected for validation. Step 3: The combination that achieved the highest accuracy score in the Train Set was confirmed if it achieved an accuracy score above 80% on the Test Set. Abbreviations: GMA, Gamma-Minimum-Average.

3.3.6. Statistical Analysis

This study used mixed effects modeling to investigate the impacts of perinatal diet and spatial location within the ARC on cell count. A mixed effects model was chosen for its ability to account for the variability introduced by the partially-crossed study design (Harrison et al., 2018; Brown, 2021). In addition to the fixed effects of diet and location, the model included random effects to account for the random variability in the number of images sampled from every subject and every location; this variation naturally arose from the differences in the number of standard-sized boxes (1125 x 1125 pixels in size, covering approximately 360 x 360 μm in area) that could fit within the area of the ARC for each hemisphere. The random effects of subject and location were partially crossed as not every subject was sampled at every atlas-matched location (Figure 3.3). For example, images from the first subject depicted in Figure 3.3 were only captured at four distinct locations: interaural positions 15.60, 14.70, 13.80, and 13.35 mm. Note that only 5 other subjects had images sampled from interaural position 13.35 mm, and each of those subjects had substantially fewer images at that location than did the first subject. Thus, the images and cell counts at 13.35 mm were heavily weighted towards the first subject. When trying to understand the impact of location on cell count at interaural position

13.35 mm, the average cell count at this location would be disproportionately impacted by a single subject and their specific background, including the likely salient impact of their perinatal diet group. Inclusion of the partially crossed random effect addressed the unequal representation of subjects and locations by controlling for the variation in the number of images derived from each.

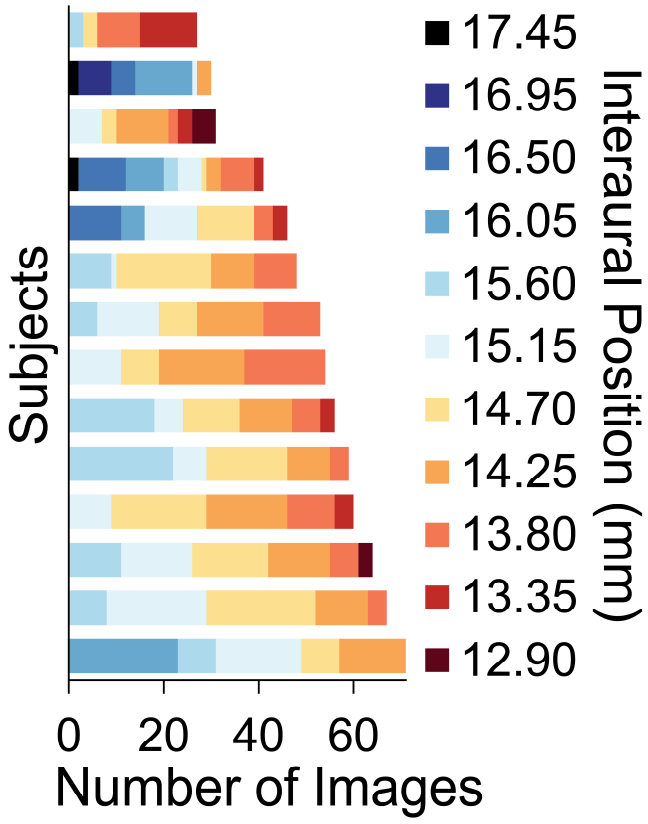

Figure 3.3. Partially-crossed sample.

A variable number of images were collected from each subject at variable locations in the ARC. This partially-crossed effect was accounted for as a random effect in the mixed effects model. Interaural position is rostral to EBZ, with 17.45 mm as the most rostral atlas-matched location.

The model was run using the lmerTest package in R (Kuznetsova et al., 2017), which implemented Satterthwaite's degrees of freedom method when calculating the type III analysis of variance (ANOVA) table for the model fits. The model formula that was ultimately selected for the final analysis was:

Cell Count ~ Perinatal Diet + Spatial Location + (1 | Subject : Spatial Location)

where *Cell Count* is the outcome variable, *Perinatal Diet* and *Spatial Location* are the fixed effects, and the remaining component constitutes the random effects. The fixed effect, *Spatial Location*, was represented by the syntax, *poly(Spatial Location, 2)* in R to denote the quadratic, second-order polynomial relationship between *Spatial Location* and *Cell Count*. The syntax, *(1 | <effects>)* indicates that the random effect is a random intercept where, holding the slope constant, the intercept is allowed to vary for each level of the random effects. The syntax, *Subject : Spatial Location* recognizes that the random effects are partially crossed and instructs the model to look for the interaction between subject and spatial location. Thus, the model expects the relationship between perinatal diet and cell count to remain constant (fixed slope) while recognizing that some locations may be predisposed to having higher cell counts than other locations (random intercept), and it allows for that variability. Similarly, the model expects the relationship between location and cell count to remain constant while recognizing that the subjects sampled at each location may be predisposed to having higher cell counts due to their perinatal diet group, and it allows for that variability as well.

Perinatal Diet and *Subject* were represented as categorical variables. The true spatial location of each image ranged along a continuous axis between interaural position 17.45 and 12.90 mm rostral to EBZ, but images were assigned one of eleven positions based on best alignment to the atlas (Paxinos et al., 2009). Thus, *Spatial Location* was treated as a continuous variable in the fixed effect to represent the continuous nature of the factor, and it was treated as a categorical variable in the random effect to account for the grouping ability of the factor.

A series of Chi-squared tests were used to determine that the formula above comprised the best fitting model (Table 3.1). An interaction effect between perinatal diet and spatial location was considered, but it was excluded from the model because it did not contribute significantly to the fit. Even when included, the interaction effect between location and perinatal diet was non-significant ($p > 0.05$), indicating that cell count varies along the rostral-caudal axis independently of the effects of the perinatal diet. Additionally, there was no main effect of offspring sex or interaction effect between sex and the other factors of interest, so sex was similarly excluded from the model. Spatial location was better fit by a quadratic term than a linear one, though there was still a main effect of spatial location on cell count with a linear fit (Figure 3.6).

3.4 Results

3.4.1. Perinatal WSD was associated with a decreased number of Iba1-stained cells in the ARC

When collapsing across all atlas-matched locations, the mixed effects model indicated a main effect of perinatal diet on Iba1-stained cell count (Figure 3.4). The cell

count was decreased in the perinatal WSD group compared to the perinatal CTR group ($p = 0.022$), with a median count of 26 cells in the WSD group compared to 29 cells in the CTR group. This result is distinct from prior effects seen in fetal tissue (Grayson et al., 2010).

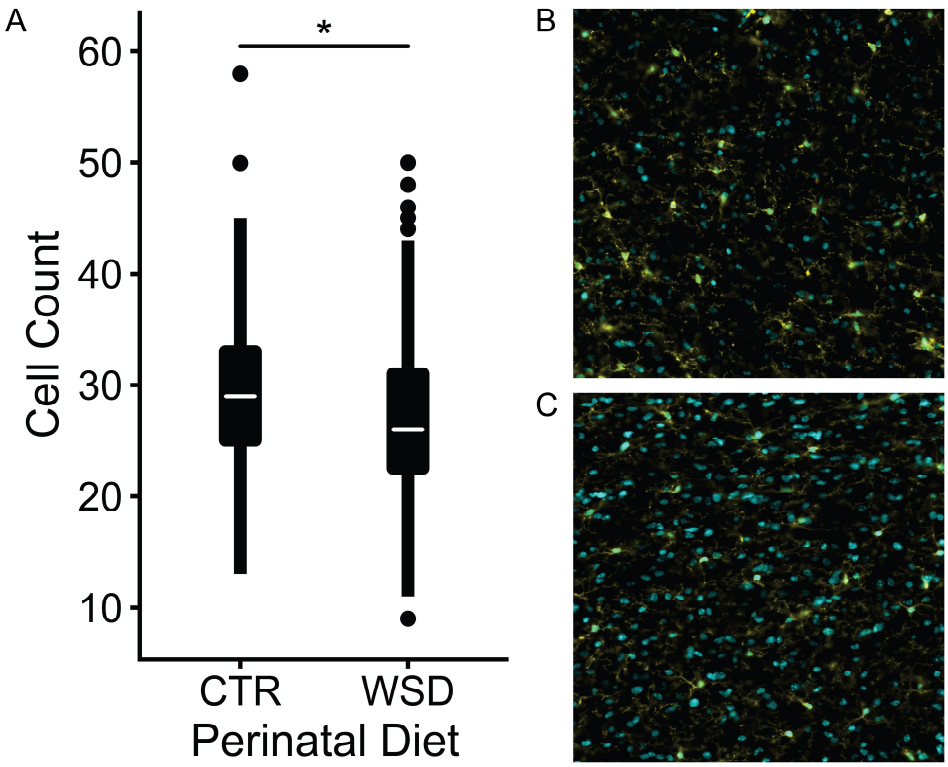

Figure 3.4. Iba1-stained cell count by perinatal diet exposure.

Perinatal WSD associated with decreased Iba1-stained cell count. **(A)** Iba1-stained cell count was decreased in the perinatal WSD group compared to the perinatal CTR group (p = 0.011). **(B)** Representative image from the perinatal CTR group displaying 29 Iba1-stained cells, the median for the group. **(C)** Representative image from the perinatal WSD group displaying 26 Iba1-stained cells, the median for the group. The images from **(B)** and **(C)** are derived from male animals and were collected from interaural position 14.25 mm rostral to EBZ. The data presented in **(A)** represent all 707 images included in the analysis deriving from all spatial locations along the rostral-caudal axis of the ARC.

3.4.2. Distribution of Iba1-stained cells was increased near the midpoint of the ARC

Iba1-stained cells were more densely located near the midpoint of the rostral-caudal length of the ARC compared with the distal ends in a distribution that was best fit by a quadratic curve (Figure 3.5). Using all 707 images captured from 14 subjects across 11 distinct atlas-matched locations in the ARC, the mixed effects model indicated a main effect of spatial location on cell count (p = 0. 029). The interaural position with the greatest Iba1-stained cell count was at 15.15 mm rostral to EBZ (n = 125 images), the midpoint of the eleven atlas-matched locations, with a median count of 30.0 cells. The distal rostral and caudal ends, at 17.45 mm (n = 4 images) and 12.90 mm (n = 8 images) respectively, had median cell counts of 26.5 and 27.5 cells, respectively. The location with the fewest number of Iba1-stained cells was at interaural position 13.35 mm (n = 27 images), directly adjacent to the most caudal location, with a median count of 22.0 cells. This analysis was additionally repeated with spatial location treated as a linear fixed effect rather than a quadratic term. This change yielded a main effect of location, suggesting a slight linear increase in cell count towards the rostral end of the ARC (Figure 3.6). However, the quadratic model was a better fitting model than the linear model (see Supplementary Material), so the cell distribution was interpreted in accordance with the quadratic fit.

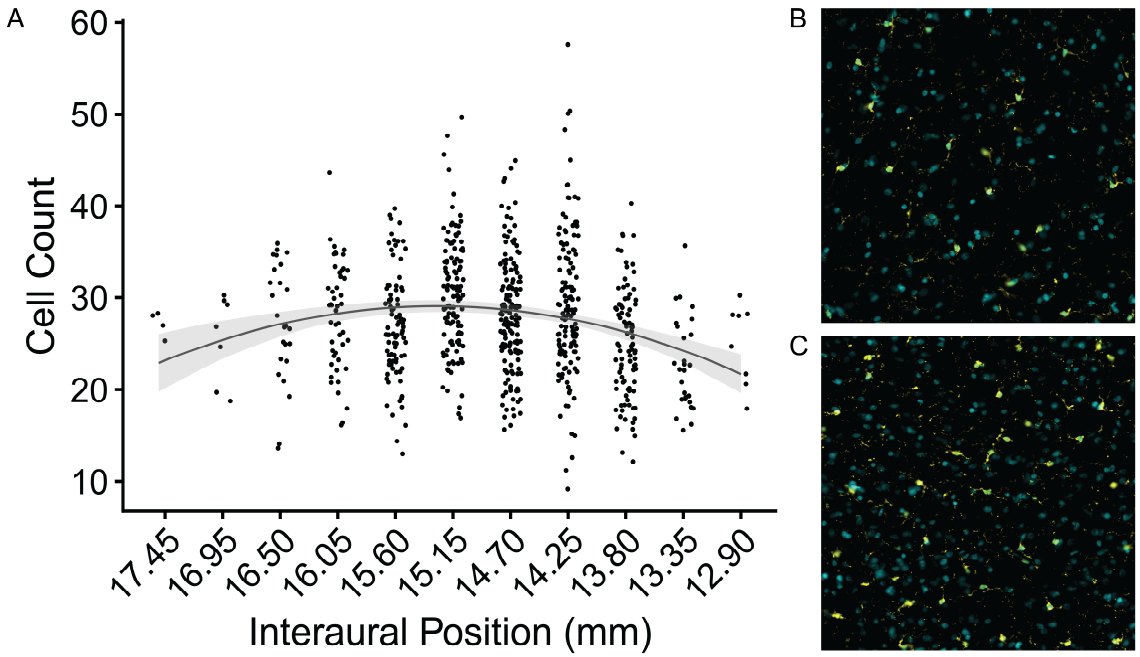

Figure 3.5. Distribution of Iba1-stained cells across the ARC.

(A) The Iba1-stained cell count distribution, fit by a quadratic curve, revealed an increased cell count towards the midpoint of the ARC along the rostral-caudal axis compared to the distal ends ($p = 0.003$). Interaural position is rostral to EBZ, with 17.45 mm as the most rostral atlas-matched location. **(B)** Representative image from interaural position 16.50 mm displaying 19 Iba1-stained cells. **(C)** Representative image from interaural position 14.70 mm displaying 43 Iba1-stained cells. The images in **(B)** and **(C)** are derived from the same animal, a one-year-old female exposed to a perinatal CTR diet. The data presented in **(A)** represent all 707 images included in the analysis deriving from all subjects across both diet groups.

3.5 Discussion

This study followed up on the previously reported finding of increased Iba1 immunoreactive area and staining density in the ARC of fetal macaques exposed to a WSD (Grayson et al., 2010). We assessed whether the increased neuroinflammation persisted in one-year-old offspring. A heightened inflammatory state can increase microglial proliferation (Sarlus and Heneka, 2017; Belhocine et al., 2022) and migration (Lively and Schlichter, 2013) and lead to a greater number of circulating macrophages that can infiltrate through the permeable BBB near the ARC. Thus, neuroinflammation was measured by counting the number of Iba1-stained cells, which include microglia and infiltrating macrophages, that were present throughout the ARC.

Two novel findings resulted from this study. First, perinatal WSD was associated with marginally lower Iba1-stained cell counts across the ARC, indicating that the elevated inflammatory state demonstrated *in utero* might not persist one year later and may even reverse slightly. Second, independent of perinatal diet, there was a modest increase in the Iba1-stained cell count in the middle of the ARC compared with the rostral and caudal ends, best fit by a quadratic curve. These findings have important implications for offspring development and the functionality of the ARC.

3.5.1. Arcuate nucleus impacts energy homeostasis and is particularly vulnerable to neuroinflammation

Although the ARC was selected particularly for its susceptibility to the infiltration of macrophages, the region is also relevant to the model of a WSD. The ARC plays a prominent role in the regulation of hunger, energy homeostasis, and body weight.

Incoming satiety signals prompt the ARC to decrease feeding and increase energy expenditure through the release of α-melanocyte-stimulating hormone (αMSH), a melanocortin receptor ligand, by the pro-opiomelanocortin (POMC) neurons of the ARC. Conversely, when receiving hunger and energy deprivation signals, the ARC increases feeding by inhibiting the POMC neurons and releasing an inverse agonist to the melanocortin receptors, agouti-related peptide (AgRP), which opposes the binding of αMSH. This activity is accomplished by the neuropeptide Y and agouti-related peptide (NPY/AgRP) neurons of the ARC. The POMC and NPY/AgRP neurons of the ARC are therefore considered to be opposing branches of the melanocortin system. Mutations to the melanocortin system result in increased feeding, decreased energy expenditure, and increased likelihood of developing obesity (Joly-Amado et al., 2014; Grayson et al., 2010).

Critically, the neuronal differentiation and gene expression of POMC and AgRP neurons are controlled through epigenetic mechanisms that are sensitive to the prenatal environment (Croizier and Bouret, 2022). In particular, perinatal exposure to a high-fat diet (HFD) in rats was associated with increased DNA CpG methylation of the *Pomc* promoter, indicating gene silencing of the neurons that typically decrease feeding, accompanied by increased body weight. The methylation was not reversed by post-weaning consumption of the standard chow, demonstrating the long-term, epigenetic impact that perinatal HFD exposure can have on neuronal functioning (Marco et al., 2014). Although the extent to which neuroinflammation synergistically advances epigenetic modifications to melanocortin circuitry is still unknown (Cesar and Pisani, 2017), neuroinflammation may impact neuronal signaling through other pathways.

Microglia play an important role in the brain by clearing debris and generating necessary immune responses, but they also play a functionally relevant role by interacting with the neurons of the ARC. Microglia express receptors for the neuropeptides produced by POMC and NPY/AgRP cells, such as αMSH and NPY, indicating that their activity could be modulated by the activity of the neuron populations in the ARC (Barnea et al., 1998; Forslin Aronsson et al., 2006; Lindberg et al., 2005). Furthermore, short-term exposure to a HFD acutely decreases AgRP mRNA expression and leptin sensitivity in NPY/AgRP neurons (Huang et al., 2003; Olofsson et al., 2013) and causes microglia in the ARC to undergo morphological and functional changes characteristic of a proinflammatory response (Thaler et al., 2012; Horvath et al., 2010), potentially implicating microglia in the dietary impacts to the melanocortin system (Jastroch et al., 2014).

The present finding fits well with this relationship. Our group previously demonstrated a reduction in AgRP mRNA expression in conjunction with an upregulation of inflammatory brain cytokines and increased microglial staining in the ARC of fetuses exposed to a prenatal WSD (Grayson et al., 2010). While not conclusive, this supports the premise that there may be an interaction between increased microglial activity and adverse effects on NPY/AgRP neurons during this period of heightened inflammation. However, in one-year-old offspring, perinatal WSD exposure was not associated with a significant difference in AgRP fiber density in the ARC, indicating that the effects from the prenatal exposure had waned. Instead, there was a significant reduction in AgRP fiber density in offspring exposed to a postnatal WSD, regardless of perinatal diet, further indicating that direct WSD exposure is needed to significantly

reduce NPY/AgRP neuron density (Sullivan et al., 2017). The follow-up study did not, however, investigate the role of microglia. The present study fills this gap by examining the number of microglia and macrophages in the ARC of one-year-old offspring. The findings of this study, that offspring with perinatal WSD exposure exhibited slightly fewer Iba1-stained cells than controls, was consistent with the absence of a significant reduction in AgRP fiber density previously reported in one-year-old offspring.

Additionally, these findings are metabolically relevant. The reduction in AgRP mRNA expression during the fetal period would suggest decreased binding of AgRP to the melanocortin receptors, resulting in increased energy expenditure. As expected, the fetal WSD offspring demonstrated reduced body weight on gestational day 130 (McCurdy et al., 2009). Once the AgRP fiber density was comparable to that of the control subjects in the one-year-old offspring, other metabolic measures similarly returned to baseline, including no difference in food intake, physical activity, energy expenditure, or total metabolic rate; body weight, however, was increased in the perinatal WSD offspring as early as 6 months after birth, demonstrating a potentially compensatory increase in growth after separation from the *in utero* environment while still prior to weaning (Sullivan et al., 2017). Importantly, the offspring that were exposed to the postnatal WSD, regardless of perinatal diet, exhibited reduced food intake and increased physical activity at one year of age, consistent with the demonstrated reduction in AgRP fiber density at that time point (Sullivan et al., 2017).

Taken together, these results indicate that the melanocortin system may interact with microglia in the ARC and is likely more susceptible to disrupted functioning during

periods of heightened inflammation associated with direct WSD exposure or during fetal development.

3.5.2. Microglia and neuroinflammation impact developmental processes such as synaptic pruning

In addition to clearing debris and potentially communicating with the melanocortin system, microglia also play an important role in synaptic pruning. While it is unclear whether microglia are actively removing synapses or simply phagocytosing them after they have been targeted for clearance by other means, there is evidence to suggest that deficits in microglial phagocytic function reduce synaptic elimination and impact circuit connectivity (Cowan and Petri, 2018; Filipello et al., 2018; Kopec et al., 2018; Kim et al., 2017). Crucially, maternal immune activation in mice has been shown to decrease expression of genes associated with phagocytosis in microglia, suggesting a relationship between maternal inflammation and decreased synaptic pruning (Kim et al., 2017; Cowan and Petri, 2018). Additionally, in mice lacking the fractalkine receptor, the number of microglia present in the developing brain was transiently reduced and synaptic pruning was delayed, suggesting that synaptic refinement is dependent upon the number of microglia (Paolicelli et al., 2011). Microglia also regulate neurogenesis by phagocytosing neural precursor cells during prenatal and early postnatal development, with increased microglial activation or quantity leading to increased phagocytosis (Cunningham et al., 2013). Thus, the decreased Iba1-stained cell count exhibited by offspring with perinatal WSD exposure might affect neurodevelopment and long-term

behavioral outcomes through reduced synaptic pruning and neural precursor cell phagocytosis.

3.5.3. Present finding of low inflammation associated with perinatal WSD is distinct from the fetal outcomes and informs a neurodevelopmental trajectory

While the present finding of decreased Iba1-stained cell count in the perinatal WSD group seemingly contradicts the increased microglial staining found in fetal ARC tissue, this difference may instead elucidate a trajectory where the heightened neuroinflammatory response in utero resolves when WSD is discontinued after weaning. This drop in cell count may be compensatory in nature, or it may be part of a longer-term reprogramming. A follow-up study at a later time point would demonstrate whether the prevalence continues to decrease throughout adolescence, stabilizes to the same levels as in control subjects, or rebounds to an elevated level. Notably, this finding is consistent with prior work by our group which found an association between perinatal WSD and decreased microglial counts in the amygdala at the same one-year postnatal time point in this NHP model (Dunn et al., 2022).

Maternal inflammation has been shown to program long-term increases in offspring inflammation (Bilbo and Schwarz, 2009; Romero et al., 2007), but diet-specific evidence suggests a trajectory where prenatal WSD may protect against offspring inflammation. In a porcine model of HFD-induced atherosclerosis, a chronic inflammatory and immune disease of artery walls, swine who had previously been exposed to a maternal HFD were at a lower risk of atherosclerosis compared to those who

were exposed to a standard maternal diet, suggesting that a maternal HFD may be protective against some types of future inflammatory risks (Norman and LeVeen, 2001). Additionally, microglia prevalence changes dynamically over the course of long-term WSD exposure. Mice showed an increase in Iba1-stained cell number in the hypothalamus after 3 and 14 days of HFD consumption but no difference from controls after 2 and 6 months (Thaler et al., 2012; Lemus et al., 2015), similar to the trajectory seen between our group's fetal and one-year-old findings. Thus, our findings are supported by literature that demonstrates the protective effect of a maternal HFD and the transient nature of an increase in Iba1-stained cells in response to a HFD.

The trajectory of microglial prevalence could impact the trajectory of energy homeostasis and neural circuit formation throughout development. Given that microglia may interact with the neuronal populations within the ARC, increased activity during the prenatal period may lead to greater disruptions to energy homeostasis, whereas fewer microglia in the postnatal period may lead to a decreased sensitivity to the system. Synaptic pruning is more likely to lead to lasting alterations to neural circuitry. Offspring exposed to a perinatal WSD may demonstrate reductions in synaptic pruning due to the potential decrease in phagocytosis-associated gene expression associated with maternal inflammation and loss of microglia availability demonstrated postnatally. As decreased synaptic pruning can lead to either hyperconnectivity or hypoconnectivity, a follow-up study would need to specifically investigate the effect of perinatal WSD on the functional connectivity of the melanocortin system (Kim et al., 2017; Cowan and Petri, 2018; Kleinhans et al., 2016; Huang et al., 2016; Ypma et al., 2016). Additionally, increased microglial activation during the prenatal period could lead to increased phagocytosis of

neural precursor cells, whereas reduced microglial prevalence during the postnatal period may slow phagocytosis, thereby establishing a trajectory of restrained followed by unrestrained cell proliferation. This impact may be evident in many brain regions, as reduced microglial prevalence was also found in the amygdala of one-year-old offspring (Dunn et al., 2022). These dynamic influences therefore have the potential to lead to significant changes in brain organization.

Alternatively, the fetal and postnatal results may appear to contradict because the different methodologies between the studies might not correlate. In the fetal study, immunoreactive area and integrative optic density were measured to capture the number of pixels that were stained for Iba1 per image. While more staining might indicate more cells, microglia also vary their Iba1 expression levels and change shape based on their activation state, with resting microglia taking up a larger area than activated microglia. Thus, the number of pixels measured does not necessarily correlate to the number of cells (Hopperton et al., 2018). Given that other measures in the prior study indicated that prenatal WSD led to increased fetal inflammation, it is more likely that the microglia assumed a smaller, activated state than a larger resting state. This would suggest a significantly greater number of activated microglia in the WSD group compared to the fewer but larger resting microglia in the CTR group; however, the alternative possibility that both groups had an equivalent number of cells, with increased Iba1 expression in the WSD group, cannot be ruled out. This alternative possibility would not necessarily contradict the present finding of slightly fewer Iba1-stained cells in the one-year-old offspring. An additional follow-up study could investigate other measures to better characterize the inflammatory state at the one year postnatal time point.

3.5.4. Spatially-dependent microglial distribution evident in the arcuate and distinct across species

This is the first study to characterize the regional distribution of Iba1-stained cells in the ARC of Japanese macaques. A few studies have explored this distribution in other species with differing findings. Thus, the distribution of microglia throughout the ARC may be distinct across species. For example, while this study found a density of Iba1-stained cells near the middle of the rostral-caudal axis, a previous study in cynomolgus monkeys found an even distribution of microglia, as identified by staining for α-napthyl butyrate esterase (Abel et al., 1999). In addition to the potential for species-specific differences and differences between the non-specific microglial markers, another possible explanation for this discrepancy could be the age difference of the subjects: the present study examined one-year-old juveniles, while the cynomolgus monkeys were adults that were at least nine years old. Additionally, it is unclear how many locations within the ARC were sampled to determine the distribution reported in adult cynomolgus macaques. An increased count in the central regions, as seen in the present study, could have been missed if too few locations were sampled.

While studies characterizing the distribution in other primate species were limited, a few studies reported the distribution in rodents. One study described a heterogeneous distribution of Iba1-stained microglia throughout the ARC in rats, as seen in the cynomolgus monkeys. However, the study was limited by a sample consisting of four male animals, and the report was not accompanied by a statistical analysis or figure to demonstrate effect size (Reis et al., 2015). A study in adult mice found a different

distribution: an increase in Iba1-stained cells weighted towards the caudal region of the ARC (Lemus et al., 2015). As this study used the same microglial marker as the present study, this discrepancy in microglial distribution is more likely due to a species-specific difference or an age difference.

A spatially-dependent microglial distribution indicates neuronal populations near denser regions may be more strongly impacted by inflammation. Thus, differences in microglial distribution across species implies that the effects of inflammation or over-nutrition on ARC-specific functions might differ across species based on where the microglia are more densely located. It is understood that the impacts of a maternal WSD vary based on the species (Williams et al., 2014), so it is possible that differences in microglial density across the ARC may mediate some of these differences.

Our results indicate an increased level of Iba1-stained cells towards the midpoint of the ARC, suggesting that an elevated inflammatory state may have a pronounced effect on the neuronal populations in that central region. One such population includes neurons that express neuropeptide Y (NPY). NPY neurons commonly express AgRP and γ-aminobutyric acid (GABA), though there are subsets of NPY neurons that do not express either neurotransmitter (Zhang et al., 2019b). In humans, NPY neurons were found primarily in the central region of the ARC and were largely absent from the rostral and caudal regions (Kalsbeek et al., 2020). Thus, increased inflammation and microglial activation would likely impact the centrally located NPY/AgRP neurons, which play a significant role in promoting feeding and reducing energy expenditure (Zhang et al., 2019b).

Consistent with a previous study by our group that demonstrated reduced AgRP fiber density and decreased feeding with postnatal WSD exposure (Sullivan et al., 2017), studies in mice have similarly demonstrated reduced AgRP and NPY mRNA expression and decreased feeding after two months of HFD consumption (Dalvi et al., 2017; Wang et al., 2002), as well as increased proinflammatory gene expression across the hypothalamus (Dalvi et al., 2017). Additionally, a patch-clamp electrophysiology study in mice demonstrated that acute microglial activation via lipopolysaccharide (LPS) administration, while increasing the firing activity of some NPY neuronal populations, inhibited the firing of most AgRP/NPY neurons in the ARC (Reis et al., 2015). Thus, there is evidence to suggest that the centrally-located density of microglia in the ARC may interact with the centrally-located NPY/AgRP neuronal population to reduce feeding during periods of elevated inflammation. On the contrary, treating mouse AgRP/NPY hypothalamic cell lines with the saturated fatty acid, palmitate, or the inflammatory cytokine, tumor necrosis factor alpha (TNF-α), significantly upregulated the expression of NPY and inflammatory markers, suggesting a potential link between increased inflammation and feeding (Dalvi et al., 2017). Moreover, increased saturated fat consumption led to decreased feeding behavior in microglia-depleted mice compared to mice with unaltered microglial levels, suggesting that microglial activation plays a role in stimulating feeding behavior (Valdearcos et al., 2014). These findings indicate that microglia may have varied effects depending on the NPY neuronal subpopulation and type of inflammatory exposure: acute *in vitro* palmitate administration may not be directly comparable to the inflammatory environment associated with chronic exposure to

a HFD. Further studies are needed to elucidate the complex interactions that determine which sources of inflammation may lead to increased or decreased energy outcomes.

3.5.5. Maternal obesity and inflammation may be additive or alternative factors to maternal diet regarding impacts to microglia count

This study found an association between perinatal WSD and decreased Iba1-stained cell count, but it is unclear as to what underlying factors led to this change. One hypothesis is that it is not the prenatal diet that creates the elevated maternal inflammatory state which impacts offspring, but maternal obesity or the combination of maternal diet and obesity. A WSD is often associated with increased adiposity, but there is metabolic variability within the human and macaque populations such that some individuals on a WSD remain lean and some individuals on a "control" diet develop obesity. We intended to use this macaque model to distinguish between the independent effects of diet and adiposity, as our group has previously demonstrated independent effects of the two factors on microglia count in the amygdala (Dunn et al., 2022). However, due to our limited sample size, perinatal WSD and maternal adiposity were highly associated, and we did not have the statistical power to distinguish between them. Other factors related to the maternal metabolic state, including insulin and leptin resistance, may additionally play a role in altering microglial activation and should be examined in future research, as well.

Another underlying mechanism we sought to investigate was maternal inflammation as measured by levels of cytokines in the blood during the third trimester of pregnancy. Using a partial least squares regression (PLSR), we found that maternal

cytokines were predictive of Iba1-stained cell count in the ARC, indicating that maternal inflammation has a lasting impact on cell count (Figure 3.7). However, the cytokines had varied impacts on the cell count, so a coherent relationship could not be drawn. We additionally investigated whether peripheral cytokines collected from the one year old offspring could predict cell count, as contemporaneous exposure to immune markers may have a stronger influence on the presence of microglia and macrophages. A separate PLSR analysis revealed that offspring markers were similarly predictive of cell count (Figure 3.8). As was observed with the maternal markers, the offspring markers had varied impacts and did not settle into coherent groupings. For example, a chemokine with proinflammatory properties, Regulated on Activation, Normal T Cell Expressed and Secreted (RANTES; Hentschke et al., 2012) was the strongest offspring marker with a positive relationship to cell count, and a separate proinflammatory cytokine, interleukin-12 (IL-12), was the strongest offspring marker with a negative relationship. As the set of proinflammatory cytokines did not have similar impacts or directionality for either the maternal or offspring set, it is difficult to conclude how a proinflammatory state in general would affect Iba1-stained cell count. The impacts of each marker appear to be distinct.

Prior work in this model characterized the relationships between maternal and offspring immune factors using latent variables comprised of groups of markers (Dunn et al., 2022). Although perinatal WSD and maternal adiposity were not associated with differences in offspring cytokines or chemokines, maternal chemokines were positively associated with offspring cytokines and negatively associated with offspring chemokines, suggesting the potential for maternal immune factors to influence cell count in the ARC

through an indirect influence on offspring immune factors (Dunn et al., 2022). However, neither maternal proinflammatory cytokines nor maternal chemokines were associated with Iba1-stained count in the amygdala of one year old offspring; this could potentially be explained by the present finding where the set of proinflammatory cytokines had divergent impacts on cell count that would have cancelled out. Further research should examine the intricate relationships between perinatal WSD exposure, maternal inflammatory factors, and offspring inflammatory factors to better contextualize the cell count results of the present study.

3.5.6. Limitations

The present study elucidates a slight relationship between perinatal diet and Iba1-stained cell count at the one year postnatal time point, but there are limitations to the conclusions that can be drawn from this observation. Critically, Iba1-stained cell count is only one measure of inflammation. A decrease in Iba1-stained cell count in the perinatal WSD group suggests that there was not enough inflammation to increase microglial proliferation or macrophage infiltration above control conditions, but other measures would be useful in confirming this inference. Assessing cell morphology would reveal more about the activation state of the microglia. Additionally, staining for inflammatory cytokines or other markers of microglial activation could elucidate the level of neuroinflammation experienced by each group. These measures would provide a more conclusive indication of neuroinflammation than Iba1-stained cell counts, but they were not pursued due to the challenges of assessing microglia morphology on single plane images and unsuccessful inflammatory marker staining. Future work in this NHP model

is underway to examine neuroinflammation across other areas of the brain with additional measures of neuroinflammation.

Another limitation is that significantly fewer images were captured on either end of the ARC than in the medial regions. Limited data points on the tails of the spread could potentially lead to inaccurate representations of the cell count distribution. Thus, the mixed effects model was repeated on a more robust data set consisting solely of images from the five consecutive medial regions with the most observations. The results were consistent with those of the full data set, confirming a main effect of spatial location best fit by a quadratic curve (see Supplementary Material). Additionally, future studies could examine the distribution of Iba1-stained cells along other axes, such as the dorsal-ventral and medial-lateral axes, to better characterize microglial prevalence throughout the ARC and uncover other neuronal populations that may be susceptible to neuroinflammatory impacts.

3.5.7. Conclusions

The neuroinflammation observed *in utero* with exposure to a perinatal WSD does not appear to persist at the one year postnatal time point. Perinatal WSD was associated with a slight decrease in Iba1-stained cells in the ARC, indicating that there may be less peripheral inflammation and fewer infiltrating macrophages than in controls. This finding, in conjunction with our prior study, suggests a response trajectory where heightened inflammation during prenatal WSD exposure drops after the WSD is discontinued at weaning, welcoming the possibility that perinatal WSD exposure could be neuroprotective at later time points. However, synaptic pruning and other microglial-

dependent processes critical for neuronal circuit formation could be impacted by the dynamic trajectory of microglial activity across development. Greater numbers of Iba1-stained cells were also found towards the midpoint of the ARC along the rostral-caudal axis independent of perinatal diet. Given the potential for interactions between microglia and ARC neurons, this could have implications for the NPY neuronal control of food intake and body weight. An important caveat to these findings is that microglial count is not infallible as a standalone measure of inflammation, so additional measures would be useful in confirming the inflammatory state of these offspring. Further research should explore the distinct effects of maternal adiposity from perinatal WSD. Additional measures of offspring inflammation and a detailed analysis of the impacts of maternal cytokines could further elucidate the underlying mechanisms that govern the relationship between maternal and postnatal inflammation and their effects on neurodevelopment.

3.6 Supplementary Materials

3.6.1. Automated Cell Counting Procedure

The procedure for determining the optimal parameters settings that would lead to the most accurate automated count included the following steps. 1) The color-merged images underwent one of four processing methods to better distinguish cell bodies from the background. 2) The processed images underwent a color threshold which isolated the teal-colored cell bodies by adjusting the lower and upper hue display limits, and a thresholding method was applied to pixels in the narrowed color range. 3) The color-thresholded, binary images underwent an object size threshold where the "Analyze Particles" function was used to generate a count of any object that covered an area greater than a set minimum size. 4) The automated count was compared to the manual count to assess the accuracy of each parameter combination. These steps are described in more detail below.

Step 1: Processing. Four processing methods were explored. The first was considered "Raw," in which no processing techniques were applied. The second was named, "Gamma," in which a gamma adjustment of 0.5 was applied. Gamma adjustment is a non-linear histogram adjustment which can be used to increase the range of intensities used by the pixels in an image. In dim images, the large majority of pixels which exist in the darker range can be made brighter and occupy a wider range of gray intensities without saturating the brightest objects, allowing for easier detection of the relatively-brighter cell bodies from the background. This function can be accessed in ImageJ via the *Process/Math/Gamma* command, set to 0.5. The third option, "Minimum," applied a minimum filter of 5.0 pixels. The minimum filter replaces the

intensity value of each pixel in the image with the smallest value present in that pixel's neighborhood. By setting the neighborhood to a 5.0 pixel radius, the overlapping centers of DAPI- and Iba1-stained cells remain bright, but their area is greatly reduced, as pixels towards the edge of the cell are replaced by the dimmer intensity of the background. This allows for sharper edge definitions and is useful for separating two nearby cells. The minimum filter function can be accessed in ImageJ via the *Process/Filters/Minimum…* command, set to 5.0 pixels. The fourth option, "Gamma-Minimum-Average" (GMA), first applied a gamma adjustment of 0.5, then a minimum filter of 5.0 pixels, and then averaged the resulting image with the original raw image. This technique combines the benefits of brightening the image with distinguishing the cell edges. Combining this with the raw image retains more of the original shape of the cells. To average the processed image with the raw image, both images must be open in ImageJ. Then, select the *Process/Image Calculator* command, set *Image1* to one of the images and *Image2* to the other, and select "Average" from the *Operation* menu.

Step 2: Color Threshold. To isolate the parts of the image that represented the teal DAPI- and Iba1-stained cells, five lower and three upper hue display limits, along with five automatic thresholding algorithms, were explored. The color threshold function is accessed in ImageJ by selecting *Image/Adjust/Color Threshold…* and setting the color space to HSB. The *Hue* display shows the range of possible hue pigments, each represented by a number between 0 and 255, and a histogram of the pigments that are represented by pixels in the image. Most images in this analysis exhibited colors ranging from yellow to cyan, roughly corresponding to a hue display range of 40 to 130, with the teal somas of the DAPI- and Iba1-stained cells ranging roughly between 50 and 115. The

Dark Background option was selected; the *Pass* option was selected for each of the *Hue*, *Saturation*, and *Brightness* components; and the default display settings were unaltered for the *Saturation* and *Brightness* components. Thus, the three features of the color threshold function that were manipulated were the lower hue display limit, ranging from 50 to 74 in increments of 6 to best determine the most-yellow pigment of dual-stained somas; the upper hue display limit, ranging from 109 to 113 in increments of 2 to best determine the most-cyan pigment of dual-stained somas; and the *Thresholding method*, which applied one of five automatic thresholding algorithms to the pixels in the image whose hue value resided within the range created by the lower and upper hue display limits.

The five thresholding algorithms that were explored were Maximum Entropy, Intermodes, Moments, Otsu, and Triangle (ImageJ, 2019). These thresholds, as well as the display limit options, were selected from all available options based on visually inspecting the binary image outputs of sample images for adequate representation of the somas without significant background interference. The Maximum Entropy algorithm maximizes the inter-class entropy of the histogram (Kapur et al., 1985). The Intermodes algorithm assumes a bimodal histogram and thresholds the average of the two local maxima that result after iteratively smoothing the histogram (Prewitt and Mendelsohn, 1966). The Moments algorithm is a moment-preserving threshold (Tsai, 1985). The Otsu algorithm minimizes the intra-class variance (Otsu, 1979). The Triangle algorithm assumes a skewed histogram, identifies the maximum peak, and searches for a threshold within the range between the peak and the farther end of the histogram (Zack et al., 1977). Applying the thresholding algorithm to the pixels within the hue display limit

range creates a binary image where the pixels that passed the threshold are represented in black against a white background (Figure 3.1F). The binary image was generated by selecting “Select” from the color threshold GUI, then selecting *Edit/Selection/Create Mask* from the main ImageJ menu.

Step 3: Object Size Threshold. ImageJ counts the number of distinct objects in the binary image that occupy an area, in square pixels, that is greater than a specified minimum area. Twenty-five minimum object sizes ranging between 40 and 280 square pixels, in increasing increments of 10 square pixels, were used for training. The “Analyze Particles” GUI was utilized and the “Size” was set to range between the desired minimum object size and “Infinity.” The default “Circularity” of 0.00-1.00 was retained to allow for any shape. Importantly, “Exclude on edges” was selected to avoid counting cells that touched an edge of the image. Optionally, a quick visualization that highlights which objects were counted can be generated by showing “Overlay Masks” (Figure 3.1G). After applying these settings, the total object count for each image was exported for comparison purposes.

Step 4. Accuracy. A measure of accuracy—the average absolute difference in accuracy from 100%—was used to assess whether the parameter combinations adequately approximated the manual counting performed by a trained observer. First, the raw accuracy was calculated for each image in a combination by dividing the automated count by the manual count. This yielded twenty raw accuracy scores where images with a greater automated count had a score greater than 1, and images with a lower automated count had a score lower than 1. The absolute value of the difference between 1 and the accuracy score was calculated for each image. For example, an image that had a manual

count of 10 and an automated count of 11 would have a raw accuracy of 1.1 and an absolute difference score of 0.1. The absolute difference scores were averaged across the twenty images to generate a single average absolute difference in accuracy score for the parameter combination. The difference between 1 and the average absolute difference score yielded the final reported accuracy score for the parameter combination. For example, Combination 8 in Figure 3.3 had an average absolute difference in accuracy of 0.096, so the combination was reported to be 90.4% accurate compared to the manual count. A final accuracy score above 80% was required to approve the automated method for use in the final data set, as 80% accuracy falls within the range of other reported accuracy and precision measures for automated cell detection (Xing and Yang, 2016; Lunde and Glover, 2020).

3.6.2. Error Rate Calculation and Application

A final step in validating the accuracy score was undertaken. It was important to ensure that the automated method was counting the same Iba1-stained cells identified by the trained observer, rather than simply counting the same number of non-cell objects and artifacts. To ensure the automated and manual methods counted the same target objects, an error rate was calculated for each combination.

First, cells in the raw, color-merged images were manually located. Using ImageJ's "Multi-point" tool, a marker was placed in the center of each cell that was counted by the observer. The set of markers was imported to the "ROI Manager" by selecting *Edit/Selection/Add to Manager*, and then *More>>/Save…* was selected in the Manager to save the set for later use.

In order to overlay the manually placed markers on the automatically counted objects, the aforementioned Object Size Threshold step had to be modified to allow the counted objects to be manipulated. Using the Analyze Particles GUI, "Show" was set to "Outlines" and the "Add to Manager" option was selected; this generated an image where each counted object appeared as an outline and was added as an ROI in the ROI Manager. Each ROI was selected, and the *Edit/Selection/Enlarge…* function was accessed from the main ImageJ menu. The ROIs were each enlarged by 8 pixel units to encompass an area slightly larger than the actual object; this was performed in case the corresponding marker from the manual count was off-center, running the risk of not overlapping the automatically counted object. These enlarged objects were filled with a medium gray color first by setting the foreground color to 124 for each of the red, green, and blue channels via *Image/Color/Color Picker…*, and then by selecting the ROI and applying *More>>/Fill* in the manager.

Next, the saved markers from the manual count were opened on the current image of the gray, automatically counted objects. Using the ROI Manager, the last marker in the list was selected, and the *Measure* function was applied. This generated a table where the "Mean" of each marker represented the color of the pixel that was overlapped by the marker. A value of 255 indicated a white background, or an absence of an automatically counted object, and a value of 124 indicated a gray background, or that the marker overlapped an automatically counted object.

Using this method, the ImageJ macro counted the number of markers that overlapped an object as "hits," the number of markers that did not overlap an object as "misses," and the number of objects that did not have an overlapping marker as "false

positives." The sum of misses and false positives were counted as the total number of "errors." The number of errors divided by the number of manually counted cells yielded an "error rate." The error rates for all twenty images were averaged for each parameter combination to yield an average error rate.

Error rate is not a complement to accuracy; an automated count of 10 could be 100% accurate when compared to a manual count of 10, but if the automated method missed one cell and counted one artifact to arrive at the sum of 10, then two errors were included in the sum. This would yield an error rate of 0.2. However, if the automated method counted errors in a pattern that consistently yielded the same total cell count as the manual count, then ultimately the automated method would be an "accurate" substitution for manual counting and could generate a data set of cell counts that would be roughly equivalent to a set of manual counts. Thus, accuracy alone was chosen as the measure used to determine whether the automated method was effective for the purpose of cell counting, and the error rate was assessed to ensure the automated count was generally valid and not wholly coincidental.

3.6.3. Determining the Best-Fitting Minimal Mixed Effects Model

A mixed-effects model was used to investigate the impacts of perinatal diet and spatial location on cell count while accounting for the partially crossed nature of the study design. During preliminary testing, it was found that there was no main effect of offspring sex or interaction effect between sex and the other factors of interest, so sex was not included as a factor during comparison testing. To determine the minimal adequate model, a series of Chi-squared tests were run to compare between progressively

more complex iterations (Table 3.1). Tests were run in R using the *anova* method from the lmerTest package (Kuznetsova et al., 2017) following the syntax, *anova(model1, model2)* where *model1* represents the mixed effects model fit to the data using the simpler formula, and *model2* represents that of the more complex formula. All models that were compared included the random effect component and varied the fixed effects. When a significant difference was found between two progressive models, the model that produced the smaller Akaike information criterion (AIC) was determined to be the better-fitting model. A more-positive log-likelihood value provided further evidence that it was the better-fitting model.

First, we established that inclusion of the random effect was justified. We compared a baseline fixed effects model (Cell Count ~ 1) to a baseline random effects model (Cell Count ~ 1 + (1 | Subject : Spatial Location)). Using a model likelihood ratio test, we determined that the baseline random effects model was significantly different from the baseline fixed effects model ($p < 0.001$) and had a lower AIC (4497.918; baseline fixed effects model AIC = 4671.834), thereby justifying its inclusion in the mixed effects model.

The first fixed effect that was added to the model was *Spatial Location*. To determine whether the relationship between *Spatial Location* and *Cell Count* was linear, quadratic, cubic, or a higher-order polynomial fit, we compared models that varied the order of the polynomial. The formula in R for the simplest, linear model was:

Cell Count ~ poly(Spatial Location, 1) + (1 | Subject : Spatial Location)

where the *1* in *poly(Spatial Location, 1)* indicated that *Spatial Location* would be treated as a first-order (linear) polynomial. Changing this number to 2 created a quadratic model, and changing it to 3 created a cubic model. When comparing the linear model to the baseline random effects model, the linear model was significantly different and had a lower AIC, indicating that *Spatial Location* added enough information to the model to merit its inclusion as a fixed effect, χ^2 (1) = 5.4186, p = 0.020. When comparing the linear model to the quadratic model, the quadratic model demonstrated a significant improvement, χ^2 (1) = 5.6405, p = 0.018. However, the cubic model did not provide significant improvement over the quadratic model, χ^2 (1) = 0.012, p = 0.913, so the quadratic polynomial was determined to be the best fit for the *Spatial Location* fixed effect. We confirmed that the quadratic model was still significantly better than the baseline random effects model, χ^2 (2) = 11.059, p = 0.004, and we used the quadratic term for *Spatial Location* in the remaining comparisons.

Table 3.1. Chi-squared test of best model fit.

The "Fixed Effects" column denotes which fixed effects were included with the random effect to complete the model formula for the comparison. The better-fitting model (bolded text in "Fixed Effects" column) was identified by a lower AIC (comparisons that reached significance) or by a simpler set of fixed effects (non-significant comparisons). Abbreviations: AIC, Akaike information criterion; Chisq, chi-squared test statistic; Df, degrees of freedom for the likelihood ratio test: the difference in number of model parameters; logLik, log-likelihood; npar, number of parameters; Pr(>Chisq), p-value.

Comparison	Fixed Effects	AIC	logLik	npar	Df	Chisq	Pr(>Chisq)
Adding Linear Spatial Location	None	4498.4	-2246.2	3	1	5.4186	0.01992
	Spatial Location (linear)	4495.0	-2243.5	4			
Adding Quadratic Spatial Location	None	4498.4	-2246.2	3	2	11.059	0.003968
	Spatial Location (quadratic)	4491.4	-2240.7	5			
Linear vs. Quadratic Spatial Location	Spatial Location (linear)	4495.0	-2243.5	4	1	5.6405	0.01755
	Spatial Location (quadratic)	4491.4	-2240.7	5			
Quadratic vs. Cubic Spatial Location	**Spatial Location (quadratic)**	4491.4	-2240.7	5	1	0.012	0.9127
	Spatial Location (cubic)	4493.4	-2240.7	6			
Adding Perinatal Diet to Spatial Location (quadratic)	Spatial Location	4491.4	-2240.7	5	1	6.7819	0.009209
	Perinatal Diet + Spatial Location	4486.6	-2237.3	6			
Adding Spatial Location (quadratic) to Perinatal Diet	Perinatal Diet	4494.5	-2243.2	4	2	11.909	0.002594
	Perinatal Diet + Spatial Location	4486.6	-2237.3	6			
Adding Interaction Effect	**Perinatal Diet + Spatial Location**	4486.6	-2237.3	6	2	0.492	0.7819
	Perinatal Diet + Spatial Location + Interaction	4490.1	-2237.1	8			

The next comparisons determined that a model that included *Perinatal Diet* and *Spatial Location* as fixed effects was better than a model that included only one of the two (*Perinatal Diet* model: χ^2 (2) = 11.909, p = 0.003; *Spatial Location* model: χ^2 (1) = 6.7819, p = 0.009). However, adding an interaction effect between *Perinatal Diet* and *Spatial Location* did not significantly improve the model, χ^2 (2) = 0.492, p = 0.782), so the simpler model that contained only *Perinatal Diet* and *Spatial Location* as the fixed effects was determined to be the best fitting model.

A limitation of this analysis is that significantly fewer images were captured on either end of the ARC than in the medial regions. For example, the regions at interaural positions 17.45 mm and 12.90 mm were represented by only 4 and 8 images, respectively (Figure 3.5, repeated in Figure 3.6A). Limited data points on the tails of the spread could potentially lead to inaccurate representations of the cell count distribution. To confirm that a relationship between spatial location and cell count truly existed, the best-fitting mixed effects model was repeated on a more conservative and robust data set consisting solely of images from the five consecutive medial regions with the most observations, each with a minimum of 88 images. These regions were 15.60, 15.15, 14.70, 14.25, and 13.80 mm rostral to EBZ. This analysis, which used 587 images captured from 14 subjects across 5 consecutive atlas-matched locations, resulted in a main effect of spatial location on cell count (p = 0.008), confirming the relationship seen across the full data set.

The reported analysis used the mixed effects model that included *Spatial Location* as a quadratic term, but it is worth noting that when the analysis was repeated with *Spatial Location* included as a linear term, the same outcomes were generated: there was

a main effect of perinatal diet and spatial location with no interaction effect. Plotting the linear relationship between spatial location and cell count would reveal a slight increase in cell count towards the rostral end of the ARC (Figure 3.6B). However, several metrics indicated that the quadratic, second-order polynomial was a better fit. In addition to emerging as the better-fitting model in the Chi-squared test (Table 3.1), the quadratic model (with *Spatial Location* as the only main effect) also had a better marginal R-squared value ($R^2 = 0.0451$) than the corresponding linear term model ($R^2 = 0.0244$), indicating that a quadratic fit of *Spatial Location* could explain about 2% more of the variance in *Cell Count* than could a linear fit. Additionally, the full model with the quadratic fit is significantly better than that with a linear fit even when using only the five medial locations with the most observations: interaural positions 15.60, 15.15, 14.70, 14.25, and 13.80 mm χ^2 (1) = 4.311, $p = 0.038$. Thus, we have concluded that the distribution of Iba1-stained cells displays an increased density in the middle of the ARC compared with the rostral and caudal ends.

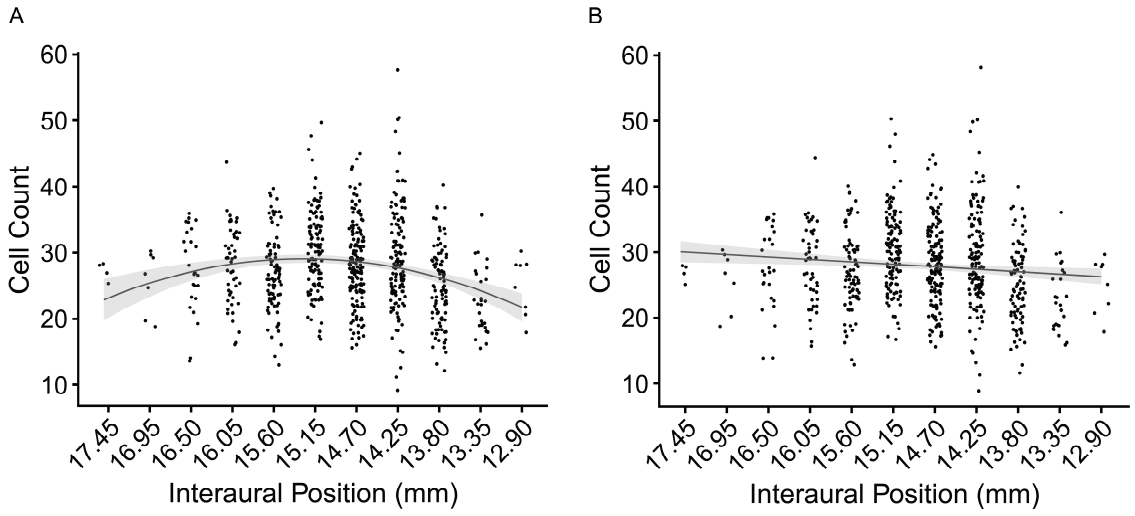

Figure 3.6. Comparison of quadratic and linear fits to the distribution of Iba1-stained cells across the ARC.

(A) Fitting the Iba1-stained cell count distribution with a quadratic curve, as seen in Figure 3.5, indicated an increased cell count towards the midpoint of the ARC (p = 0.003). **(B)** When using a mixed effects model that included spatial location as a linear fixed effect rather than a quadratic term, Iba1-stained cell count increased linearly towards the rostral end of the ARC (p = 0.029). Interaural position is rostral to EBZ, with 17.45 mm as the most rostral atlas-matched location.

3.6.4. Maternal inflammation may impact microglia count

Given that consuming a WSD can lead to an elevated inflammatory state, maternal inflammation may potentially mediate the relationship between perinatal WSD and decreased Iba1-stained cell count observed in this study. We therefore explored whether markers of maternal inflammation would similarly correlate with a decreased Iba1-stained cell count.

Maternal inflammation was assessed by measuring the levels of inflammatory markers in the blood during the third trimester of pregnancy. Plasma concentrations were determined using an IL-6 ELISA and Monkey Magnetic 29-Plex cytokine panel (ThermoFisher Scientific, Waltham, MA, USA), and a data cleaning procedure was conducted to process the raw concentrations into usable measures, as previously described (Dunn et al., 2022). The 14 markers selected for the analysis included four proinflammatory cytokines, three pleiotropic cytokines, six chemokines, and one growth factor.

A total of 17 dam-offspring dyads were selected for this analysis. Of the offspring, six were exposed to a perinatal CTR and post-weaning CTR diet, five were exposed to a perinatal WSD and post-weaning CTR diet, and six were exposed to a perinatal WSD and post-weaning WSD. As previously stated, this latter group was excluded from the main analyses that tested the effects of perinatal diet and spatial location on cell count due to the incongruent post-weaning diet exposure, but it is worth noting that this exclusion was done for the sake of simplicity: there was no main effect of post-weaning diet when included as a factor in the mixed effects model, but reporting the equivalent results when excluding the incongruent post-weaning diet group made for a simpler, more coherent interpretation than the alternative of introducing a covariate in the model in order to include the subjects. As post-weaning diet had no effect on cell count, including the post-weaning WSD group in this analysis increased the sample size without introducing a confounding variable. A larger sample size was useful, as there was only one observation per juvenile subject: the median cell count of all images collected across the entire span of the ARC.

A partial least squares regression with three components strongly predicted offspring median cell count from the group of 14 maternal inflammatory markers. The relationship between observed and predicted median cell counts was strong and positive (r = 0.83; Figure 3.7A), and results were significant as determined by the difference in the distributions of the out-of-sample prediction errors (d = 0.60, mean absolute error; Figure 3.7B) using leave-3-out cross-validation (680 unique combinations when leaving 3 subjects out of a sample of 17 subjects) compared to errors obtained by repeating the same approach but shuffling the data in the training partition 4,000 times (null model). The same out-of-sample validation schema was used to determine the optimal number of components. Peak performance was found with three components, but results were similar with two and four components. This out-of-sample validation schema reduces the risk of overfitting and maximizes the likelihood that the estimates are generalizable (Rudolph et al., 2017; Silva-Batista et al., 2020).

This result indicates that a strong relationship exists between maternal inflammation and offspring microglia and macrophage count at the one year postnatal time point. However, when examining the individual contributions of each of the 14 inflammatory markers towards the relationship, a pattern did not readily emerge (Figure 3.7C). For example, the four proinflammatory cytokines spanned the range of beta-weight magnitudes, with MIF standing as the marker that contributed most strongly to a positive relationship between maternal inflammation and offspring cell count, and IL-1b standing as the marker with the second strongest negative contribution to such a relationship. If all four had instead demonstrated strong, negative beta-weights near a value of -1, this would have suggested that a high concentration of maternal

proinflammatory cytokines is associated with a decrease in median cell count. However, coherent patterns such as this could not be drawn from the more nuanced results. More research is needed to explore the myriad ways that maternal inflammation may affect offspring neurodevelopment.

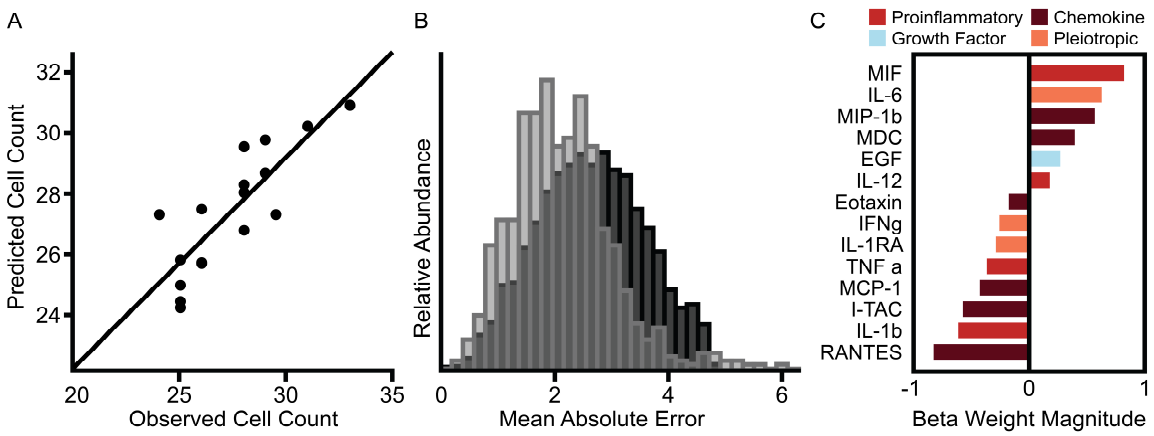

Figure 3.7. Maternal cytokines predict offspring Iba1-stained cell count in the ARC. A partial least squares regression with three components strongly predicted offspring median cell count from the group of 14 maternal inflammatory markers. **(A)** Observed offspring median cell count was strongly and positively correlated with the count predicted by maternal markers ($r = 0.83$). **(B)** The distribution of the mean absolute error arising from the use of maternal markers to predict cell count (light gray) was moderately shifted to the left of that of the null model (dark gray; $d = 0.60$), indicating a reduction in error. **(C)** The beta-weight magnitudes demonstrate the relative contributions of the individual maternal inflammatory markers to a positive relationship between an increase in the plasma concentration of the set of markers and the offspring median cell count. Abbreviations from **(C)**: EGF, epidermal growth factor; IFNg, interferon gamma; IL-1b, interleukin 1 beta; IL-1RA, interleukin 1 receptor antagonist; IL-6, interleukin 6; IL-12, interleukin 12; I-TAC, interferon-inducible T-cell alpha chemoattractant; MCP-1, monocyte chemoattractant protein-1; MDC, macrophage-derived chemokine; MIF, macrophage migration inhibitory factor; MIP-1b, macrophage inflammatory protein-1 beta; RANTES, regulated upon activation, normal T cell expressed and secreted; TNF a, tumor necrosis factor alpha.

3.6.5. Offspring inflammation may impact microglia count

We investigated whether markers of offspring inflammation would correlate with Iba1-stained cell count, as contemporaneous exposure to immune markers may have a stronger influence on the presence of microglia and macrophages distinct from the impacts of maternal markers.

Offspring inflammation was assessed by measuring the levels of inflammatory markers in the blood in one-year-old offspring. Plasma concentrations were determined using a Monkey Magnetic 29-Plex cytokine panel (ThermoFisher Scientific, Waltham, MA, USA), and a data cleaning procedure was conducted to process the raw concentrations into usable measures, as previously described (Dunn et al., 2022). The 14 markers selected for the analysis included three proinflammatory cytokines, two pleiotropic cytokines, six chemokines, and three growth factors.

A total of 16 offspring subjects were selected for this analysis: four were exposed to a perinatal CTR and post-weaning CTR diet, seven were exposed to a perinatal WSD and post-weaning CTR diet, and five were exposed to a perinatal WSD and post-weaning WSD. As previously stated, this latter group was excluded from the main analyses that tested the effects of perinatal diet and spatial location on cell count due to the incongruent post-weaning diet exposure for the sake of simplicity. As post-weaning diet had no effect on cell count, including the post-weaning WSD group in this analysis increased the sample size without introducing a confounding variable. A larger sample size was useful, as there was only one observation per juvenile subject: the median cell count of all images collected across the entire span of the ARC.

A partial least squares regression with five components strongly predicted offspring median cell count from the group of 14 offspring inflammatory markers. The relationship between observed and predicted median cell counts was strong and positive (r = 0.94; Figure 3.8A), and results were significant as determined by the difference in the distributions of the out-of-sample prediction errors (d = 0.83, mean absolute error; Figure 3.8B) using leave-3-out cross-validation (560 unique combinations when leaving 3 subjects out of a sample of 16 subjects) compared to errors obtained by repeating the same approach but shuffling the data in the training partition 4,000 times (null model). The same out-of-sample validation schema was used to determine the optimal number of components. Peak performance was found with five components, but results were similar with four and six components. This out-of-sample validation schema reduces the risk of overfitting and maximizes the likelihood that the estimates are generalizable (Rudolph et al., 2017; Silva-Batista et al., 2020).

This result indicates that a strong relationship exists between offspring inflammation and offspring microglia and macrophage count at the one year postnatal time point. However, when examining the individual contributions of each of the 14 inflammatory markers towards the relationship, a pattern did not readily emerge (Figure 3.8C). For example, the three proinflammatory cytokines spanned the range of beta-weight magnitudes, with IL-1b standing as a marker with a weak contribution to a positive relationship between offspring inflammation and cell count, and IL-12 standing as the marker with the strongest negative contribution to such a relationship. If all three had instead demonstrated strong, negative beta-weights near a value of -2, this would have suggested that a high concentration of offspring proinflammatory cytokines is

associated with a decrease in median cell count. However, coherent patterns such as this could not be drawn from the more nuanced results.

Interestingly, RANTES is a chemokine with proinflammatory functionality, and it was the strongest offspring marker with a positive relationship to cell count and the strongest maternal marker with a negative contribution to increased cell count. This suggests that an elevated level of maternal RANTES has an opposite effect on Iba1-stained cell count in the ARC from an elevated level of RANTES within the juvenile subject when collected at the same time point as the cell count. This could indicate that increased maternal RANTES, like maternal WSD and similar proinflammatory exposures, may program for reduced inflammation in one year old offspring, whereas elevated levels of inflammation within the juvenile subject recruit or are produced by the inflammatory cells likely to engage in inflammatory responses, microglia and macrophages. More research is needed to explore the myriad ways that offspring inflammatory markers may impact microglia and macrophage presence in the ARC.

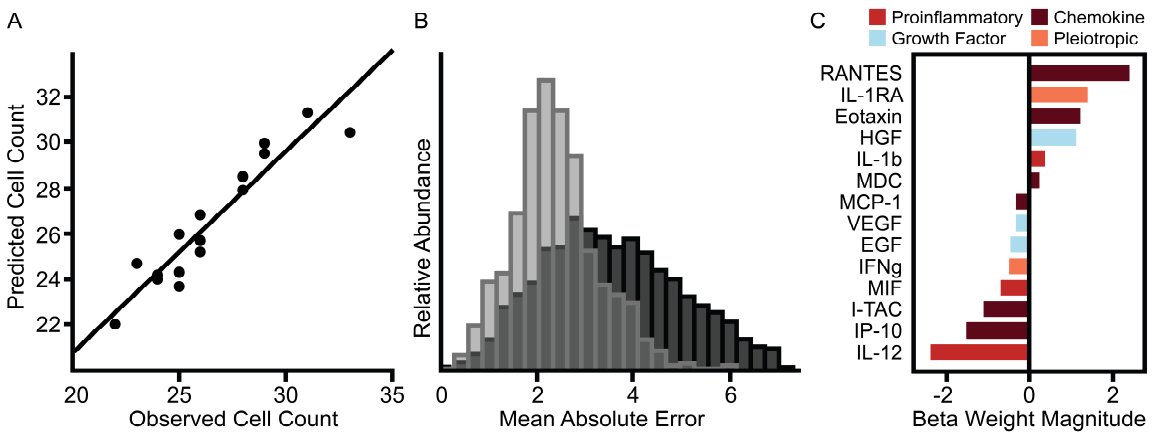

Figure 3.8. Offspring cytokines predict offspring Iba1-stained cell count in the ARC. A partial least squares regression with five components strongly predicted offspring median cell count from the group of 14 offspring inflammatory markers. **(A)** Observed offspring median cell count was strongly and positively correlated with the count predicted by offspring markers ($r = 0.94$). **(B)** The distribution of the mean absolute error arising from the use of offspring markers to predict cell count (light gray) was moderately shifted to the left of that of the null model (dark gray; $d = 0.83$), indicating a reduction in error. **(C)** The beta-weight magnitudes demonstrate the relative contributions of the individual offspring inflammatory markers to a positive relationship between an increase in the plasma concentration of the set of markers and the offspring median cell count. Abbreviations from **(C)**: EGF, epidermal growth factor; HGF, hepatocyte growth factor; IFNg, interferon gamma; IL-1b, interleukin 1 beta; IL-1RA, interleukin 1 receptor antagonist; IL-12, interleukin 12; IP-10, interferon gamma-induced protein 10; I-TAC, interferon-inducible T-cell alpha chemoattractant; MCP-1, monocyte chemoattractant protein-1; MDC, macrophage-derived chemokine; MIF, macrophage migration inhibitory factor; RANTES, regulated upon activation, normal T cell expressed and secreted; VEGF, vascular endothelial growth factor.

CHAPTER 4. DISCUSSION

4.1 Summary of Findings

The goal of this dissertation was to characterize the impacts of prenatal WSD exposure, which is a potential risk factor for SPD, on offspring neurodevelopment. Two aspects of neurodevelopment were explored across two main studies. First, the functional connectivity of areas involved in sensory and emotional processing were examined for differences associated with perinatal WSD exposure throughout development. Second, a potential mediator of altered circuit formation, neuroinflammation, was assessed at an early developmental time point. Together, these findings explore the role of a perinatal environmental exposure in the context of SPD.

4.1.1. Overview of Findings from Study 1

A machine learning model was able to train on differences in the connectivity of 378 connections within and between the sensory networks and the amygdala to classify offspring by perinatal diet exposure only when offspring were 4 months of age. The model was unable to detect connectivity differences at 6, 11, 21, and 36 months of age, suggesting that perinatal WSD exposure does not lead to long-lasting alterations in the functional connectivity of sensory and emotional processing areas. The features that were the most important to improving accurate predictions in the 4 month old model consisted of decreased connectivity within the somatomotor network, within the visual network, and between the somatomotor and auditory networks; increased connectivity between the auditory and visual networks; and mixed effects between the somatomotor and visual

networks. Although amygdala connectivity was expected to be implicated given the negative emotional component of SOR and integration of the amygdala in non-classical sensory processing pathways, amygdala connectivity was only weakly impacted at 4 months of age, with connections to the somatomotor network contributing more to model performance than connections from other networks to the amygdala. The same set of connections were assessed in children who reported a measure of SOR at roughly the equivalent developmental stage of the 36 month old macaques. Consistent with the macaque finding, the FRF model was also unable to predict the SOR score from the functional connectivity of the children. Taken together, these results suggest that a prenatal risk factor for ASD, which is a disorder that is highly comorbid with SPD, disrupts sensory connectivity during infancy, but these connections are largely robust against long-term impacts over time, similar to what is seen in children that still report SOR during preadolescence. These findings support the theory that SPD may stem from impaired sensory processing, especially at very early ages.

4.1.2. Overview of Findings from Study 2

Although prenatal WSD exposure was associated with increased microglial staining in the fetal ARC (Grayson et al., 2010), perinatal WSD exposure was not associated with an increased number of microglia and infiltrating macrophages in the ARC one year after birth. Instead, the perinatal WSD offspring displayed a slightly decreased number of microglia and macrophages. This finding illustrates a response trajectory where inflammation is elevated during perinatal WSD exposure but resolves after the WSD is discontinued at weaning. The slight decrease in cell count suggests a

potentially compensatory or neuroprotective effect at this time point. A slight decrease in microglia could impact neural circuitry by reducing synaptic pruning and neural precursor cell phagocytosis. Reduced microglial prevalence was also found in the amygdala of one-year-old WSD offspring (Dunn et al., 2022), further indicating that impacts to circuitry could occur in regions outside of the ARC.

This study also found a greater density of microglia and macrophages in the middle of the ARC compared with the rostral and caudal ends. This distribution, best fit by a quadratic curve, was independent of perinatal diet exposure. Centrally located neuronal populations may be more vulnerable to microglia-neuron interactions during periods of elevated inflammation, including during the prenatal period of WSD exposure. One such neuronal population consists of NPY neurons, indicating that inflammatory conditions could disrupt the control of food intake and body weight. The findings from this study have important implications for the trajectory of offspring neurodevelopment and brain organization.

4.2 Trajectory of Perinatal WSD Exposure on Functional Connectivity and Neuroinflammation

The two studies of this dissertation found a consistent trajectory regarding the impacts of perinatal WSD exposure on brain connectivity and neuroinflammation. Study 1 explored functional connectivity from as early as 4 months of age through 36 months of age in Japanese macaques. Study 2 reported on neuroinflammation from the prenatal period and followed up on microglial outcomes one year after birth in the same macaque model. In both studies, perinatal WSD exposure was found to have a larger impact on

offspring outcomes during the period of exposure, and outcomes resolved quickly thereafter.

Specifically, this entailed widespread differences in the functional connectivity of sensory systems at 4 months of age which diminished even during perinatal exposure at 6 months of age, and it encompassed increased markers of neuroinflammation during the prenatal period but decreased markers one year after birth. This consistency supports the view that the brain is resilient against long-term impacts from perinatal WSD exposure. In fact, indistinguishable patterns of functional connectivity during perinatal WSD exposure and a slight decrease in postnatal neuroinflammation can be interpreted as positive indicators; the former speaks to the robustness of neural circuitry formation in the face of direct and continued WSD exposure, and the latter proposes a potentially neuroprotective outcome where prenatal inflammation primes for less postnatal inflammation. These conclusions are, however, limited by the scope of the studies; further research could uncover differences in functional connectivity that were too small or too varied to be detected in the small sample size at 6 months, and additional measures of neuroinflammation could lead to a more comprehensive, and potentially opposite, understanding of the neuroinflammatory state at the one year time point.

Additionally, while a preliminary analysis in Study 1 found no difference in the number of microglia and macrophages in the amygdala at 36 months of age (Figure 2.6), there was a slight trend towards an increased prevalence in the perinatal WSD group. If the trend reaches significance in a more robust study, this would reveal a trajectory where neuroinflammation in perinatal WSD offspring is heightened *in utero*, as evidenced in the fetal ARC (Grayson et al., 2010), reduced in early childhood, as suggested by fewer Iba1-

stained cells in the ARC (Study 2) and amygdala (Dunn et al., 2022), and resurfaces during preadolescence, as suggested by the trend in the amygdala (Study 1). This particular trajectory would identify preadolescence as another period that may be subjected to disruptions in neural circuit formation and functioning.

Furthermore, it is important to consider that while the perinatal WSD exposure does not appear to have major detrimental impacts in older offspring, it is not without its effects. Although decreased neuroinflammation is often regarded as a sign of health, a reduction in the number of microglia, even if slight, could have noticeable impacts on synaptic pruning and other microglial processes implicated in circuit formation. Similarly, while no major differences in functional connectivity were found in 36 month old macaques, humans with SOR at the same developmental age demonstrated differences in a small set of sensory connections in a study by Schwarzlose and colleagues (2023) despite poor FRF model performance in the current study, suggesting that small effects might be found in the WSD offspring by a more sensitive analytical approach. Thus, it is possible that perinatal WSD exposure continues to impact offspring in subtle ways. Further research is recommended to better uncover the extent of these impacts.

Overall, the two studies elucidate a distinct trajectory that highlights the prenatal and early postnatal periods as being more susceptible to neuroinflammatory and neural circuitry impacts associated with WSD exposure. While most studies in children with SPD tend to observe the early childhood and preadolescent periods, the present studies suggest that greater challenges with sensory processing and related behaviors may be present during infancy. Future efforts should focus on the first year of life to identify

early markers of SPD and develop therapeutic treatments or interventions. Further research is required to understand how impacts initiated during this period may lead to the behaviors characteristic of neurodevelopmental disorders like SPD that continue in later childhood.

4.3 Neuroinflammation as a Mediator for Altered Neural Circuitry

Another area for further research is in regards to the relationship between neuroinflammation and functional connectivity. The two studies of this dissertation identified a consistent response trajectory across connectivity and neuroinflammation, indicating that a relationship could exist between the two domains. It is well known that microglia do, in fact, shape functional connectivity by controlling neurogenesis and synapse elimination, and it would be interesting to explore direct links between perinatal WSD exposure, microglial activity, and the connectivity of regions implicated in the 4 month old offspring. Given that the FRF model was only able to differentiate between diet groups based on the connectivity at 4 months of age, it would seem that the microglial process of neural precursor cell phagocytosis may be more impacted and responsible for the altered circuitry than synaptic pruning, as the former is prominent during the third trimester, and the latter does not peak until later ages (Cunningham et al., 2013; Eltokhi et al., 2020). A follow-up study could explore whether microglial phagocytosis is amplified in the regions that demonstrated decreased connectivity at 4 months of age. Increased neuroinflammation and microglial prevalence are associated with increased phagocytosis of neural precursor cells (Cunningham et al., 2013), so it is

possible that the inflammatory effects of the prenatal WSD exposure (Grayson et al., 2010) reduced the total number of neurons that reached maturation in these areas, leading to decreased connectivity such as was seen in the intra-somatosensory network at 4 months of age.

Studying the detailed dynamics of microglial phagocytosis at every region that displayed altered connectivity might be a burdensome endeavor, especially if some of those regions turned out to be poor candidates for microglial involvement due to being spared from a strong neuroinflammatory response. A comprehensive precursor experiment could identify candidates by assessing neuroinflammation across the brain using MRI. The use of MRI would enable cross-mapping between domains: the areas that are implicated in altered functional connectivity could be rapidly compared to a brain-wide map of neuroinflammation. This comparison would uncover associated regions that should be targeted for more extensive investigation. The brain-wide map of neuroinflammation would be generated by acquiring structural MRI scans under ferumoxytol contrast. Ferumoxytol is an ultrasmall superparagmagnetic iron oxide (USPIO) nanoparticle that is Food and Drug Administration (FDA)-approved for the treatment of iron deficiency in adult chronic kidney disease patients. Due to its superparamagnetic quality, it is also used as an imaging contrast agent. Ferumoxytol has an intravascular half-life of 10-14 hours (Hasan et al., 2012), so it is cleared relatively quickly. However, during neuroinflammation, ferumoxytol is trafficked into tissue at sites of reactive lesions and altered BBB permeability (McConnell et al., 2016) where it is phagocytosed by inflammatory cells like macrophages (Hubert et al., 2019; Hasan et al., 2012). Clearance through phagocytosis takes longer than intravascular clearance.

Imaging 24 hours after administration therefore leads to peak contrast enhancement intensity in areas that are sites of neuroinflammation (Hasan et al., 2012). Using this approach, sites of neuroinflammation could be mapped to the functional connectome to identify regions of overlap, potentially implicating neuroinflammation in the altered connectivity. This experiment was considered for the present study, but there was insufficient time to optimize scan settings before the juvenile macaques had aged out of the study.

Similarly, a future direction for the current study would be to relate the functional connectivity findings to neuroinflammatory outcomes using the FRF. Instead of predicting perinatal WSD exposure, measures like microglial density or the concentration of an inflammatory cytokine in offspring could be predicted by the set of functional connections. Some of this data currently exists for a subset of offspring who underwent imaging at 36 months of age. Following imaging, the number of microglia and macrophages, identified by Iba1 staining, was quantified as previously described (Dunn et al., 2022). Thus, amygdala connectivity could be used to predict Iba1-stained cell counts in the amygdala at roughly the same time point. A pilot analysis using data from these two domains was conducted for this dissertation and was reported in the Supplementary Material of Study 1. In summary, all connections between the amygdala and the sensory networks, totaling 53 connections including the connection between both hemispheres of the amygdala, were selected as training features. The FRF regression model implemented 6-fold cross-validation with 5 repetitions, 3000 trees, and 90% of the data reserved for the training set. Unfortunately, the model did not achieve significant performance metrics, likely due to the small sample size ($N = 10$). Although the FRF

model was unable to use the connectivity of the 53 amygdala connections to predict the average number of microglia and macrophages across the amygdala, other analyses could examine the relationship between Iba1-stained cell count and each individual connection or network grouping to find focal areas of impact. Further work should also seek to increase the sample size to increase power and enable more robust investigation. If an analysis revealed a relationship between the two measures, then this would provide further evidence for a relationship between microglial activity and impaired neural circuitry. Synaptic pruning might be a more likely mediator for alterations in circuitry in this age group as the microglial process would still be taking place, whereas controlling neurogenesis through phagocytosis is predominant at earlier time points (Eltokhi et al., 2020; Cunningham et al., 2013). Increased synaptic pruning can lead to increased or decreased connectivity depending on the context (Kim et al., 2017; Cowan and Petri, 2018; Kleinhans et al., 2016; Huang et al., 2016; Ypma et al., 2016), so the results of the analysis would be useful in understanding the impacts of synaptic pruning within the amygdala as microglial count rises. Additional studies could further identify the mechanisms by which neuroinflammation, potentially from WSD exposure, transiently reconstructs neural circuitry during early development.

4.4 Alternatives to Perinatal WSD: Maternal Adiposity and Inflammation may be Distinct Drivers of SPD Outcomes

While prenatal WSD is associated with an increased incidence of neurodevelopmental disorders like ASD, it is important to remember that there may be an underlying mediator between the diet and the increased incidence. Two potential

mediators are adiposity and inflammation, as both are increased with WSD consumption, and both are similarly associated with an increased incidence of neurodevelopmental disorders following prenatal exposure (DeCapo et al., 2019; Careaga et al., 2017; Parker-Athill and Tan, 2010; Guma et al., 2019). It is possible that these three factors have distinct effects that have been conflated in the literature. For example, it is possible that maternal adiposity has more predictive power than maternal WSD due to the direct influences of adiposity, yet WSD continues to be implicated due to its association with an increased likelihood of increasing adiposity. In this scenario, it is not necessarily the WSD exposure that determines the neurodevelopmental outcome, but rather how the body of the pregnant person responds to the diet, especially in terms of whether adiposity is increased or an inflammatory response is launched.

There is evidence in the literature that suggests this conflation may be occurring. In human studies that involve prenatal exposures, accounts of WSD are typically based on self-reporting rather than experimentally controlled dietary interventions (Bastías-Pérez et al., 2020). Self-reporting errors can make it difficult to accurately ascertain the diet composition that would be associated with the neurodevelopmental outcome. Instead, more objective measures that are generally correlated with adiposity, like body mass index (BMI) and weight, are more commonly used to explore associations with neurodevelopmental disorders in offspring. These measures are often associated with an increased incidence of ASD in humans (Moss and Chugani, 2014; Reynolds et al., 2014; Krakowiak et al., 2012; Li et al., 2016; Mina et al., 2017). In order to further study the effects of these metabolic measures on prenatal development in animal models, a method must be implemented to increase adiposity in the dams. While certain genetic factors are

associated with increased adiposity, a major environmental contributor is diet, as diets with more than 30% of the daily energy intake deriving from fats can easily induce obesity in humans (Bastías-Pérez et al., 2020). This environmental factor is pertinent, as WSD consumption is highly prevalent among the US population (Hohos and Skaznik-Wikiel, 2017; Hintze et al., 2018). High-fat diets are therefore regularly selected as a convenient, relevant means for inducing the implicated adiposity measures in animal models.

As mentioned previously, adverse dietary manipulations are generally not acceptable in human studies of prenatal development, thereby leading to the reliance on self-reporting. As such, most studies that can examine the precise impacts of prenatal WSD on neurodevelopment require the use of animal models (Bastías-Pérez et al., 2020). Most animal studies that examine the impacts of WSD, or WSD-induced obesity, implement rodent models (Even et al., 2017; Urbonaite et al., 2022). The potential issue is that not all rodent strains replicate the full metabolic spectrum of humans (Bastías-Pérez et al., 2020; Buettner et al., 2007; Even et al., 2017). For example, inbred mouse strains like C57BL/6J are highly susceptible to obesity when fed a high-fat diet (Rossmeisl et al., 2003; Fernandes et al., 2021). Sprague-Dawley rats tend to display more variation in weight gain, but some studies still report almost complete overlap between the HFD-fed and obese subsets (Lauterio et al., 1994; Bilbo and Tsang, 2010). Thus, animal models that claim to expose an association between prenatal WSD exposure and a neurodevelopmental outcome may instead be demonstrating an association between exposure to increased maternal adiposity and the neurodevelopmental outcome.

Furthermore, many rodent studies utilize high-fat diets that derive 60% of the kcal from fat to induce obesity rapidly and save on costs, whereas a more physiologically relevant diet for comparison to human obesity would contain 45% fat content (Bastías-Pérez et al., 2020; Mitchell et al., 2022a; Hintze et al., 2018). A study in mice that compared diets with 45% and 60% fat content revealed differences in the sets of metabolites that were altered compared to metabolites in mice that were fed a low-fat diet, demonstrating that diet composition affects the metabolic response (Showalter et al., 2018). Data from studies that use diets with 60% fat content might therefore be irrelevant to human outcomes. Thus, outcomes that have been attributed to prenatal WSD exposure may more appropriately be attributed to extreme metabolic perturbations not commonly experienced in the human population.

Studies that carefully match the metabolic variation of the animal species and strain, the fat content of the diet, and the types of fat in the diet to the corresponding features typical for humans may provide more accurate insight into the true impacts of prenatal WSD exposure on offspring neurodevelopment. These studies should seek to control for maternal adiposity in order to distinguish any independent effects of the two highly conflated factors. Perhaps the most physiologically relevant study regarding this subject matter was conducted by Lyall and colleagues (2013) in humans. The researchers found no significant difference in offspring ASD risk with certain types of fat intake (saturated fat, monounsaturated fat, and *trans*-fat) when adjusting for the BMI of the pregnant individual, even though there was an association between increased BMI and total fat intake. On the contrary, increased polyunsaturated fatty acid intake was associated with a decreased risk of ASD (Lyall et al., 2013). Measures of fat intake do

not fully replicate the WSD, which also includes high sugar content, but this evidence suggests that the fats in the diet alone may not account for the increased incidence of ASD phenotypes typically seen in animal studies. The authors additionally acknowledge several limitations, including sources of error in the reporting of dietary consumption and a limited sample size of 317 pregnant individuals who reported a child with ASD compared to 17,728 controls. Nevertheless, a review of studies that examined prenatal factors associated with ASD identified this study by Lyall and colleagues (2013) as being the only one to examine maternal fat and fatty acid intake on ASD incidence at the time of publication (Lyall et al., 2014). Given the shortage of WSD studies in humans, a comprehensive review of carefully controlled and physiologically relevant animal studies in this field may better determine the extent to which prenatal WSD exposure and maternal adiposity independently contribute to neurodevelopmental outcomes.

The NHP model used in this study is exceptionally suited to address the issue of conflated factors. The NHP subjects match the metabolic responses that are characteristic of humans, including a variation in the weight gain, BMI, and adiposity measures among subjects from both diet groups (Harris et al., 2016). The composition of the WSD is additionally controlled to be more representative of the WSD typically consumed by humans. Thus, while results from this NHP model may conflict with the largely rodent-based literature in some areas, this may be due to the greater match between NHP and human outcomes. Moreover, prior studies in this model have avoided conflating environmental factors by distinguishing between the independent and interrelated effects of maternal diet, adiposity, and inflammation on offspring neurodevelopment (Thompson et al., 2018).

An exploration of maternal factors on offspring inflammation found unique effects of maternal adiposity and WSD exposure. Maternal WSD was associated with increased maternal pre-pregnancy adiposity, yet the former and latter were associated with decreased and increased Iba1-stained cell counts in the offspring amygdala one year after birth, respectively (Dunn et al., 2022). Additionally, while maternal cytokine and chemokine levels from the third trimester were not associated with Iba1-stained cell counts in the amygdala of offspring, there was an impact on offspring inflammatory markers one year after birth. Maternal adiposity was associated with decreased maternal chemokines, which were in turn associated with decreased offspring cytokines and increased offspring chemokines. This comprehensive analysis elucidates the complexity of interactions that lead to offspring outcomes. The findings from Study 2 are consistent with the prior analysis, as both revealed decreased Iba1-stained cell counts associated with perinatal WSD exposure one year after birth. The findings would suggest that, had a greater sample size allowed for the independent analysis of maternal adiposity, an increased Iba1-stained cell count in the ARC may have been associated with maternal adiposity in Study 2, as well. Admittedly, given the high overlap of offspring exposed to either perinatal WSD or maternal adiposity, it is possible, though less likely in the context of the amygdala findings, that the ARC findings could be attributed to maternal adiposity rather than perinatal WSD exposure. Interestingly, while the prior study did not find an association between maternal cytokine and chemokine levels and Iba1-stained cell counts in the amygdala, a PLSR analysis reported in the Supplementary Material of Study 2 demonstrated an association between maternal cytokine and chemokines levels and Iba1-stained cell counts in the ARC. A coherent understanding of the impacts could not be

drawn, however, suggesting that individual cytokines may have opposing impacts on the number of microglia and macrophages present in the ARC of offspring one year after birth. This could explain why the prior study, which looked for impacts from predetermined combinations of cytokines and chemokines rather than components automatically detected from the PLSR, did not find a strong association. The PLSR analysis supports the idea that alternative factors like maternal inflammatory markers may have complex impacts on offspring outcomes that are inconsistent with the impacts of perinatal WSD exposure.

Maternal adiposity and perinatal WSD exposure also have opposing effects on idiosyncratic behavior, as well as opposing effects on maternal IL-12 levels which are then negatively associated with offspring social engagement behaviors, at 6.6 months of age (Mitchell et al., 2022b). Perinatal WSD exposure was additionally associated with increased anxiety and stereotypy, while maternal adiposity was associated with increased impulsive and disruptive behaviors, at 11 months of age (Thompson et al., 2018). These findings further demonstrate the disparate effects of prenatal WSD and adiposity exposures on offspring neurodevelopment. Further research should examine the independent impacts of these two prenatal factors on behaviors common to SPD.

Analysis of offspring cortical thickness growth over time has also revealed independent impacts from perinatal WSD exposure and third trimester maternal IL-6 levels (Ramirez et al., 2021). Among other distinct effects in different regions, perinatal WSD exposure was associated with decreased bilateral cortical thickness in the pole of the temporal cortex at 4 months of age, whereas increased maternal IL-6 was associated with increased thickness. Additionally, perinatal WSD exposure and maternal IL-6

exposure had largely overlapping effects on cortical surface area, with a much greater number of additional functional networks impacted by diet than by IL-6. This study demonstrates that perinatal WSD exposure may have a separate impact on cortical volume from maternal inflammation. The findings from Study 1 partially align to the results of the prior analysis. Study 1 found decreased intra-somatomotor network connectivity as the most informative difference associated with perinatal WSD exposure at 4 months of age. This could potentially be explained by the decreased cortical surface area of the somatomotor network found in WSD offspring at the same time point, as a smaller area could signal fewer neurons and weaker connections. The only other difference found at this time point among the networks assessed in Study 1, for either perinatal exposure, was decreased cortical surface area in the limbic network associated with perinatal WSD exposure. A hypothesis of this dissertation was that perinatal WSD exposure would be associated with increased amygdala connectivity, so decreased cortical surface area does not align well to that hypothesis, though it does support the expectation that the amygdala would be impacted. The findings from Study 1 demonstrated small differences in amygdala connectivity at 4 months of age that were not ranked highly for model importance, with mixed directionality of impacts. However, these findings do not necessarily conflict, as the amygdala is just one region within the limbic network; it is possible that other regions within the network could have demonstrated decreased connectivity, aligning with decreased surface area, had they been included in the FRF model. For example, while maternal IL-6 was not associated with a change in limbic network cortical surface area, it was associated with smaller left

amygdala volume at 4 months of age, demonstrating that amygdala changes can be insufficient to drive network-wide changes (Ramirez et al., 2020).

Given the differences in impacts on brain structure between perinatal WSD and maternal IL-6 exposure, it would be interesting to follow up on Study 1 and determine whether controlling for maternal IL-6 or adiposity would yield different results. Of the 69 offspring included in Study 1, 50 had measures of maternal pre-pregnancy adiposity. Of these, 60% of the offspring exposed to a perinatal CTR diet were from dams with a percent body fat greater than 19.6%, defined as high adiposity for this study, whereas only 53.3% of the WSD offspring were exposed to high maternal adiposity. However, dams with more than 29.05% body fat were considered to have very high adiposity. Only 15% of all perinatal CTR offspring were exposed to the influences of very high adiposity, whereas this exposure was prevalent in 40% of perinatal WSD offspring. This stratification in adiposity levels across diet groups enables future analyses to explore the independent impacts of perinatal WSD and maternal adiposity exposures on functional connectivity measures. In fact, one analysis that attempted to explore the independent impact of maternal adiposity was included in the Supplementary Material of Study 1. As none of the subjects in the 36 month age group had missing maternal adiposity data, it was possible to use their functional connectivity strengths to predict maternal adiposity in the same manner as perinatal WSD group was predicted. However, neither a regression model predicting percent body fat nor a classification model predicting binary adiposity categories yielded significant performance metrics. Thus, maternal adiposity, like perinatal WSD exposure, did not lead to strong or widespread differences in connectivity at 36 months of age. However, this does not rule out the possibility that maternal

adiposity could have a different impact on functional connectivity from perinatal WSD exposure during periods of heightened vulnerability, such as during the 4 month old time point. Prior studies in this animal model suggest that this may be the case, though further research is needed to confirm this hypothesis.

Considering the above, it is clear that perinatal WSD exposure may have distinct impacts from maternal adiposity, and some of the literature may inadvertently conflate the two factors. Similarly, diet- and adiposity-mediated impacts to maternal inflammatory markers may also lead to distinct outcomes. Thus, it is important to consider all three factors, in addition to other measures, when evaluating impacts to offspring neurodevelopment. The current field of SPD research has yet to establish prenatal WSD exposure as a risk factor, perhaps due to the difficulties in acquiring accurate dietary reporting in human models, but this dissertation reveals findings that merit further investigation into the compounding or contrasting impacts of diet and other factors on the development of SPD in offspring.

4.5 Appropriate Animal Model Applications

When designing future studies, it is important to consider whether a NHP or rodent model would be better suited to address the research question. For example, NHP models replicate the full range of metabolic variation seen in humans, so studies that seek to provide clinically relevant metabolic insights or distinguish between the independent effects of diet and adiposity might consider preferentially adopting a NHP model or, if needed, a rodent model that has been carefully chosen for its metabolic similarities to humans (Even et al., 2017). In general, NHP models will offer greater similarities to

humans than will rodent models given the genetic relationships between the species, but not every research question will need to maximize physiological or behavioral relevance.

Preliminary lines of study that benefit from surveying a multitude of cytokines, metabolic factors, or brain regions could be initiated in rodents, and promising interactions could be repeated and expanded upon in NHP models. This strategy could be useful when following up on the supplemental result in Study 2 that demonstrated that maternal cytokines predicted offspring Iba1-stained cell count in differential ways. Many inflammatory mechanisms are conserved across species (Godec et al., 2016; Estes et al., 2018), so a rodent model could be sufficient for a preliminary exploration of how prenatal inflammatory dynamics shape neural circuitry.

Similarly, experiments that require large sample sizes or longitudinal approaches could leverage the cost-effectiveness and shorter developmental timelines of rodents before moving to a NHP model. This could be useful when following up on the functional connectivity findings from Study 1. A major limitation to brain-wide association studies that aim to relate variability in functional connectivity to psychopathology is that large sample sizes consisting of thousands of subjects are needed for reproducible, reliable results (Marek et al., 2022). Smaller sample sizes are sufficient in conjunction with repeated sampling, such as in longitudinal designs, or with induced effects, like a lesion, but these study modifications require substantial time and cost when conducted in NHP models. Critically, mice have demonstrated the same large-scale functional network properties identified in NHPs, so rs-fcMRI can be used to translate findings between mice and humans through NHP alignment (Stafford et al., 2014). Thus, rodent models can be leveraged to relate invasive or longitudinal physiological and

behavioral findings to brain-wide functional connectivity, potentially across large sample sizes when research groups conducting similar studies share their data in open-source repositories, to provide a baseline understanding of clinically relevant targets for future validation in NHP models.

Notably, any question that benefits from genetic manipulations, such as a knockout of microglial phagocytosis genes to examine the specific impacts to neurogenesis, synaptic pruning, and resulting functional connectivity, would be better applied in rodent models, as transgenic NHP methods are limited and labor-intensive (Liang et al., 2022). Relating genetic findings to human psychopathology through functional connectivity could therefore be a unique capability of rodent models.

While rodent studies benefit from low costs, short life spans, high reproduction rates, and precise genetic control to offer insights into detailed physiological dynamics, NHP models provide clinical relevance through highly conserved attributes including metabolic and immune functioning, gestational and neurodevelopmental timelines, placental structure and function, brain organization, and complex behavior (Sullivan and Kievit, 2016; Estes et al., 2018; Carter, 2007; Miranda-Dominguez et al., 2014). NHP models are therefore exceptionally positioned to validate findings from the vast body of rodent literature related to the impacts of prenatal WSD on offspring neurodevelopment, as was conducted for this dissertation. Future studies should continue to recruit NHP models as appropriate to affirm rodent findings and guide promising paths for further investigation.

4.6 Conclusions

The findings from this dissertation characterize the longitudinal outcomes of perinatal WSD exposure on functional connectivity and neuroinflammation in the context of SPD. The shared trajectory of strong impacts during the prenatal and early postnatal periods followed by rapid attenuation illustrates the transient impact of perinatal WSD exposure on long-term outcomes. These early periods are likely more susceptible to disruptions from WSD exposure due to the dynamic neural structuring occurring at those time points.

While these studies are limited by small sample sizes and an inability to fully test for the independent impacts of maternal adiposity and inflammation, they provide insights that are consistent with other findings in this NHP model and across the literature, and they contribute critical advancements on multiple fronts. These findings expand the developmental range that is typically explored in human SPD studies by characterizing functional connectivity from infancy through preadolescence; in doing so, this work has identified early infancy as a period when challenges in sensory processing may be particularly pronounced. Future work should investigate this period for sensory difficulties, markers for early detection of SPD, and therapeutic interventions. Furthermore, the differences found in the connectivity of sensory and emotional processing areas at 4 months of age support the theory that SPD arises from impairments in sensory processing, contributing to a growing body of research that promotes this perspective in the field. Additionally, these findings have uncovered a trajectory of neuroinflammation that aligns with the connectivity results, informing how this potential mediator of altered circuitry may impact sensory processing across development.

Importantly, this work combines the unique advantages of exploring dietary impacts in a metabolically relevant animal model with the application of a cross-species functional connectivity approach. Analyzing the same brain regions between species has allowed the WSD findings to be more appropriately compared to clinically relevant human outcomes. Ultimately, these studies advance what is known about the development of SPD and pave the way for future translational discoveries and therapies.

REFERENCES

ABCD Study. (2022). *Data Analysis, Informatics & Resource Center (DAIRC)*. Available online at: https://abcdstudy.org/study-sites/daic/ (accessed December 23, 2022).

Abel, T. W., Voytko, M. L., and Rance, N. E. (1999). The effects of hormone replacement therapy on hypothalamic neuropeptide gene expression in a primate model of menopause. *J. Clin. Endocrinol. Metab.* 84(6), 2111–2118. doi: 10.1210/jcem.84.6.5689

ABIDE. (2017). *Autism Brain Imaging Data Exchange*. Available online at: http://fcon_1000.projects.nitrc.org/indi/abide/ (accessed December 23, 2022).

Aguzzi, A., Barres, B. A., and Bennett, M. L. (2013). Microglia: scapegoat, saboteur, or something else?. *Science* 339(6116), 156–161. doi: 10.1126/science.1227901

Ahn, R. R., Miller, L. J., Milberger, S., and McIntosh, D. N. (2004). Prevalence of parents' perceptions of sensory processing disorders among kindergarten children. *Am. J. Occup. Ther.* 58(3), 287–293. doi: 10.5014/ajot.58.3.287

American Psychiatric Association. (2013a). *Diagnostic and statistical manual of mental disorders*, 5th Edn. Washington, DC: American Psychiatric Association.

American Psychiatric Association. (2013b). *Insurance Implications of DSM-5*. Available online at: https://www.psychiatry.org/File%20Library/Psychiatrists/Practice/DSM/APA_DSM_Insurance-Implications-of-DSM-5.pdf (accessed December 23, 2022).

Anderson, G., and Maes, M. (2014). Redox regulation and the autistic spectrum: role of

tryptophan catabolites, immuno-inflammation, autoimmunity and the amygdala. *Curr. Neuropharmacol.* 12(2), 148–167. doi: 10.2174/1570159X11666131120223757

Andersson, J. L., Skare, S., and Ashburner, J. (2003). How to correct susceptibility distortions in spin-echo echo-planar images: application to diffusion tensor imaging. *Neuroimage* 20(2), 870–888. doi: 10.1016/S1053-8119(03)00336-7

Andescavage, N. N., du Plessis, A., McCarter, R., Serag, A., Evangelou, I., Vezina, G., Robertson, R., and Limperopoulos, C. (2017). Complex trajectories of brain development in the healthy human fetus. *Cereb. Cortex* 27(11), 5274–5283. doi: 10.1093/cercor/bhw306

Andrews, D. S., Aksman, L., Kerns, C. M., Lee, J. K., Winder-Patel, B. M., Harvey, D. J., Waizbard-Bartov, E., Heath, B., Solomon, M., Rogers, S. J., Altmann, A., Nordahl, C. W., and Amaral, D. G. (2022). Association of amygdala development with different forms of anxiety in autism spectrum disorder. *Biol. Psychiatry* 91(11), 977–987. doi: 10.1016/j.biopsych.2022.01.016

Anghel, S. I., and Wahli, W. (2007). Fat poetry: a kingdom for PPAR gamma. *Cell Res.* 17(6), 486–511. doi: 10.1038/cr.2007.48

ANTs. (2022). *Advanced Normalization Tools*. Available online at: http://stnava.github.io/ANTs/ (accessed December 23, 2022).

Attwell, D., and Iadecola, C. (2002). The neural basis of functional brain imaging signals. *Trends Neurosci.* 25(12), 621–625. doi: 10.1016/s0166-2236(02)02264-6

Bale, T. L., Baram, T. Z., Brown, A. S., Goldstein, J. M., Insel, T. R., McCarthy, M. M.,

Nemeroff, C. B., Reyes, T. M., Simerly, R. B., Susser, E. S., and Nestler, E. J. (2010). Early life programming and neurodevelopmental disorders. *Biol. Psychiatry* 68(4), 314–319. doi: 10.1016/j.biopsych.2010.05.028

Bar-Shalita, T., and Cermak, S. A. (2016). Atypical sensory modulation and psychological distress in the general population. *Am. J. Occup. Ther.* 70(4), 7004250010. doi: 10.5014/ajot.2016.018648

Baranek, G. T., Roberts, J. E., David, F. J., Sideris, J., Mirrett, P. L., Hatton, D. D., and Bailey, D. B., Jr (2008). Developmental trajectories and correlates of sensory processing in young boys with fragile X syndrome. *Phys. Occup. Ther. Pediatr.* 28(1), 79–98. doi: 10.1300/j006v28n01_06

Barnea, A., Aguila-Mansilla, N., Bigio, E. H., Worby, C., and Roberts, J. (1998). Evidence for regulated expression of neuropeptide Y gene by rat and human cultured astrocytes. *Regul. Pept.* 75-76, 293–300. doi: 10.1016/s0167-0115(98)00081-0

Basha, S., Surendran, N., and Pichichero, M. (2014). Immune responses in neonates. *Expert Rev. Clin. Immunol.* 10(9), 1171–1184. doi:10.1586/1744666X.2014.942288

Bastías-Pérez, M., Serra, D., and Herrero, L. (2020). Dietary options for rodents in the study of obesity. *Nutrients* 12(11), 3234. doi: 10.3390/nu12113234

Beauchamp, M. S., Yasar, N. E., Frye, R. E., and Ro, T. (2008). Touch, sound and vision in human superior temporal sulcus. *Neuroimage* 41(3), 1011–1020. doi: 10.1016/j.neuroimage.2008.03.015

Belhocine, S., Machado Xavier, A., Distéfano-Gagné, F., Fiola, S., Rivest, S., and

Gosselin, D. (2022). Context-dependent transcriptional regulation of microglial proliferation. *Glia* 70(3), 572–589. doi: 10.1002/glia.24124

Ben-Sasson, A., Carter, A. S., and Briggs-Gowan, M. J. (2009). Sensory over-responsivity in elementary school: Prevalence and social-emotional correlates. *J. Abnorm. Child Psychol.* 37(5), 705–716. doi: 10.1007/s10802-008-9295-8

Ben-Sasson, A., Carter, A.S., and Briggs-Gowan, M.J. (2010). The development of sensory over-responsivity from infancy to elementary school. *J. Abnorm. Child Psychol.* 38, 1193–1202. doi: 10.1007/s10802-010-9435-9

Bezgin, G., Vakorin, V. A., van Opstal, A. J., McIntosh, A. R., and Bakker, R. (2012). Hundreds of brain maps in one atlas: registering coordinate-independent primate neuro-anatomical data to a standard brain. *Neuroimage* 62(1), 67–76. doi: 10.1016/j.neuroimage.2012.04.013

Bilbo, S. D., and Schwarz, J. M. (2009). Early-life programming of later-life brain and behavior: a critical role for the immune system. *Front. Behav. Neurosci.* 3, 14. doi: 10.3389/neuro.08.014.2009

Bilbo, S. D., and Tsang, V. (2010). Enduring consequences of maternal obesity for brain inflammation and behavior of offspring. *FASEB J.* 24(6), 2104–2115. doi: 10.1096/fj.09-144014

Bolton, J. L., and Bilbo, S. D. (2014). Developmental programming of brain and behavior by perinatal diet: focus on inflammatory mechanisms. *Dialogues Clin. Neurosci.* 16(3), 307–320. doi: 10.31887/DCNS.2014.16.3/jbolton

Bordeleau, M., Fernández de Cossío, L., Chakravarty, M. M., and Tremblay, M. È.

(2021). From maternal diet to neurodevelopmental disorders: a story of neuroinflammation. *Front. Cell. Neurosci.* 14, 612705. doi: 10.3389/fncel.2020.612705

Brown, V. A. (2021). An introduction to linear mixed-effects modeling in R. *Adv. Methods Pract. Psychol. Sci.* 4(1). doi: 10.1177/2515245920960351

Buettner, R., Schölmerich, J., and Bollheimer, L. C. (2007). High-fat diets: modeling the metabolic disorders of human obesity in rodents. *Obesity (Silver Spring)* 15(4), 798–808. doi: 10.1038/oby.2007.608

Cabinian, A., Sinsimer, D., Tang, M., Zumba, O., Mehta, H., Toma, A., Sant'Angelo, D., Laouar, Y., and Laouar, A. (2016). Transfer of maternal immune cells by breastfeeding: maternal cytotoxic T lymphocytes present in breast milk localize in the Peyer's patches of the nursed infant. *PloS One* 11(6), e0156762. doi: 10.1371/journal.pone.0156762

Careaga, M., Murai, T., and Bauman, M. D. (2017). Maternal immune activation and autism spectrum disorder: from rodents to nonhuman and human primates. *Biol. Psychiatry* 81(5), 391–401. doi: 10.1016/j.biopsych.2016.10.020

Carpenter, K. L. H., Baranek, G. T., Copeland, W. E., Compton, S., Zucker, N., Dawson, G., and Egger, H. L. (2019). Sensory over-responsivity: An early risk factor for anxiety and behavioral challenges in young children. *J. Abnorm. Child Psychol.* 47, 1075–1088. doi: 10.1007/s10802-018-0502-y

Carter, A. M. (2007). Animal models of human placentation—a review. *Placenta*, 28 Suppl A, S41–S47. doi: 10.1016/j.placenta.2006.11.002

Carter, A. S., Ben-Sasson, A., and Briggs-Gowan, M. J. (2011). Sensory over-responsivity, psychopathology, and family impairment in school-aged children. *J. Am. Acad. Child Adolesc. Psychiatry* 50(12), 1210–1219. doi: 10.1016/j.jaac.2011.09.010

Cesar, H. C., and Pisani, L. P. (2017). Fatty-acid-mediated hypothalamic inflammation and epigenetic programming. *J. Nutr. Biochem.* 42, 1–6. doi: 10.1016/j.jnutbio.2016.08.008

Chang, Y. S., Owen, J. P., Desai, S. S., Hill, S. S., Arnett, A. B., Harris, J., Marco, E. J., and Mukherjee, P. (2014). Autism and sensory processing disorders: shared white matter disruption in sensory pathways but divergent connectivity in social-emotional pathways. *PloS One* 9(7), e103038. doi: 10.1371/journal.pone.0103038

Chavhan, G. B., Babyn, P. S., Thomas, B., Shroff, M. M., and Haacke, E. M. (2009). Principles, techniques, and applications of T2*-based MR imaging and its special applications. *Radiographics* 29(5), 1433–1449. doi: 10.1148/rg.295095034

Christensen, L. B., Woods, T. A., Carmody, A. B., Caughey, B., and Peterson, K. E. (2014). Age-related differences in neuroinflammatory responses associated with a distinct profile of regulatory markers on neonatal microglia. *J. Neuroinflammation* 11, 70. doi: 10.1186/1742-2094-11-70

Cinti, S., Mitchell, G., Barbatelli, G., Murano, I., Ceresi, E., Faloia, E., Wang, S., Fortier, M., Greenberg, A. S., and Obin, M. S. (2005). Adipocyte death defines macrophage localization and function in adipose tissue of obese mice and humans. *J. Lipid Res.* 46(11), 2347–2355. doi: 10.1194/jlr.M500294-JLR200

Collection 3165 - ABCD-BIDS Community Collection (ABCC). (2022a). *ABCD-BIDS Community Collection (ABCC) Documentation Summary*. Available online at: https://collection3165.readthedocs.io/en/stable/ (accessed December 23, 2022).

Collection 3165 - ABCD-BIDS Community Collection (ABCC). (2022b). *Pipeline*. Available online at: https://collection3165.readthedocs.io/en/stable/pipeline/ (accessed December 23, 2022).

Comstock, S. M., Pound, L. D., Bishop, J. M., Takahashi, D. L., Kostrba, A. M., Smith, M. S., and Grove, K. L. (2012). High-fat diet consumption during pregnancy and the early post-natal period leads to decreased α cell plasticity in the nonhuman primate. *Mol. Metab.* 2(1), 10–22. doi: 10.1016/j.molmet.2012.11.001

Cordova, M., Shada, K., Demeter, D. V., Doyle, O., Miranda-Dominguez, O., Perrone, A., Schifsky, E., Graham, A., Fombonne, E., Langhorst, B., Nigg, J., Fair, D. A., and Feczko, E. (2020). Heterogeneity of executive function revealed by a functional random forest approach across ADHD and ASD. *Neuroimage Clin.* 26, 102245. doi: 10.1016/j.nicl.2020.102245

Cowan, M., and Petri, W. A., Jr. (2018). Microglia: immune regulators of neurodevelopment. *Front. Immunol.* 9, 2576. doi: 10.3389/fimmu.2018.02576

Crane, L., Goddard, L., and Pring, L. (2009). Sensory processing in adults with autism spectrum disorders. *Autism.* 13(3), 215–228. doi: 10.1177/1362361309103794

Critz, C., Blake, K., and Nogueira, E. (2015). Sensory processing challenges in children. *J. Nurse Pract.* 11(7): 710-716. doi: 10.1016/j.nurpra.2015.04.016

Croizier, S., and Bouret, S. G. (2022). Molecular control of the development of

hypothalamic neurons involved in metabolic regulation. *J. Chem. Neuroanat.* 123, 102117. doi: 10.1016/j.jchemneu.2022.102117

Cunningham, C. L., Martínez-Cerdeño, V., and Noctor, S. C. (2013). Microglia regulate the number of neural precursor cells in the developing cerebral cortex. *J. Neurosci.* 33(10), 4216–4233. doi: 10.1523/JNEUROSCI.3441-12.2013

Dale, A. M., Fischl, B., and Sereno, M. I. (1999). Cortical surface-based analysis: I. Segmentation and surface reconstruction. *Neuroimage* 9(2), 179–194. doi: 10.1006/nimg.1998.0395

Dalvi, P. S., Chalmers, J. A., Luo, V., Han, D. Y., Wellhauser, L., Liu, Y., Tran, D. Q., Castel, J., Luquet, S., Wheeler, M. B., and Belsham, D. D. (2017). High fat induces acute and chronic inflammation in the hypothalamus: effect of high-fat diet, palmitate and TNF-α on appetite-regulating NPY neurons. *Int. J. Obes. (Lond.)* 41, 149–158. doi: 10.1038/ijo.2016.183

DeCapo, M., Thompson, J. R., Dunn, G., and Sullivan, E. L. (2019). Perinatal nutrition and programmed risk for neuropsychiatric disorders: a focus on animal models. *Biol. Psychiatry* 85(2), 122–134. doi: 10.1016/j.biopsych.2018.08.006

Denizli, M., Capitano, M. L., and Kua, K. L. (2022). Maternal obesity and the impact of associated early-life inflammation on long-term health of offspring. *Front. Cell. Infect. Microbiol.* 12, 940937. doi: 10.3389/fcimb.2022.940937

Donahue, C. J., Sotiropoulos, S. N., Jbabdi, S., Hernandez-Fernandez, M., Behrens, T. E., Dyrby, T. B., Coalson, T., Kennedy, H., Knoblauch, K., Van Essen, D. C., and Glasser, M. F. (2016). Using diffusion tractography to predict cortical connection

strength and distance: a quantitative comparison with tracers in the monkey. *J. Neurosci.* 36(25), 6758–6770. doi: 10.1523/JNEUROSCI.0493-16.2016

Dong, J., Lei, J., Elsayed, N. A., Lee, J. Y., Shin, N., Na, Q., Chudnovets, A., Jia, B., Wang, X., and Burd, I. (2020). The effect of intrauterine inflammation on mTOR signaling in mouse fetal brain. *Dev. Neurobiol.* 80(5-6), 149–159. doi: 10.1002/dneu.22755

Duan, Y., Zeng, L., Zheng, C., Song, B., Li, F., Kong, X., and Xu, K. (2018). Inflammatory links between high fat diets and diseases. *Front. Immunol.* 9, 2649. doi: 10.3389/fimmu.2018.02649

Dunn, G. A., Mitchell, A. J., Selby, M., Fair, D. A., Gustafsson, H. C., and Sullivan, E. L. (2022). Maternal diet and obesity shape offspring central and peripheral inflammatory outcomes in juvenile non-human primates. *Brain Behav. Immun.* 102, 224–236. doi: 10.1016/j.bbi.2022.02.024

Dunn, G. A., Nigg, J. T., and Sullivan, E. L. (2019). Neuroinflammation as a risk factor for attention deficit hyperactivity disorder. *Pharmacol. Biochem. Behav.* 182, 22–34. doi: 10.1016/j.pbb.2019.05.005

Dunn, W., and Westman, K. (1997). The sensory profile: the performance of a national sample of children without disabilities. *Am. J. Occup. Ther.* 51(1), 25–34. doi: 10.5014/ajot.51.1.25

Edlow, A. G., Castro, V. M., Shook, L. L., Kaimal, A. J., and Perlis, R. H. (2022). Neurodevelopmental outcomes at 1 year in infants of mothers who tested positive for SARS-CoV-2 during pregnancy. *JAMA Netw. Open* 5(6), e2215787. doi:

10.1001/jamanetworkopen.2022.15787

El Akoum, S., Lamontagne, V., Cloutier, I., and Tanguay, J. F. (2011). Nature of fatty acids in high fat diets differentially delineates obesity-linked metabolic syndrome components in male and female C57BL/6J mice. *Diabetol. Metab. Syndr.* 3, 34. doi: 10.1186/1758-5996-3-34

Ellulu, M. S., Patimah, I., Khaza'ai, H., Rahmat, A., and Abed, Y. (2017). Obesity and inflammation: the linking mechanism and the complications. *Arch. Med. Sci.* 13(4), 851–863. doi: 10.5114/aoms.2016.58928

Eltokhi, A., Janmaat, I. E., Genedi, M., Haarman, B. C. M., and Sommer, I. E. C. (2020). Dysregulation of synaptic pruning as a possible link between intestinal microbiota dysbiosis and neuropsychiatric disorders. *J. Neurosci. Res.* 98(7), 1335–1369. doi: 10.1002/jnr.24616

Entringer, S., Buss, C., and Wadhwa, P. D. (2015). Prenatal stress, development, health and disease risk: A psychobiological perspective-2015 Curt Richter Award Paper. *Psychoneuroendocrinology* 62, 366–375. doi: 10.1016/j.psyneuen.2015.08.019

Estes, J. D., Wong, S. W., and Brenchley, J. M. (2018). Nonhuman primate models of human viral infections. *Nat. Rev. Immunol.* 18(6), 390–404. doi: 10.1038/s41577-018-0005-7

Even, P. C., Virtue, S., Morton, N. M., Fromentin, G., and Semple, R. K. (2017). Editorial: Are rodent models fit for investigation of human obesity and related diseases?. *Front. Nutr.* 4, 58. doi: 10.3389/fnut.2017.00058

Fair, D. A., Nigg, J. T., Iyer, S., Bathula, D., Mills, K. L., Dosenbach, N. U., Schlaggar,

B. L., Mennes, M., Gutman, D., Bangaru, S., Buitelaar, J. K., Dickstein, D. P., Di Martino, A., Kennedy, D. N., Kelly, C., Luna, B., Schweitzer, J. B., Velanova, K., Wang, Y. F., Mostofsky, S., Castellanos, F. X., and Milham, M. P. (2013). Distinct neural signatures detected for ADHD subtypes after controlling for micro-movements in resting state functional connectivity MRI data. *Front. Syst. Neurosci.* 6, 80. doi: 10.3389/fnsys.2012.00080

Feczko, E., Balba, N. M., Miranda-Dominguez, O., Cordova, M., Karalunas, S. L., Irwin, L., Demeter, D. V., Hill, A. P., Langhorst, B. H., Grieser Painter, J., Van Santen, J., Fombonne, E. J., Nigg, J. T., and Fair, D. A. (2018). Subtyping cognitive profiles in Autism Spectrum Disorder using a Functional Random Forest algorithm. *Neuroimage* 172, 674–688. doi: 10.1016/j.neuroimage.2017.12.044

Feczko, E., Miranda-Dominguez, O., Marr, M., Graham, A. M., Nigg, J. T., and Fair, D. A. (2019). The heterogeneity problem: approaches to identify psychiatric subtypes. *Trends Cogn. Sci.* 23(7), 584–601. doi: 10.1016/j.tics.2019.03.009

Fernandes, D. J., Spring, S., Roy, A. R., Qiu, L. R., Yee, Y., Nieman, B. J., Lerch, J. P., and Palmert, M. R. (2021). Exposure to maternal high-fat diet induces extensive changes in the brain of adult offspring. *Transl. Psychiatry* 11(1), 149. doi: 10.1038/s41398-021-01274-1

Filipello, F., Morini, R., Corradini, I., Zerbi, V., Canzi, A., Michalski, B., Erreni, M., Markicevic, M., Starvaggi-Cucuzza, C., Otero, K., Piccio, L., Cignarella, F., Perrucci, F., Tamborini, M., Genua, M., Rajendran, L., Menna, E., Vetrano, S., Fahnestock, M., Paolicelli, R. C., and Matteoli, M. (2018). The microglial innate immune receptor TREM2 is required for synapse elimination and normal brain

connectivity. *Immunity* 48(5), 979–991.e8. doi: 10.1016/j.immuni.2018.04.016

Fischl, B., Sereno, M. I., and Dale, A. M. (1999). Cortical surface-based analysis. II: Inflation, flattening, and a surface-based coordinate system. *Neuroimage* 9(2), 195–207. doi: 10.1006/nimg.1998.0396

Forslin Aronsson, S., Spulber, S., Popescu, L. M., Winblad, B., Post, C., Oprica, M., and Schultzberg, M. (2006). alpha-Melanocyte-stimulating hormone is neuroprotective in rat global cerebral ischemia. *Neuropeptides* 40(1), 65–75. doi: 10.1016/j.npep.2005.10.006

Fox, M. D., and Raichle, M. E. (2007). Spontaneous fluctuations in brain activity observed with functional magnetic resonance imaging. *Nat. Rev. Neurosci.* 8(9), 700–711. doi: 10.1038/nrn2201

Fox, M. D., Snyder, A. Z., Vincent, J. L., Corbetta, M., Van Essen, D. C., and Raichle, M. E. (2005). The human brain is intrinsically organized into dynamic, anticorrelated functional networks. *Proc. Natl. Acad. Sci. U. S. A.* 102(27), 9673–9678. doi: 10.1073/pnas.0504136102

Frade, J. M., and Barde, Y. A. (1998). Microglia-derived nerve growth factor causes cell death in the developing retina. *Neuron* 20(1), 35–41. doi: 10.1016/s0896-6273(00)80432-8

FreeSurfer. (2022). FreeSurfer software suite. Available online at: https://surfer.nmr.mgh.harvard.edu/ (accessed December 23, 2022).

Frias, A. E., Morgan, T. K., Evans, A. E., Rasanen, J., Oh, K. Y., Thornburg, K. L., and Grove, K. L. (2011). Maternal high-fat diet disturbs uteroplacental hemodynamics

and increases the frequency of stillbirth in a nonhuman primate model of excess nutrition. *Endocrinology* 152(6), 2456–2464. doi: 10.1210/en.2010-1332

Fujiyama, Y., Hokari, R., Miura, S., Watanabe, C., Komoto, S., Oyama, T., Kurihara, C., Nagata, H., and Hibi, T. (2007). Butter feeding enhances TNF-alpha production from macrophages and lymphocyte adherence in murine small intestinal microvessels. *J. Gastroenterol. Hepatol.* 22(11), 1838–1845. doi: 10.1111/j.1440-1746.2007.04905.x

Funaki M. (2009). Saturated fatty acids and insulin resistance. *J. Med. Invest.* 56(3-4), 88–92. doi: 10.2152/jmi.56.88

Gao, W., Alcauter, S., Elton, A., Hernandez-Castillo, C. R., Smith, J. K., Ramirez, J., and Lin, W. (2015). Functional network development during the first year: relative sequence and socioeconomic correlations. *Cereb. Cortex* 25(9), 2919–2928. doi: 10.1093/cercor/bhu088

Gao, W., Lin, W., Grewen, K., and Gilmore, J. H. (2017). Functional connectivity of the infant human brain: plastic and modifiable. *Neuroscientist* 23(2), 169–184. doi: 10.1177/1073858416635986

Garavan, H., Bartsch, H., Conway, K., Decastro, A., Goldstein, R. Z., Heeringa, S., Jernigan, T., Potter, A., Thompson, W., and Zahs, D. (2018). Recruiting the ABCD sample: Design considerations and procedures. *Dev. Cogn. Neurosci.* 32, 16–22. doi: 10.1016/j.dcn.2018.04.004

Garidou, L., Pomié, C., Klopp, P., Waget, A., Charpentier, J., Aloulou, M., Giry, A., Serino, M., Stenman, L., Lahtinen, S., Dray, C., Iacovoni, J. S., Courtney, M.,

Collet, X., Amar, J., Servant, F., Lelouvier, B., Valet, P., Eberl, G., Fazilleau, N., Douin-Echinard, V., Heymes, C., and Burcelin, R. (2015). The gut microbiota regulates intestinal CD4 T cells expressing RORγt and controls metabolic disease. *Cell Metab.* 22(1), 100–112. doi: 10.1016/j.cmet.2015.06.001

Garofalo, R. (2010). Cytokines in human milk. *J. Pediatr.* 156(2 Suppl), S36–S40. doi: 10.1016/j.jpeds.2009.11.019

Gawlińska, K., Gawliński, D., Borczyk, M., Korostyński, M., Przegaliński, E., and Filip, M. (2021). A maternal high-fat diet during early development provokes molecular changes related to autism spectrum disorder in the rat offspring brain. *Nutrients* 13(9), 3212. doi: 10.3390/nu13093212

Github. (2022a). *DCAN-Labs/biceps.* Available online at: https://github.com/DCAN-Labs/biceps (accessed December 23, 2022).

Github. (2022b). *DCAN-Labs/functional-random-forest*. Available online at: https://github.com/DCAN-Labs/functional-random-forest (accessed December 23, 2022).

Github. (2023). *and02709/ISSPCA*. Available online at: https://github.com/and02709/ISSPCA (accessed March 9, 2023).

Glasser, M. F., Sotiropoulos, S. N., Wilson, J. A., Coalson, T. S., Fischl, B., Andersson, J. L., Xu, J., Jbabdi, S., Webster, M., Polimeni, J. R., Van Essen, D. C., Jenkinson, M., and WU-Minn HCP Consortium (2013). The minimal preprocessing pipelines for the Human Connectome Project. *Neuroimage* 80, 105–124. doi: 10.1016/j.neuroimage.2013.04.127

Goasdoué, K., Miller, S. M., Colditz, P. B., and Björkman, S. T. (2017). Review: The blood-brain barrier; protecting the developing fetal brain. *Placenta* 54, 111–116. doi: 10.1016/j.placenta.2016.12.005

Goda, Y., and Davis, G. W. (2003). Mechanisms of synapse assembly and disassembly. *Neuron* 40(2), 243–264. doi: 10.1016/s0896-6273(03)00608-1

Godec, J., Tan, Y., Liberzon, A., Tamayo, P., Bhattacharya, S., Butte, A. J., Mesirov, J. P., and Haining, W. N. (2016). Compendium of immune signatures identifies conserved and species-specific biology in response to inflammation. *Immunity* 44(1), 194–206. doi: 10.1016/j.immuni.2015.12.006

Gordon, E. M., Laumann, T. O., Adeyemo, B., Huckins, J. F., Kelley, W. M., and Petersen, S. E. (2016). Generation and evaluation of a cortical area parcellation from resting-state correlations. *Cereb. Cortex* 26(1), 288–303. doi: 10.1093/cercor/bhu239

Gourley, L., Wind, C., Henninger, E. M., and Chinitz, S. (2013). Sensory processing difficulties, behavioral problems, and parental stress in a clinical population of young children. *J. Child Fam. Stud.* 22(7), 912–921. doi: 10.1007/s10826-012-9650-9

Graham, A. M., Pfeifer, J. H., Fisher, P. A., Lin, W., Gao, W., and Fair, D. A. (2015). The potential of infant fMRI research and the study of early life stress as a promising exemplar. *Dev. Cogn. Neurosci.* 12, 12–39. doi: 10.1016/j.dcn.2014.09.005

Graham, A. M., Rasmussen, J. M., Rudolph, M. D., Heim, C. M., Gilmore, J. H., Styner,

M., Potkin, S. G., Entringer, S., Wadhwa, P. D., Fair, D. A., and Buss, C. (2018). Maternal systemic interleukin-6 during pregnancy is associated with newborn amygdala phenotypes and subsequent behavior at 2 years of age. *Biol. Psychiatry* 83(2), 109–119. doi: 10.1016/j.biopsych.2017.05.027

Grant, W. F., Gillingham, M. B., Batra, A. K., Fewkes, N. M., Comstock, S. M., Takahashi, D., Braun, T. P., Grove, K. L., Friedman, J. E., and Marks, D. L. (2011). Maternal high fat diet is associated with decreased plasma n-3 fatty acids and fetal hepatic apoptosis in nonhuman primates. *PloS One*, 6(2), e17261. doi: 10.1371/journal.pone.0017261

Grayson, B. E., Allen, S. E., Billes, S. K., Williams, S. M., Smith, M. S., and Grove, K. L. (2006). Prenatal development of hypothalamic neuropeptide systems in the nonhuman primate. *Neuroscience* 143(4), 975–986. doi: 10.1016/j.neuroscience.2006.08.055

Grayson, B. E., Levasseur, P. R., Williams, S. M., Smith, M. S., Marks, D. L., and Grove, K. L. (2010). Changes in melanocortin expression and inflammatory pathways in fetal offspring of nonhuman primates fed a high-fat diet. *Endocrinology* 151(4), 1622–1632. doi: 10.1210/en.2009-1019

Grayson, D. S., and Fair, D. A. (2017). Development of large-scale functional networks from birth to adulthood: A guide to the neuroimaging literature. *Neuroimage* 160, 15–31. doi: 10.1016/j.neuroimage.2017.01.079

Grayson, D. S., Bliss-Moreau, E., Machado, C. J., Bennett, J., Shen, K., Grant, K. A., Fair, D. A., and Amaral, D. G. (2016). The rhesus monkey connectome predicts

disrupted functional networks resulting from pharmacogenetic inactivation of the amygdala. *Neuron* 91(2), 453–466. doi: 10.1016/j.neuron.2016.06.005

GUI_environments. (2022). *Overview*. Available online at: https://gui-environments-documentation.readthedocs.io/en/latest/GUI_environments/ (accessed December 23, 2022).

Guma, E., Plitman, E., and Chakravarty, M. M. (2019). The role of maternal immune activation in altering the neurodevelopmental trajectories of offspring: A translational review of neuroimaging studies with implications for autism spectrum disorder and schizophrenia. *Neurosci. Biobehav. Rev.* 104, 141–157. doi: 10.1016/j.neubiorev.2019.06.020

Gustafsson, H. C., Sullivan, E. L., Nousen, E. K., Sullivan, C. A., Huang, E., Rincon, M., Nigg, J. T., and Loftis, J. M. (2018). Maternal prenatal depression predicts infant negative affect via maternal inflammatory cytokine levels. *Brain Behav. Immun.* 73, 470–481. doi: 10.1016/j.bbi.2018.06.011

Haddad-Tóvolli, R., Dragano, N., Ramalho, A., and Velloso, L. A. (2017). Development and function of the blood-brain barrier in the context of metabolic control. *Front. Neurosci.* 11, 224. doi: 10.3389/fnins.2017.00224

Hagler, D. J., Jr, Hatton, S., Cornejo, M. D., Makowski, C., Fair, D. A., Dick, A. S., Sutherland, M. T., Casey, B. J., Barch, D. M., Harms, M. P., Watts, R., Bjork, J. M., Garavan, H. P., Hilmer, L., Pung, C. J., Sicat, C. S., Kuperman, J., Bartsch, H., Xue, F., Heitzeg, M. M., Laird, A. R., Trinh, T. T., Gonzalez, R., Tapert, S. F., Riedel, M. C., Squeglia, L. M., Hyde, L. W., Rosenberg, M. D., Earl, E. A., Howlett, K. D.,

Baker, F. C., Soules, M., Diaz, J., de Leon, O. R., Thompson, W. K., Neale, M. C., Herting, M., Sowell, E. R., Alvarez, R. P., Hawes, S. W., Sanchez, M., Bodurka, J., Breslin, F. J., Morris, A. S., Paulus, M. P., Simmons, W. K., Polimeni, J. R., van der Kouwe, A., Nencka, A. S., Gray, K. M., Pierpaoli, C., Matochik, J. A., Noronha, A., Aklin, W. M., Conway, K., Glantz, M., Hoffman, E., Little, R., Lopez, M., Pariyadath, V., Weiss, S. R., Wolff-Hughes, D. L., DelCarmen-Wiggins, R., Feldstein Ewing, S. W., Miranda-Dominguez, O., Nagel, B. J., Perrone, A. J., Sturgeon, D. T., Goldstone, A., Pfefferbaum, A., Pohl, K. M., Prouty, D., Uban, K., Bookheimer, S. Y., Dapretto, M., Galvan, A., Bagot, K., Giedd, J., Infante, M. A., Jacobus, J., Patrick, K., Shilling, P. D., Desikan, R., Li, Y., Sugrue, L., Banich, M. T., Friedman, N., Hewitt, J. K., Hopfer, C., Sakai, J., Tanabe, J., Cottler, L. B., Nixon, S. J., Chang, L., Cloak, C., Ernst, T., Reeves, G., Kennedy, D. N., Heeringa, S., Peltier, S., Schulenberg, J., Sripada, C., Zucker, R. A., Iacono, W. G., Luciana, M., Calabro, F. J., Clark, D. B., Lewis, D. A., Luna, B., Schirda, C., Brima, T., Foxe, J. J., Freedman, E. G., Mruzek, D. W., Mason, M. J., Huber, R., McGlade, E., Prescot, A., Renshaw, P. F., Yurgelun-Todd, D. A., Allgaier, N. A., Dumas, J. A., Ivanova, M., Potter, A., Florsheim, P., Larson, C., Lisdahl, K., Charness, M. E., Fuemmeler, B., Hettema, J. M., Maes, H. H., Steinberg, J., Anokhin, A. P., Glaser, P., Heath, A. C., Madden, P. A., Baskin-Sommers, A., Constable, R. T., Grant, S. J., Dowling, G. J., Brown, S. A., Jernigan, T. L., and Dale, A. M. (2019). Image processing and analysis methods for the Adolescent Brain Cognitive Development Study. *Neuroimage* 202, 116091. doi: 10.1016/j.neuroimage.2019.116091

Harris, R. A., Alcott, C. E., Sullivan, E. L., Takahashi, D., McCurdy, C. E., Comstock,

S., Baquero, K., Blundell, P., Frias, A. E., Kahr, M., Suter, M., Wesolowski, S., Friedman, J. E., Grove, K. L., and Aagaard, K. M. (2016). Genomic variants associated with resistance to high fat diet induced obesity in a primate model. *Sci. Rep.* 6, 36123. doi: 10.1038/srep36123

Harrison, X. A., Donaldson, L., Correa-Cano, M. E., Evans, J., Fisher, D. N., Goodwin, C. E. D., et al. (2018). A brief introduction to mixed effects modelling and multi-model inference in ecology. *PeerJ* 6, e4794. doi: 10.7717/peerj.4794

Hasan, D. M., Amans, M., Tihan, T., Hess, C., Guo, Y., Cha, S., Su, H., Martin, A. J., Lawton, M. T., Neuwelt, E. A., Saloner, D. A., and Young, W. L. (2012). Ferumoxytol-enhanced MRI to image inflammation within human brain arteriovenous malformations: a pilot investigation. *Transl. Stroke Res.* 3(Suppl 1), 166–173. doi: 10.1007/s12975-012-0172-y

Heeringa, S. G., and Berglund, P. A. (2020). A guide for population-based analysis of the Adolescent Brain Cognitive Development (ABCD) study baseline data. bioRxiv [Preprint]. Available at: https://www.biorxiv.org/content/10.1101/2020.02.10.942011v1 (Accessed December 23, 2022).

Heim, C. M., Entringer, S., and Buss, C. (2019). Translating basic research knowledge on the biological embedding of early-life stress into novel approaches for the developmental programming of lifelong health. *Psychoneuroendocrinology* 105, 123–137. doi: 10.1016/j.psyneuen.2018.12.011

Hentschke, M. R., Krauspenhar, B., Guwzinski, A., Caruso, F. B., Silveira, I. D.,

Antonello, I. C., Gadonski, G., Poli-de-Figueiredo, C. E., and da Costa, B. E. (2012). PP040. Expression of RANTES (CCL5) in maternal plasma, fetal plasma and placenta in pre-eclampsia and normotensive controls. *Pregnancy Hypertens.* 2(3), 263. doi: 10.1016/j.preghy.2012.04.151Hintze, K. J., Benninghoff, A. D., Cho, C. E., and Ward, R. E. (2018). Modeling the Western diet for preclinical investigations. *Adv. Nutr*. 9(3), 263–271. doi: 10.1093/advances/nmy002

Hohos, N. M., and Skaznik-Wikiel, M. E. (2017). High-fat diet and female fertility. *Endocrinology* 158(8), 2407–2419. doi: 10.1210/en.2017-00371

Hong, C. P., Park, A., Yang, B. G., Yun, C. H., Kwak, M. J., Lee, G. W., Kim, J. H., Jang, M. S., Lee, E. J., Jeun, E. J., You, G., Kim, K. S., Choi, Y., Park, J. H., Hwang, D., Im, S. H., Kim, J. F., Kim, Y. K., Seoh, J. Y., Surh, C. D., Kim, Y. M., and Jang, M. H. (2017). Gut-specific delivery of T-helper 17 cells reduces obesity and insulin resistance in mice. *Gastroenterology* 152(8), 1998–2010. doi: 10.1053/j.gastro.2017.02.016

Hopperton, K. E., Mohammad, D., Trépanier, M. O., Giuliano, V., and Bazinet, R. P. (2018). Markers of microglia in post-mortem brain samples from patients with Alzheimer's disease: a systematic review. *Mol. Psychiatry* 23(2), 177–198). doi: 10.1038/mp.2017.246

Horvath, T. L., Sarman, B., García-Cáceres, C., Enriori, P. J., Sotonyi, P., Shanabrough, M., Borok, E., Argente, J., Chowen, J. A., Perez-Tilve, D., Pfluger, P. T., Brönneke, H. S., Levin, B. E., Diano, S., Cowley, M. A., and Tschöp, M. H. (2010). Synaptic input organization of the melanocortin system predicts diet-induced hypothalamic reactive gliosis and obesity. *Proc. Natl. Acad. Sci. U. S. A.* 107(33), 14875–14880.

doi: 10.1073/pnas.1004282107

Howard, A. L., Robinson, M., Smith, G. J., Ambrosini, G. L., Piek, J. P., and Oddy, W. H. (2011). ADHD is associated with a "Western" dietary pattern in adolescents. *J. Atten. Disord.* 15(5), 403–411. doi: 10.1177/1087054710365990

Huang, W. C., Chen, Y., and Page, D. T. (2016). Hyperconnectivity of prefrontal cortex to amygdala projections in a mouse model of macrocephaly/autism syndrome. *Nat. Commun.* 7, 13421. doi: 10.1038/ncomms13421

Huang, X. F., Han, M., South, T., and Storlien, L. (2003). Altered levels of POMC, AgRP and MC4-R mRNA expression in the hypothalamus and other parts of the limbic system of mice prone or resistant to chronic high-energy diet-induced obesity. *Brain Res.* 992(1), 9–19. doi: 10.1016/j.brainres.2003.08.019

Hubert, V., Dumot, C., Ong, E., Amaz, C., Canet-Soulas, E., Chauveau, F., and Wiart, M. (2019). MRI coupled with clinically-applicable iron oxide nanoparticles reveals choroid plexus involvement in a murine model of neuroinflammation. *Sci. Rep.* 9(1), 10046. doi: 10.1038/s41598-019-46566-1

Huettel, S. A., Song, A. W., and McCarthy, G. (2008). *Functional Magnetic Resonance Imaging*, 2nd Edn. Sunderland, MA: Sinauer Associates Inc.

Hunyady, B., Mezey, E., and Palkovits, M. (2000). Gastrointestinal immunology: cell types in the lamina propria--a morphological review. *Acta Physiol. Hung.* 87(4), 305–328.

ImageJ. (2019). *Auto Threshold*. Available online at: https://imagej.net/plugins/auto-threshold (accessed September 22, 2022).

Jastroch, M., Morin, S., Tschöp, M. H., and Yi, C. X. (2014). The hypothalamic neural-glial network and the metabolic syndrome. *Best Pract. Res. Clin. Endocrinol. Metab.* 28(5), 661–671. doi: 10.1016/j.beem.2014.02.002

Jenkinson, M., Beckmann, C. F., Behrens, T. E., Woolrich, M. W., and Smith, S. M. (2012). FSL. *Neuroimage* 62(2), 782–790. doi: 10.1016/j.neuroimage.2011.09.015

Jo, J., Gavrilova, O., Pack, S., Jou, W., Mullen, S., Sumner, A. E., Cushman, S. W., and Periwal, V. (2009). Hypertrophy and/or hyperplasia: dynamics of adipose tissue growth. *PLoS Comput. Biol.* 5(3), e1000324. doi: 10.1371/journal.pcbi.1000324

Joly-Amado, A., Cansell, C., Denis, R. G., Delbes, A. S., Castel, J., Martinez, S., and Luquet, S. (2014). The hypothalamic arcuate nucleus and the control of peripheral substrates. *Best Pract. Res. Clin. Endocrinol. Metab.* 28(5), 725–737. doi: 10.1016/j.beem.2014.03.003

Joshi, N. P., Mane, A. R., Sahay, A. S., Sundrani, D. P., Joshi, S. R., and Yajnik, C. S. (2022). Role of placental glucose transporters in determining fetal growth. *Reprod. Sci.* 29(10), 2744–2759. doi: 10.1007/s43032-021-00699-9

Kabaran, S., and Besler, H. T. (2015). Do fatty acids affect fetal programming?. *J. Health Popul. Nutr.* 33, 14. doi: 10.1186/s41043-015-0018-9

Kalsbeek, M. J., Wolff, S. E., Korpel, N. L., la Fleur, S. E., Romijn, J. A., Fliers, E., Kalsbeek, A., Swaab, D. F., Huitinga, I., Hol, E. M., and Yi, C. X. (2020). The impact of antidiabetic treatment on human hypothalamic infundibular neurons and microglia. *JCI Insight* 5(16), e133868. doi: 10.1172/jci.insight.133868

Kapur, J. N., Sahoo, P. K., and Wong, A. K. (1985). A new method for gray-level picture

thresholding using the entropy of the histogram. *Comput. Vis. Graph. Image Process.* 29, 273-285. doi: 10.1016/0734-189X(85)90125-2

Karastergiou, K., and Mohamed-Ali, V. (2010). The autocrine and paracrine roles of adipokines. *Mol. Cell. Endocrinol.* 318(1-2), 69–78. doi: 10.1016/j.mce.2009.11.011

Kawano, Y., Edwards, M., Huang, Y., Bilate, A. M., Araujo, L. P., Tanoue, T., Atarashi, K., Ladinsky, M. S., Reiner, S. L., Wang, H. H., Mucida, D., Honda, K., and Ivanov, I. I. (2022). Microbiota imbalance induced by dietary sugar disrupts immune-mediated protection from metabolic syndrome. *Cell* 185(19), 3501–3519.e20. doi: 10.1016/j.cell.2022.08.005

Kawano, Y., Nakae, J., Watanabe, N., Kikuchi, T., Tateya, S., Tamori, Y., Kaneko, M., Abe, T., Onodera, M., and Itoh, H. (2016). Colonic pro-inflammatory macrophages cause insulin resistance in an intestinal Ccl2/Ccr2-dependent manner. *Cell Metab.* 24(2), 295–310. doi: 10.1016/j.cmet.2016.07.009

Kern, J. K., Geier, D. A., Sykes, L. K., and Geier, M. R. (2016). Relevance of neuroinflammation and encephalitis in autism. *Front. Cell. Neurosci.* 9, 519. doi: 10.3389/fncel.2015.00519

Kim, H. J., Cho, M. H., Shim, W. H., Kim, J. K., Jeon, E. Y., Kim, D. H., and Yoon, S. Y. (2017). Deficient autophagy in microglia impairs synaptic pruning and causes social behavioral defects. *Mol. Psychiatry* 22(11), 1576–1584. doi: 10.1038/mp.2016.103

Kim, K. A., Gu, W., Lee, I. A., Joh, E. H., and Kim, D. H. (2012). High fat diet-induced gut microbiota exacerbates inflammation and obesity in mice via the TLR4 signaling

pathway. *PloS One*, 7(10), e47713. doi: 10.1371/journal.pone.0047713

Kleinhans, N. M., Reiter, M. A., Neuhaus, E., Pauley, G., Martin, N., Dager, S., and Estes, A. (2016). Subregional differences in intrinsic amygdala hyperconnectivity and hypoconnectivity in autism spectrum disorder. *Autism Res.* 9(7), 760–772. doi: 10.1002/aur.1589

Knuesel, I., Chicha, L., Britschgi, M., Schobel, S. A., Bodmer, M., Hellings, J. A., Toovey, S., and Prinssen, E. P. (2014). Maternal immune activation and abnormal brain development across CNS disorders. *Nat. Rev. Neurol.* 10(11), 643–660. doi: 10.1038/nrneurol.2014.187

Konrad, D., and Wueest, S. (2014). The gut-adipose-liver axis in the metabolic syndrome. *Physiology (Bethesda)* 29(5), 304–313. doi: 10.1152/physiol.00014.2014

Kopec, A. M., Smith, C. J., Ayre, N. R., Sweat, S. C., and Bilbo, S. D. (2018). Microglial dopamine receptor elimination defines sex-specific nucleus accumbens development and social behavior in adolescent rats. *Nat. Commun.* 9(1), 3769. doi: 10.1038/s41467-018-06118-z

Krakowiak, P., Walker, C. K., Bremer, A. A., Baker, A. S., Ozonoff, S., Hansen, R. L., and Hertz-Picciotto, I. (2012). Maternal metabolic conditions and risk for autism and other neurodevelopmental disorders. *Pediatrics* 129(5), e1121–e1128. doi: 10.1542/peds.2011-2583

Kuznetsova A., Brockhoff P. B., and Christensen R. H. B. (2017). lmerTest package: tests in linear mixed effects models. *J. Stat. Softw.* 82(13), 1–26. doi: 10.18637/jss.v082.i13

Kwon, E. J., and Kim, Y. J. (2017). What is fetal programming?: a lifetime health is under the control of in utero health. *Obstet. Gynecol. Sci.* 60(6), 506–519. doi: 10.5468/ogs.2017.60.6.506

Lauterio, T. J., Bond, J. P., and Ulman, E. A. (1994). Development and characterization of a purified diet to identify obesity-susceptible and resistant rat populations. *J. Nutr.* 124(11), 2172–2178. doi: 10.1093/jn/124.11.2172

Leekam, S. R., Nieto, C., Libby, S. J., Wing, L., and Gould, J. (2007). Describing the sensory abnormalities of children and adults with autism. *J. Autism Dev. Disord.* 37(5), 894–910. doi: 10.1007/s10803-006-0218-7

Lemus, M. B., Bayliss, J. A., Lockie, S. H., Santos, V. V., Reichenbach, A., Stark, R., and Andrews, Z. B. (2015). A stereological analysis of NPY, POMC, Orexin, GFAP astrocyte, and Iba1 microglia cell number and volume in diet-induced obese male mice. *Endocrinology* 156(5), 1701–1713. doi: 10.1210/en.2014-1961

Levitt P. (2003). Structural and functional maturation of the developing primate brain. *J. Pediatr.* 143(4 Suppl), S35–S45. doi: 10.1067/s0022-3476(03)00400-1

Li, M., Fallin, M. D., Riley, A., Landa, R., Walker, S. O., Silverstein, M., Caruso, D., Pearson, C., Kiang, S., Dahm, J. L., Hong, X., Wang, G., Wang, M. C., Zuckerman, B., and Wang, X. (2016). The association of maternal obesity and diabetes with autism and other developmental disabilities. *Pediatrics* 137(2), e20152206. doi: 10.1542/peds.2015-2206

Li, Q., and Barres, B. A. (2018). Microglia and macrophages in brain homeostasis and disease. *Nat. Rev. Immunol.* 18(4), 225–242. doi: 10.1038/nri.2017.125

Li, T., Chiou, B., Gilman, C. K., Luo, R., Koshi, T., Yu, D., Oak, H. C., Giera, S., Johnson-Venkatesh, E., Muthukumar, A. K., Stevens, B., Umemori, H., and Piao, X. (2020). A splicing isoform of GPR56 mediates microglial synaptic refinement via phosphatidylserine binding. *EMBO J.* 39(16), e104136. doi: 10.15252/embj.2019104136

Liang, W., He, J., Mao, C., Yu, C., Meng, Q., Xue, J., Wu, X., Li, S., Wang, Y., and Yi, H. (2022). Gene editing monkeys: Retrospect and outlook. *Front. Cell Dev. Biol.* 10, 913996. doi: 10.3389/fcell.2022.913996

Lindberg, C., Hjorth, E., Post, C., Winblad, B., and Schultzberg, M. (2005). Cytokine production by a human microglial cell line: effects of ßamyloid and α-melanocyte-stimulating hormone. *Neurotox. Res.* 8(3), 267-276. doi: 10.1007/BF03033980

Lively, S., and Schlichter, L. C. (2013). The microglial activation state regulates migration and roles of matrix-dissolving enzymes for invasion. *J. Neuroinflammation* 10, 75. doi: 10.1186/1742-2094-10-75

Logothetis, N. K., and Wandell, B. A. (2004). Interpreting the BOLD signal. *Annu. Rev. Physiol.* 66, 735–769. doi: 10.1146/annurev.physiol.66.082602.092845

Lucker, J. R., and Doman, A. (2015). Neural mechanisms involved in hypersensitive hearing: Helping children with ASD who are overly sensitive to sounds. *Autism Res. Treat.* 2015, 369035. doi: 10.1155/2015/369035

Lumeng, C. N., and Saltiel, A. R. (2011). Inflammatory links between obesity and metabolic disease. *J. Clin. Invest.* 121(6), 2111–2117. doi: 10.1172/JCI57132

Lunde, A., and Glover, J. C. (2020). A versatile toolbox for semi-automatic cell-by-cell

object-based colocalization analysis. *Sci. Rep.* 10(1), 19027. doi: 10.1038/s41598-020-75835-7

Lyall, K., Munger, K. L., O'Reilly, É. J., Santangelo, S. L., and Ascherio, A. (2013). Maternal dietary fat intake in association with autism spectrum disorders. *Am. J. Epidemiol.* 178(2), 209–220. doi: 10.1093/aje/kws433

Lyall, K., Schmidt, R. J., and Hertz-Picciotto, I. (2014). Maternal lifestyle and environmental risk factors for autism spectrum disorders. *Int. J. Epidemiol.* 43(2), 443–464. doi: 10.1093/ije/dyt282

Malonek, D., Dirnagl, U., Lindauer, U., Yamada, K., Kanno, I., and Grinvald, A. (1997). Vascular imprints of neuronal activity: relationships between the dynamics of cortical blood flow, oxygenation, and volume changes following sensory stimulation. *Proc. Natl. Acad. Sci. U. S. A.* 94(26), 14826–14831. doi: 10.1073/pnas.94.26.14826

Marco, A., Kisliouk, T., Tabachnik, T., Meiri, N., and Weller, A. (2014). Overweight and CpG methylation of the Pomc promoter in offspring of high-fat-diet-fed dams are not "reprogrammed" by regular chow diet in rats. *FASEB J.* 28(9), 4148–4157. doi: 10.1096/fj.14-255620

Marek, S., Tervo-Clemmens, B., Calabro, F. J., Montez, D. F., Kay, B. P., Hatoum, A. S., Donohue, M. R., Foran, W., Miller, R. L., Hendrickson, T. J., Malone, S. M., Kandala, S., Feczko, E., Miranda-Dominguez, O., Graham, A. M., Earl, E. A., Perrone, A. J., Cordova, M., Doyle, O., Moore, L. A., Conan, G. M., Uriarte, J., Snider, K., Lynch, B. J., Wilgenbusch, J. C., Pengo, T., Tam, A., Chen, J., Newbold,

D. J., Zheng, A., Seider, N. A., Van, A. N., Metoki, A., Chauvin, R. J., Laumann, T. O., Greene, D. J., Petersen, S. E., Garavan, H., Thompson, W. K., Nichols, T. E., Yeo, B. T. T., Barch, D. M., Luna, B., Fair, D. A., and Dosenbach, N. U. F. (2022). Reproducible brain-wide association studies require thousands of individuals. *Nature* 603(7902), 654–660. doi: 10.1038/s41586-022-04492-9

Marr, M. C. (2020). *Intergenerational transmission of childhood maltreatment: characterizing potential mechanisms and offspring neurobehavioral outcomes*. [Doctoral dissertation]. [Portland (OR)]: Oregon Health & Science University

MATLAB. (2022). Natick, Massachusetts: The MathWorks Inc.

Maury, E., and Brichard, S. M. (2010). Adipokine dysregulation, adipose tissue inflammation and metabolic syndrome. *Mol. Cell. Endocrinol*. 314(1), 1–16. doi: 10.1016/j.mce.2009.07.031

May-Benson, T. A., Koomar, J. A., and Teasdale, A. (2009). Incidence of pre-, peri-, and post-natal birth and developmental problems of children with sensory processing disorder and children with autism spectrum disorder. *Front. Integr. Neurosci.* 3, 31. doi: 10.3389/neuro.07.031.2009

McConnell, H. L., Schwartz, D. L., Richardson, B. E., Woltjer, R. L., Muldoon, L. L., and Neuwelt, E. A. (2016). Ferumoxytol nanoparticle uptake in brain during acute neuroinflammation is cell-specific. *Nanomedicine.* 12(6), 1535–1542. doi: 10.1016/j.nano.2016.03.009

McCurdy, C. E., Bishop, J. M., Williams, S. M., Grayson, B. E., Smith, M. S., Friedman, J. E., and Grove, K. L. (2009). Maternal high-fat diet triggers lipotoxicity in the fetal

livers of nonhuman primates. *J. Clin. Invest.* 119(2), 323–335. doi: 10.1172/JCI32661

Menassa, D. A., and Gomez-Nicola, D. (2018). Microglial dynamics during human brain development. *Front. Immunol.* 9, 1014. doi: 10.3389/fimmu.2018.01014

Michelsen, T. M., Holme, A. M., Holm, M. B., Roland, M. C., Haugen, G., Powell, T. L., Jansson, T., and Henriksen, T. (2019). Uteroplacental glucose uptake and fetal glucose consumption: a quantitative study in human pregnancies. *J. Clin. Endocrinol. Metab.* 104(3), 873–882. doi: 10.1210/jc.2018-01154

Milham, M. P., Ai, L., Koo, B., Xu, T., Amiez, C., Balezeau, F., Baxter, M. G., Blezer, E. L. A., Brochier, T., Chen, A., Croxson, P. L., Damatac, C. G., Dehaene, S., Everling, S., Fair, D. A., Fleysher, L., Freiwald, W., Froudist-Walsh, S., Griffiths, T. D., Guedj, C., Hadj-Bouziane, F., Ben Hamed, S., Harel, N., Hiba, B., Jarraya, B., Jung, B., Kastner, S., Klink, P. C., Kwok, S. C., Laland, K. N., Leopold, D. A., Lindenfors, P., Mars, R. B., Menon, R. S., Messinger, A., Meunier, M., Mok, K., Morrison, J. H., Nacef, J., Nagy, J., Rios, M. O., Petkov, C. I., Pinsk, M., Poirier, C., Procyk, E., Rajimehr, R., Reader, S. M., Roelfsema, P. R., Rudko, D. A., Rushworth, M. F. S., Russ, B. E., Sallet, J., Schmid, M. C., Schwiedrzik, C. M., Seidlitz, J., Sein, J., Shmuel, A., Sullivan, E. L., Ungerleider, L., Thiele, A., Todorov, O. S., Tsao, D., Wang, Z., Wilson, C. R. E., Yacoub, E., Ye, F. Q., Zarco, W., Zhou, Y. D., Margulies, D. S., Schroeder, C. E. (2018). An open resource for non-human primate imaging. *Neuron* 100(1), 61–74.e2. doi: 10.1016/j.neuron.2018.08.039

Miller, E. B., Zhang, P., Ching, K., Pugh, E. N., Jr, and Burns, M. E. (2019). In vivo

imaging reveals transient microglia recruitment and functional recovery of photoreceptor signaling after injury. *Proc. Natl. Acad. Sci. U. S. A.* 116(33), 16603–16612. doi: 10.1073/pnas.1903336116

Miller, L. J., Anzalone, M. E., Lane, S. J., Cermak, S. A., and Osten, E. T. (2007). Concept evolution in sensory integration: a proposed nosology for diagnosis. *Am. J. Occup. Ther.* 61(2), 135–140. doi: 10.5014/ajot.61.2.135

Mina, T. H., Lahti, M., Drake, A. J., Räikkönen, K., Minnis, H., Denison, F. C., Norman, J. E., and Reynolds, R. M. (2017). Prenatal exposure to very severe maternal obesity is associated with adverse neuropsychiatric outcomes in children. *Psychol. Med.* 47(2), 353–362. doi: 10.1017/S0033291716002452

Miranda-Dominguez, O., Mills, B. D., Grayson, D., Woodall, A., Grant, K. A., Kroenke, C. D., and Fair, D. A. (2014). Bridging the gap between the human and macaque connectome: a quantitative comparison of global interspecies structure-function relationships and network topology. *J. Neurosci.* 34(16), 5552–5563. doi: 10.1523/JNEUROSCI.4229-13.2014

Miranda-Dominguez, O., Ramirez, J. S. B., Mitchell, A. J., Perrone, A., Earl, E., Carpenter, S., Feczko, E., Graham, A., Jeon, S., Cohen, N. J., Renner, L., Neuringer, M., Kuchan, M. J., Erdman, J. W., Jr, and Fair, D. (2022). Carotenoids improve the development of cerebral cortical networks in formula-fed infant macaques. *Sci. Rep.* 12(1), 15220. doi: 10.1038/s41598-022-19279-1

Mitchell, A. J., Dunn, G. A., and Sullivan, E. L. (2022a). The influence of maternal metabolic state and nutrition on offspring neurobehavioral development: a focus on

preclinical models. *Biol. Psychiatry Cogn. Neurosci. Neuroimaging* 7(5), 450–460. doi: 10.1016/j.bpsc.2021.11.014

Mitchell, A. J., Khambadkone, S. G., Dunn, G., Bagley, J., Tamashiro, K. L. K., Fair, D., Gustafsson, H., and Sullivan, E. L. (2022b). Maternal Western-style diet reduces social engagement and increases idiosyncratic behavior in Japanese macaque offspring. *Brain Behav. Immun.* 105, 109–121. doi: 10.1016/j.bbi.2022.07.004

Mitchell, H. H., Hamilton, T. S., Steggerda, F. R., and Bean, H. W. (1945). The chemical composition of the adult human body and its bearing on the biochemistry of growth. *J. Biol. Chem.* 158, 625-637. doi: 10.1016/s0021-9258(19)51339-4

Møller, A. R. (2006). *Hearing: Anatomy, Physiology, and Disorders of the Auditory System*, 2nd Edn. San Diego, CA: Academic Press.

Møller, A. R., Kern, J. K., and Grannemann, B. (2005). Are the non-classical auditory pathways involved in autism and PDD?. *Neurol. Res.* 27(6), 625–629. doi: 10.1179/016164105X25117

Møller, A. R., and Rollins, P. R. (2002). The non-classical auditory pathways are involved in hearing in children but not in adults. *Neurosci. Lett.* 319(1), 41–44. doi: 10.1016/s0304-3940(01)02516-2

Moss, B. G., and Chugani, D. C. (2014). Increased risk of very low birth weight, rapid postnatal growth, and autism in underweight and obese mothers. *Am. J. Health Promot.* 28(3), 181–188. doi: 10.4278/ajhp.120705-QUAN-325

Moussavi, N., Gavino, V., and Receveur, O. (2008). Could the quality of dietary fat, and not just its quantity, be related to risk of obesity?. *Obesity (Silver Spring)* 16(1), 7–

15. doi: 10.1038/oby.2007.14

Mulligan, S., Douglas, S., and Armstrong, C. (2021). Characteristics of idiopathic sensory processing disorder in young children. *Front. Integr. Neurosci.* 15, 647928. doi: 10.3389/fnint.2021.647928

Musiek, F., Mohanani, A., Wierzbinski, E., Kilgore, G., Hunter, J., and Marotto, J. (2011). The non-classical pathway: Too great to be ignored. *Hear. J.* 64(10), 6-8. doi: 10.1097/01.HJ.0000406765.34487.d4

Nayak, D., Roth, T. L., and McGavern, D. B. (2014). Microglia development and function. *Annu. Rev. Immunol.* 32, 367–402. doi: 10.1146/annurev-immunol-032713-120240

Neniskyte, U., and Gross, C. T. (2017). Errant gardeners: glial-cell-dependent synaptic pruning and neurodevelopmental disorders. *Nat. Rev. Neurosci.* 18(11), 658–670. doi: 10.1038/nrn.2017.110

NIMH Data Archive. (2022). *ABCD Data Repository*. Available online at: https://nda.nih.gov/abcd/ (accessed December 23, 2022).

Norman, J. F., and LeVeen, R. F. (2001). Maternal atherogenic diet in swine is protective against early atherosclerosis development in offspring consuming an atherogenic diet post-natally. *Atherosclerosis* 157(1), 41–47. doi: 10.1016/s0021-9150(00)00668-7

Ogawa, S., Lee, T. M., Kay, A. R., and Tank, D. W. (1990). Brain magnetic resonance imaging with contrast dependent on blood oxygenation. *Proc. Natl. Acad. Sci. U. S. A.* 87(24), 9868–9872. doi: 10.1073/pnas.87.24.9868

Olofsson, L. E., Unger, E. K., Cheung, C. C., and Xu, A. W. (2013). Modulation of AgRP-neuronal function by SOCS3 as an initiating event in diet-induced hypothalamic leptin resistance. *Proc. Natl. Acad. Sci. U. S. A.* 110(8), E697-E706. doi: 10.1073/pnas.1218284110

Otsu, N. (1979). A threshold selection method from gray level histograms. *IEEE Trans. Syst. Man Cybern.* 9, 62-66. doi: 10.1109/TSMC.1979.4310076

Owen, J. P., Marco, E. J., Desai, S., Fourie, E., Harris, J., Hill, S. S., Arnett, A. B., and Mukherjee, P. (2013). Abnormal white matter microstructure in children with sensory processing disorders. *Neuroimage Clin.* 2, 844–853. doi: 10.1016/j.nicl.2013.06.009

Paolicelli, R. C., Bolasco, G., Pagani, F., Maggi, L., Scianni, M., Panzanelli, P., Giustetto, M., Ferreira, T. A., Guiducci, E., Dumas, L., Ragozzino, D., and Gross, C. T. (2011). Synaptic pruning by microglia is necessary for normal brain development. *Science* 333(6048), 1456–1458. doi: 10.1126/science.1202529

Parker-Athill, E. C., and Tan, J. (2010). Maternal immune activation and autism spectrum disorder: interleukin-6 signaling as a key mechanistic pathway. *Neurosignals* 18(2), 113–128. doi: 10.1159/000319828

Parush, S., Sohmer, H., Steinberg, A., and Kaitz, M. (2007). Somatosensory function in boys with ADHD and tactile defensiveness. *Physiol. Behav.* 90(4), 553–558. doi: 10.1016/j.physbeh.2006.11.004

Paxinos, G., Huang, X.-F., Petrides, M. and Toga, A. W. (2009). *The Rhesus Monkey Brain in Stereotaxic Coordinates*, 2nd Edn. San Diego: Elsevier Academic Press.

Peet, G., Bennett, F. C., and Bennett, M. L. (2020). Please eat (only part) of me: synaptic phosphatidylserine cues microglia to feast: Two new studies identify how a common apoptotic cell flag is used to sculpt neural circuits. *EMBO J.* 39(16), e105924. doi: 10.15252/embj.2020105924

Peleg-Raibstein, D., Luca, E., and Wolfrum, C. (2012). Maternal high-fat diet in mice programs emotional behavior in adulthood. *Behav. Brain Res.* 233(2), 398–404. doi: 10.1016/j.bbr.2012.05.027

Pons, V., and Rivest, S. (2020). Beneficial roles of microglia and growth factors in MS, a brief review. *Front. Cell. Neurosci.* 14, 284. doi: 10.3389/fncel.2020.00284

Pont-Lezica, L., Beumer, W., Colasse, S., Drexhage, H., Versnel, M., and Bessis, A. (2014). Microglia shape corpus callosum axon tract fasciculation: functional impact of prenatal inflammation. *Eur. J. Neurosci.* 39(10), 1551–1557. doi: 10.1111/ejn.12508

Power, J. D., Barnes, K. A., Snyder, A. Z., Schlaggar, B. L., and Petersen, S. E. (2012). Spurious but systematic correlations in functional connectivity MRI networks arise from subject motion. *Neuroimage* 59(3), 2142–2154. doi: 10.1016/j.neuroimage.2011.10.018

Power, J. D., Mitra, A., Laumann, T. O., Snyder, A. Z., Schlaggar, B. L., and Petersen, S. E. (2014). Methods to detect, characterize, and remove motion artifact in resting state fMRI. *Neuroimage* 84, 320–341. doi: 10.1016/j.neuroimage.2013.08.048

Prewitt, J. M., and Mendelsohn, M. L. (1966). The analysis of cell images. *Ann. N. Y. Acad. Sci.* 128(3), 1035-1053. doi: 10.1111/j.1749-6632.1965.tb11715.x

Quraishi, A. N., and Illsley, N. P. (1999). Transport of sugars across human placental membranes measured by light scattering. *Placenta* 20(2-3), 167–174. doi: 10.1053/plac.1998.0365

Raichle, M. E., and Mintun, M. A. (2006). Brain work and brain imaging. *Annu. Rev. Neurosci.* 29, 449–476. doi: 10.1146/annurev.neuro.29.051605.112819

Ramirez, J. S. B. (2019). *Maternal nutrition and inflammation as a risk factor for future mental health disorders*. [Doctoral dissertation]. [Portland (OR)]: Oregon Health & Science University

Ramirez, J. S. B., Graham, A. M., Thompson, J. R., Zhu, J. Y., Sturgeon, D., Bagley, J. L., Thomas, E., Papadakis, S., Bah, M., Perrone, A., Earl, E., Miranda-Dominguez, O., Feczko, E., Fombonne, E. J., Amaral, D. G., Nigg, J. T., Sullivan, E. L., and Fair, D. A. (2020). Maternal interleukin-6 is associated with macaque offspring amygdala development and behavior. *Cereb Cortex* 30(3), 1573–1585. doi: 10.1093/cercor/bhz188

Ramirez, J. S. B., Hermosillo, R., Thomas, E., Zhu, J. Y., Sturgeon, D., Schifsky, E., Galassi, A., Thompson, J. R., Bagley, J. L., Milham, M. P., Miranda-Dominguez, O., Papadakis, S., Bah, M., Mitchell, A. J., Xu, T., Graham, A. M., Feczko, E., Sullivan, E. L., and Fair, D. A. (2021). Vertex-wise characterization of non-human primate cortical development with prenatal insights. bioRxiv [Preprint]. Available at: https://www.biorxiv.org/content/10.1101/2021.09.23.461551v1.full (Accessed December 23, 2022).

Rasmussen, J. M., Graham, A. M., Entringer, S., Gilmore, J. H., Styner, M., Fair, D. A.,

Wadhwa, P. D., and Buss, C. (2019). Maternal interleukin-6 concentration during pregnancy is associated with variation in frontolimbic white matter and cognitive development in early life. *Neuroimage* 185, 825–835. doi: 10.1016/j.neuroimage.2018.04.020

Reis, W. L., Yi, C. X., Gao, Y., Tschöp, M. H., and Stern, J. E. (2015). Brain innate immunity regulates hypothalamic arcuate neuronal activity and feeding behavior. *Endocrinology* 156(4), 1303–1315. doi: 10.1210/en.2014-1849

Reynolds, L. C., Inder, T. E., Neil, J. J., Pineda, R. G., and Rogers, C. E. (2014). Maternal obesity and increased risk for autism and developmental delay among very preterm infants. *J. Perinatol.* 34(9), 688–692. doi: 10.1038/jp.2014.80

Reynolds, L. P., Borowicz, P. P., Caton, J. S., Vonnahme, K. A., Luther, J. S., Hammer, C. J., Maddock Carlin, K. R., Grazul-Bilska, A. T., and Redmer, D. A. (2010). Developmental programming: the concept, large animal models, and the key role of uteroplacental vascular development. *J. Anim. Sci.* 88(13 Suppl), E61–E72. doi: 10.2527/jas.2009-2359

Rijnsburger, M., Unmehopa, U. A., Eggels, L., Serlie, M. J., and la Fleur, S. E. (2019). One-week exposure to a free-choice high-fat high-sugar diet does not disrupt blood-brain barrier permeability in fed or overnight fasted rats. *Nutr. Neurosci.* 22(8), 541–550. doi: 10.1080/1028415X.2017.1418727

Rivera, H. M., Kievit, P., Kirigiti, M. A., Bauman, L. A., Baquero, K., Blundell, P., Dean, T. A., Valleau, J. C., Takahashi, D. L., Frazee, T., Douville, L., Majer, J., Smith, M. S., Grove, K. L., and Sullivan, E. L. (2015). Maternal high-fat diet and

obesity impact palatable food intake and dopamine signaling in nonhuman primate offspring. *Obesity (Silver Spring)* 23(11), 2157–2164. doi: 10.1002/oby.21306

Robinson, E. C., Jbabdi, S., Glasser, M. F., Andersson, J., Burgess, G. C., Harms, M. P., Smith, S. M., Van Essen, D. C., and Jenkinson, M. (2014). MSM: a new flexible framework for Multimodal Surface Matching. *Neuroimage* 100, 414–426. doi: 10.1016/j.neuroimage.2014.05.069

Rock, R. B., Gekker, G., Hu, S., Sheng, W. S., Cheeran, M., Lokensgard, J. R., and Peterson, P. K. (2004). Role of microglia in central nervous system infections. *Clin. Microbiol. Rev.* 17(4), 942–964. doi: 10.1128/CMR.17.4.942-964.2004

Rohr, M. W., Narasimhulu, C. A., Rudeski-Rohr, T. A., and Parthasarathy, S. (2020). Negative effects of a high-fat diet on intestinal permeability: a review. *Adv. Nutr*. 11(1), 77–91. doi: 10.1093/advances/nmz061

Romero, E., Ali, C., Molina-Holgado, E., Castellano, B., Guaza, C., and Borrell, J. (2007). Neurobehavioral and immunological consequences of prenatal immune activation in rats. Influence of antipsychotics. *Neuropsychopharmacology* 32(8), 1791-1804. doi: 10.1038/sj.npp.1301292

Rossmeisl, M., Rim, J. S., Koza, R. A., and Kozak, L. P. (2003). Variation in type 2 diabetes--related traits in mouse strains susceptible to diet-induced obesity. *Diabetes* 52(8), 1958–1966. doi: 10.2337/diabetes.52.8.1958

Rudolph, M. D., Graham, A. M., Feczko, E., Miranda-Dominguez, O., Rasmussen, J. M., Nardos, R., Entringer, S., Wadhwa, P. D., Buss, C., and Fair, D. A. (2018). Maternal IL-6 during pregnancy can be estimated from newborn brain connectivity and

predicts future working memory in offspring. *Nat. Neurosci.* 21(5), 765–772. doi: 10.1038/s41593-018-0128-y

Rudolph, M. D., Miranda-Domínguez, O., Cohen, A. O., Breiner, K., Steinberg, L., Bonnie, R. J., Scott, E. S., Taylor-Thompson, K., Chein, J., Fettich, K. C., Richeson, J. A., Dellarco, D. V., Galván, A., Casey, B. J., and Fair, D. A. (2017). At risk of being risky: the relationship between "brain age" under emotional states and risk preference. *Dev. Cogn. Neurosci.* 24, 93–106. doi: 10.1016/j.dcn.2017.01.010

Russo, N., Foxe, J. J., Brandwein, A. B., Altschuler, T., Gomes, H., and Molholm, S. (2010). Multisensory processing in children with autism: high-density electrical mapping of auditory–somatosensory integration. *Autism Res*. 3(5), 253–267. doi: 10.1002/aur.152

Salati, J. A., Roberts, V. H. J., Schabel, M. C., Lo, J. O., Kroenke, C. D., Lewandowski, K. S., Lindner, J. R., Grove, K. L., and Frias, A. E. (2019). Maternal high-fat diet reversal improves placental hemodynamics in a nonhuman primate model of diet-induced obesity. *Int. J. Obes. (Lond.)* 43(4), 906–916. doi: 10.1038/s41366-018-0145-7

Saragosa-Harris, N. M., Chaku, N., MacSweeney, N., Guazzelli Williamson, V., Scheuplein, M., Feola, B., Cardenas-Iniguez, C., Demir-Lira, E., McNeilly, E. A., Huffman, L. G., Whitmore, L., Michalska, K. J., Damme, K. S., Rakesh, D., and Mills, K. L. (2022). A practical guide for researchers and reviewers using the ABCD Study and other large longitudinal datasets. *Dev. Cogn. Neurosci.* 55, 101115. doi: 10.1016/j.dcn.2022.101115

Sarlus, H., and Heneka, M. T. (2017). Microglia in Alzheimer's disease. *J. Clin. Invest.* 127(9), 3240–3249. doi: 10.1172/JCI90606

Saunders, N. R., Dreifuss, J. J., Dziegielewska, K. M., Johansson, P. A., Habgood, M. D., Møllgård, K., and Bauer, H. C. (2014). The rights and wrongs of blood-brain barrier permeability studies: a walk through 100 years of history. *Front. Neurosci.* 8, 404. doi: 10.3389/fnins.2014.00404

Schepanski, S., Buss, C., Hanganu-Opatz, I. L., and Arck, P. C. (2018). Prenatal immune and endocrine modulators of offspring's brain development and cognitive functions later in life. *Front. Immunol.* 9, 2186. doi: 10.3389/fimmu.2018.02186

Schindelin, J., Arganda-Carreras, I., Frise, E., Kaynig, V., Longair, M., Pietzsch, T., Preibisch, S., Rueden, C., Saalfeld, S., Schmid, B., Tinevez, J. Y., White, D. J., Hartenstein, V., Eliceiri, K., Tomancak, P., and Cardona, A. (2012). Fiji: an open-source platform for biological-image analysis. *Nat. Methods* 9(7), 676-682. doi: 10.1038/nmeth.2019

Schoen, S. A., Miller, L. J., and Green, K. E. (2008). Pilot study of the Sensory Over-Responsivity Scales: assessment and inventory. *Am. J. Occup. Ther.* 62(4), 393–406. doi: 10.5014/ajot.62.4.393

Schulkin, J. (2007). Autism and the amygdala: an endocrine hypothesis. *Brain Cogn.* 65(1), 87–99. doi: 10.1016/j.bandc.2006.02.009

Schumann, C. M., Hamstra, J., Goodlin-Jones, B. L., Lotspeich, L. J., Kwon, H., Buonocore, M. H., Lammers, C. R., Reiss, A. L., and Amaral, D. G. (2004). The amygdala is enlarged in children but not adolescents with autism; the hippocampus

is enlarged at all ages. *J. Neurosci.* 24(28), 6392–6401. doi: 10.1523/JNEUROSCI.1297-04.2004

Schwarzlose, R. F., Tillman, R., Hoyniak, C. P., Luby, J. L., and Barch, D. M. (2023). Sensory over-responsivity: A feature of childhood psychiatric illness associated with altered functional connectivity of sensory networks. *Biol. Psychiatry* 93(1), 92–101. doi: 10.1016/j.biopsych.2022.09.004

Scola, G., and Duong, A. (2017). Prenatal maternal immune activation and brain development with relevance to psychiatric disorders. *Neuroscience* 346, 403–408. doi: 10.1016/j.neuroscience.2017.01.033

Scott, J. A., Grayson, D., Fletcher, E., Lee, A., Bauman, M. D., Schumann, C. M., Buonocore, M. H., and Amaral, D. G. (2016). Longitudinal analysis of the developing rhesus monkey brain using magnetic resonance imaging: birth to adulthood. *Brain Struct. Funct.* 221(5), 2847–2871. doi: 10.1007/s00429-015-1076-x

Scott-Hewitt, N., Perrucci, F., Morini, R., Erreni, M., Mahoney, M., Witkowska, A., Carey, A., Faggiani, E., Schuetz, L. T., Mason, S., Tamborini, M., Bizzotto, M., Passoni, L., Filipello, F., Jahn, R., Stevens, B., and Matteoli, M. (2020). Local externalization of phosphatidylserine mediates developmental synaptic pruning by microglia. *EMBO J.* 39(16), e105380. doi: 10.15252/embj.2020105380

Shemer, A., Erny, D., Jung, S., and Prinz, M. (2015). Microglia plasticity during health and disease: an immunological perspective. *Trends Immunol.* 36(10), 614–624. doi: 10.1016/j.it.2015.08.003

Shen, M. D., Swanson, M. R., Wolff, J. J., Elison, J. T., Girault, J. B., Kim, S. H., Smith, R. G., Graves, M. M., Weisenfeld, L. A. H., Flake, L., MacIntyre, L., Gross, J. L., Burrows, C. A., Fonov, V. S., Collins, D. L., Evans, A. C., Gerig, G., McKinstry, R. C., Pandey, J., St John, T., Zwaigenbaum, L., Estes, A. M., Dager, S. R., Schultz, R. T., Styner, M. A., Botteron, K. N., Hazlett, H. C., Piven, J., and IBIS Network. (2022). Subcortical brain development in autism and fragile X syndrome: evidence for dynamic, age- and disorder-specific trajectories in infancy. *Am. J. Psychiatry* 179(8), 562–572. doi: 10.1176/appi.ajp.21090896

Showalter, M. R., Nonnecke, E. B., Linderholm, A. L., Cajka, T., Sa, M. R., Lönnerdal, B., Kenyon, N. J., and Fiehn, O. (2018). Obesogenic diets alter metabolism in mice. *PloS One* 13(1), e0190632. doi: 10.1371/journal.pone.0190632

Sidman, R. L., and Rakic, P. (1973). Neuronal migration, with special reference to developing human brain: a review. *Brain Res.* 62(1), 1–35. doi: 10.1016/0006-8993(73)90617-3

Silva-Batista, C., Ragothaman, A., Mancini, M., Carlson-Kuhta, P., Harker, G., Jung, S. H., Nutt, J. G., Fair, D. A., Horak, F. B., and Miranda-Domínguez, O. (2021). Cortical thickness as predictor of response to exercise in people with Parkinson's disease. *Hum. Brain. Mapp.* 42*,* 139– 153. doi: 10.1002/hbm.25211

Smith, J. A., Das, A., Ray, S. K., and Banik, N. L. (2012). Role of pro-inflammatory cytokines released from microglia in neurodegenerative diseases. *Brain Res. Bull.* 87(1), 10–20. doi: 10.1016/j.brainresbull.2011.10.004

Smith, S. M., Jenkinson, M., Woolrich, M. W., Beckmann, C. F., Behrens, T. E.,

Johansen-Berg, H., Bannister, P. R., De Luca, M., Drobnjak, I., Flitney, D. E., Niazy, R. K., Saunders, J., Vickers, J., Zhang, Y., De Stefano, N., Brady, J. M., and Matthews, P. M. (2004). Advances in functional and structural MR image analysis and implementation as FSL. *Neuroimage* 23 Suppl 1, S208–S219. doi: 10.1016/j.neuroimage.2004.07.051

Snodgrass, R. G., Huang, S., Choi, I. W., Rutledge, J. C., and Hwang, D. H. (2013). Inflammasome-mediated secretion of IL-1β in human monocytes through TLR2 activation; modulation by dietary fatty acids. *J. Immunol.* 191(8), 4337–4347. doi: 10.4049/jimmunol.1300298

Spann, M. N., Monk, C., Scheinost, D., and Peterson, B. S. (2018). Maternal immune activation during the third trimester is associated with neonatal functional connectivity of the salience network and fetal to toddler behavior. *J. Neurosci.* 38(11), 2877–2886. doi: 10.1523/JNEUROSCI.2272-17.2018

Squarzoni, P., Oller, G., Hoeffel, G., Pont-Lezica, L., Rostaing, P., Low, D., Bessis, A., Ginhoux, F., and Garel, S. (2014). Microglia modulate wiring of the embryonic forebrain. *Cell Rep.* 8(5), 1271–1279. doi: 10.1016/j.celrep.2014.07.042

Stafford, J. M., Jarrett, B. R., Miranda-Dominguez, O., Mills, B. D., Cain, N., Mihalas, S., Lahvis, G. P., Lattal, K. M., Mitchell, S. H., David, S. V., Fryer, J. D., Nigg, J. T., and Fair, D. A. (2014). Large-scale topology and the default mode network in the mouse connectome. *Proc. Natl. Acad. Sci. U. S. A.* 111(52), 18745–18750. doi: 10.1073/pnas.1404346111

Sturgeon, D., Earl, E., Madison, T., Perrone, A., Kathy, Rueter, A., hough129, and

Rockets2theMoon. (2022). DCAN-Labs/abcd-hcp-pipeline. Zenodo. (2022). doi: 10.5281/zenodo.2587209

Sullivan, E. L., and Kievit, P. (2016). "The Implications of Maternal Obesity on Offspring Physiology and Behavior in the Nonhuman Primate," in Parental Obesity: Intergenerational Programming and Consequences, eds. Green, L., Hester, R. (New York, NY: Springer New York), 201–234.

Sullivan, E. L., Grayson, B., Takahashi, D., Robertson, N., Maier, A., Bethea, C. L., Smith, M. S., Coleman, K., and Grove, K. L. (2010). Chronic consumption of a high-fat diet during pregnancy causes perturbations in the serotonergic system and increased anxiety-like behavior in nonhuman primate offspring. *J. Neurosci.* 30(10), 3826–3830. doi: 10.1523/JNEUROSCI.5560-09.2010

Sullivan, E. L., Nousen, E. K., Chamlou, K. A., and Grove, K. L. (2012). The impact of maternal high-fat diet consumption on neural development and behavior of offspring. *Int. J. Obes. Suppl.* 2(Suppl 2), S7–S13. doi: 10.1038/ijosup.2012.15

Sullivan, E. L., Rivera, H. M., True, C. A., Franco, J. G., Baquero, K., Dean, T. A., Valleau, J. C., Takahashi, D. L., Frazee, T., Hanna, G., Kirigiti, M. A., Bauman, L. A., Grove, K. L., and Kievit, P. (2017). Maternal and postnatal high-fat diet consumption programs energy balance and hypothalamic melanocortin signaling in nonhuman primate offspring. *Am. J. Physiol. Regul. Integr. Comp. Physiol.* 313(2), R169–R179. doi: 10.1152/ajpregu.00309.2016

Sutton, E. F., Gilmore, L. A., Dunger, D. B., Heijmans, B. T., Hivert, M. F., Ling, C., Martinez, J. A., Ozanne, S. E., Simmons, R. A., Szyf, M., Waterland, R. A.,

Redman, L. M., and Ravussin, E. (2016). Developmental programming: State-of-the-science and future directions-Summary from a Pennington Biomedical symposium. *Obesity (Silver Spring)* 24(5), 1018–1026. doi: 10.1002/oby.21487

Suzuki, T., and Hara, H. (2010). Dietary fat and bile juice, but not obesity, are responsible for the increase in small intestinal permeability induced through the suppression of tight junction protein expression in LETO and OLETF rats. *Nutr. Metab. (Lond.).* 7, 19. doi: 10.1186/1743-7075-7-19

Tau, G. Z., and Peterson, B. S. (2010). Normal development of brain circuits. *Neuropsychopharmacology* 35(1), 147–168. doi: 10.1038/npp.2009.115

Teng, K. T., Chang, C. Y., Chang, L. F., and Nesaretnam, K. (2014). Modulation of obesity-induced inflammation by dietary fats: mechanisms and clinical evidence. *Nutr. J.* 13, 12. doi: 10.1186/1475-2891-13-12

Thaler, J. P., Yi, C. X., Schur, E. A., Guyenet, S. J., Hwang, B. H., Dietrich, M. O., Zhao, X., Sarruf, D. A., Izgur, V., Maravilla, K. R., Nguyen, H. T., Fischer, J. D., Matsen, M. E., Wisse, B. E., Morton, G. J., Horvath, T. L., Baskin, D. G., Tschöp, M. H., and Schwartz, M. W. (2012). Obesity is associated with hypothalamic injury in rodents and humans. *J. Clin. Invest.*, 122(1), 153–162. doi: 10.1172/JCI59660

Thion, M. S., Ginhoux, F., and Garel, S. (2018). Microglia and early brain development: An intimate journey. *Science* 362(6411), 185–189. doi: 10.1126/science.aat0474

Thomason, M. E., Grove, L. E., Lozon, T. A., Jr, Vila, A. M., Ye, Y., Nye, M. J., Manning, J. H., Pappas, A., Hernandez-Andrade, E., Yeo, L., Mody, S., Berman, S., Hassan, S. S., and Romero, R. (2015). Age-related increases in long-range

connectivity in fetal functional neural connectivity networks in utero. *Dev. Cogn. Neurosci.* 11, 96–104. doi: 10.1016/j.dcn.2014.09.001

Thompson, J. R., Gustafsson, H. C., DeCapo, M., Takahashi, D. L., Bagley, J. L., Dean, T. A., Kievit, P., Fair, D. A., and Sullivan, E. L. (2018). Maternal diet, metabolic state, and inflammatory response exert unique and long-lasting influences on offspring behavior in non-human primates. *Front. Endocrinol. (Lausanne)* 9, 161. doi: 10.3389/fendo.2018.00161

Thompson, J. R., Valleau, J. C., Barling, A. N., Franco, J. G., DeCapo, M., Bagley, J. L., and Sullivan, E. L. (2017). Exposure to a high-fat diet during early development programs behavior and impairs the central serotonergic system in juvenile non-human primates. *Front. Endocrinol.* 8, 164. doi: 10.3389/fendo.2017.00164

Tobi, E. W., Goeman, J. J., Monajemi, R., Gu, H., Putter, H., Zhang, Y., Slieker, R. C., Stok, A. P., Thijssen, P. E., Müller, F., van Zwet, E. W., Bock, C., Meissner, A., Lumey, L. H., Eline Slagboom, P., and Heijmans, B. T. (2014). DNA methylation signatures link prenatal famine exposure to growth and metabolism. *Nat. Commun.* 5, 5592. doi: 10.1038/ncomms6592

Toga, A. W., Thompson, P. M., and Sowell, E. R. (2006). Mapping brain maturation. *Trends Neurosci.* 29(3), 148–159. doi: 10.1016/j.tins.2006.01.007

Tomchek, S. D., and Dunn, W. (2007). Sensory processing in children with and without autism: a comparative study using the short sensory profile. *Am. J. Occup. Ther.* 61(2), 190–200. doi: 10.5014/ajot.61.2.190

Translating Time (2022). *Translate*. Available online at:

https://www.translatingtime.org/translate/ (accessed December 23, 2022).

Tremblay, M. È., Stevens, B., Sierra, A., Wake, H., Bessis, A., and Nimmerjahn, A. (2011). The role of microglia in the healthy brain. *J. Neurosci.* 31(45), 16064–16069. doi: 10.1523/JNEUROSCI.4158-11.2011

Tsai, W.-H. (1985). Moment-preserving thresholding: a new approach. *Comput. Vis. Graph. Image Process.* 29(3), 377-393. doi: 10.1016/0734-189X(85)90133-1

Urbonaite, G., Knyzeliene, A., Bunn, F. S., Smalskys, A., and Neniskyte, U. (2022). The impact of maternal high-fat diet on offspring neurodevelopment. *Front. Neurosci.* 16, 909762. doi: 10.3389/fnins.2022.909762

Valdearcos, M., Robblee, M. M., Benjamin, D. I., Nomura, D. K., Xu, A. W., and Koliwad, S. K. (2014). Microglia dictate the impact of saturated fat consumption on hypothalamic inflammation and neuronal function. *Cell Rep.* 9(6), 2124–2138. doi: 10.1016/j.celrep.2014.11.018

van den Heuvel, M. P., Kersbergen, K. J., de Reus, M. A., Keunen, K., Kahn, R. S., Groenendaal, F., de Vries, L. S., and Benders, M. J. (2015). The neonatal connectome during preterm brain development. *Cereb. Cortex* 25(9), 3000–3013. doi: 10.1093/cercor/bhu095

Van Essen, D. C., and Glasser, M. F. (2018). Parcellating cerebral cortex: how invasive animal studies inform noninvasive mapmaking in humans. *Neuron* 99(4), 640–663. doi: 10.1016/j.neuron.2018.07.002

Vasistha, N. A., Pardo-Navarro, M., Gasthaus, J., Weijers, D., Müller, M. K., García-González, D., Malwade, S., Korshunova, I., Pfisterer, U., von Engelhardt, J.,

Hougaard, K. S., and Khodosevich, K. (2020). Maternal inflammation has a profound effect on cortical interneuron development in a stage and subtype-specific manner. *Mol. Psychiatry*, 25(10), 2313–2329. doi: 10.1038/s41380-019-0539-5

Vincent, J. L., Patel, G. H., Fox, M. D., Snyder, A. Z., Baker, J. T., Van Essen, D. C., Zempel, J. M., Snyder, L. H., Corbetta, M., and Raichle, M. E. (2007). Intrinsic functional architecture in the anaesthetized monkey brain. *Nature* 447(7140), 83–86. doi: 10.1038/nature05758

Wang, H., Storlien, L. H., and Huang, X. F. (2002). Effects of dietary fat types on body fatness, leptin, and ARC leptin receptor, NPY, and AgRP mRNA expression. *Am. J. Physiol. Endocrinol. Metab.* 282(6), E1352–E1359. doi: 10.1152/ajpendo.00230.2001

Williams, L., Seki, Y., Vuguin, P. M., and Charron, M. J. (2014). Animal models of in utero exposure to a high fat diet: a review. *Biochim. Biophys. Acta.* 1842(3), 507–519. doi: 10.1016/j.bbadis.2013.07.006

Woolrich, M. W., Jbabdi, S., Patenaude, B., Chappell, M., Makni, S., Behrens, T., Beckmann, C., Jenkinson, M., and Smith, S. M. (2009). Bayesian analysis of neuroimaging data in FSL. *Neuroimage* 45(1 Suppl), S173–S186. doi: 10.1016/j.neuroimage.2008.10.055

Workman, A. D., Charvet, C. J., Clancy, B., Darlington, R. B., and Finlay, B. L. (2013). Modeling transformations of neurodevelopmental sequences across mammalian species. *J. Neurosci.* 33(17), 7368–7383. doi: 10.1523/JNEUROSCI.5746-12.2013

Xing, F., and Yang, L. (2016). Robust nucleus/cell detection and segmentation in digital

pathology and microscopy images: a comprehensive review. *IEEE Rev. Biomed. Eng.* 9, 234–263. doi: 10.1109/RBME.2016.2515127

Xu, T., Falchier, A., Sullivan, E. L., Linn, G., Ramirez, J. S. B., Ross, D., Feczko, E., Opitz, A., Bagley, J., Sturgeon, D., Earl, E., Miranda-Domínguez, O., Perrone, A., Craddock, R. C., Schroeder, C. E., Colcombe, S., Fair, D. A., and Milham, M. P. (2018). Delineating the macroscale areal organization of the macaque cortex in vivo. *Cell Rep.* 23(2), 429–441. doi: 10.1016/j.celrep.2018.03.049

Xu, T., Nenning, K. H., Schwartz, E., Hong, S. J., Vogelstein, J. T., Goulas, A., Fair, D. A., Schroeder, C. E., Margulies, D. S., Smallwood, J., Milham, M. P., and Langs, G. (2020). Cross-species functional alignment reveals evolutionary hierarchy within the connectome. *Neuroimage* 223, 117346. doi: 10.1016/j.neuroimage.2020.117346

Xu, T., Sturgeon, D., Ramirez, J. S. B., Froudist-Walsh, S., Margulies, D. S., Schroeder, C. E., Fair, D. A., and Milham, M. P. (2019). Interindividual variability of functional connectivity in awake and anesthetized rhesus macaque monkeys. *Biol. Psychiatry Cogn. Neurosci. Neuroimaging* 4(6), 543–553. doi: 10.1016/j.bpsc.2019.02.005

Yoshida, H., Miura, S., Kishikawa, H., Hirokawa, M., Nakamizo, H., Nakatsumi, R. C., Suzuki, H., Saito, H., and Ishii, H. (2001). Fatty acids enhance GRO/CINC-1 and interleukin-6 production in rat intestinal epithelial cells. *J. Nutr.* 131(11), 2943–2950. doi: 10.1093/jn/131.11.2943

Ypma, R. J., Moseley, R. L., Holt, R. J., Rughooputh, N., Floris, D. L., Chura, L. R., Spencer, M. D., Baron-Cohen, S., Suckling, J., Bullmore, E. T., and Rubinov, M. (2016). Default mode hypoconnectivity underlies a sex-related autism spectrum.

Biol. Psychiatry Cogn. Neurosci. Neuroimaging 1(4), 364–371. doi: 10.1016/j.bpsc.2016.04.006

Zack, G. W., Rogers, W. E., and Latt, S. A. (1977). Automatic measurement of sister chromatid exchange frequency. *J. Histochem. Cytochem.* 25(7), 741-753. doi: 10.1177/25.7.70454m

Zhang, H., Shen, D., and Lin, W. (2019a). Resting-state functional MRI studies on infant brains: A decade of gap-filling efforts. *Neuroimage* 185, 664–684. doi: 10.1016/j.neuroimage.2018.07.004

Zhang, J., Zhang, N., Du, S., He, H., Xu, Y., Cai, H., Guo, X., and Ma, G. (2018). The effects of hydration status on cognitive performances among young adults in Hebei, China: A randomized controlled trial (RCT). *Int. J. Environ. Res. Public Health* 15(7), 1477. doi: 10.3390/ijerph15071477

Zhang, L., Hernandez-Sanchez, D., and Herzog, H. (2019b). Regulation of feeding-related behaviors by arcuate neuropeptide Y neurons. *Endocrinology* 160(6), 1411–1420. doi: 10.1210/en.2019-00056